

Crest stability of XblocPlus armoured low crested breakwaters

Master thesis

Tim Ruwiel

 **TU Delft**

 **bam**

Crest stability of XblocPlus armoured low crested breakwaters

Master thesis

by

Tim Ruwiel

Student number: 4509277
Project duration: September 1, 2019 – May 27, 2020
Thesis committee: Assis. Prof. Dr. ir. A. Antonini, TU Delft
Ir. D. Janssen, TU Delft
Prof. Dr. ir. W. Uijttewaal, TU Delft
Ir. B. Reedijk, BAM Infraconsult
Ir. M. Van de Koppel, BAM Infraconsult

An electronic version of this thesis is available at <http://repository.tudelft.nl/>.

Preface

This thesis forms the final part of my studies to obtain the title Master of Science in Civil Engineering at the Delft University of Technology. The main topic of the thesis is the crest stability of XblocPlus armoured low crested breakwaters.

First of all, I would like to thank the members of my thesis committee for giving their feedback on my work and technical advice based on their own experience. In particular, I would like to thank Bas Reedijk and Michael van de Koppel for being my daily supervisors. Furthermore, I would like to thank everyone from the water department of BAM Infraconsult. If necessary, everyone was willing to help me to answer my questions.

During the thesis period, I could perform physical model tests in the lab of BAM. During my Master's, I gained theoretical knowledge about this testing method. However, I am thankful that I could add some practical experience to my knowledge about physical model testing. Also a big thank you to those who were my lab buddy.

At last, I would like to thank by family, girlfriend and friends for their support during my master's. Given that my parents allowed me to convert their garage into a temporary crest block factory, clearly demonstrates that.

Tim Ruwiel
Delft, May 2020

Abstract

XblocPlus is a single layer armour unit that is recently developed by BAM Infraconsult. It is the successor of the Xbloc. An important advantage of the XblocPlus is the relatively high construction speed compared to the Xbloc. The increased construction speed is caused by the possibility to place XblocPlus in a uniform pattern and the relatively large surface area that can be covered with a small number of blocks. A disadvantage of XblocPlus is the limited block stability at the top armour rows of a low crested structure. The limited stability is caused by the reduced interlocking capacity of the blocks on the top armour row. In previously performed studies, a back support is placed behind the blocks to stabilise the top armour row on the front slope. The back support of a concrete element, significantly improves the stability of these armour blocks. However, at normative wave conditions, the stability of the top armour row on the front slope is still insufficient to meet the target stability ($N_{s,c} = 3.0$). The stability of the top row on the rear slope is not investigated in other studies. Consequently, no conclusions can be drawn about the stability of the crest blocks on the rear slope. In this study, physical model tests in a wave flume were performed to assess the effect of crest modifications on the stability of the top armour rows on the front and rear slope. The main objective of this study is to design a stable breakwater crest that has the best hydraulic performance with respect to the economically most feasible breakwater dimensions.

After an exploratory study into the meaning of the main objective, it can be concluded that a relative crest width of 1 is desirable. The relative crest width is determined as the ratio between the crest width (B) and the significant wave height ($H_{s,d}$). The principle of previous studies is used to set a reference situation. This crest configuration contains a concrete element between the top armour rows that functions as a support (table 1). This is a rather wide structure with a relative crest width equal to 2.7. After testing the reference situation, the top row on the front slope turned out to be normative for the crest stability. The stability found at failure coincides with the stability found in previous studies. The blocks on the top row of the rear slope remained stable. Also after reduction of the crest width to a relative crest width of 1.9, the crest blocks on the rear slope remained stable whereas the crest blocks on the front slope failed. It can be concluded that the blocks on the top row of the front slope are normative for the crest stability. The weight of these blocks is too low to meet the target stability.

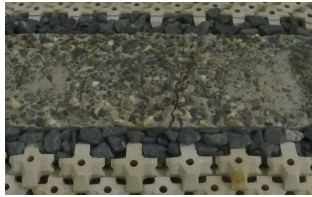
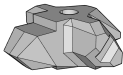

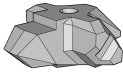
Name	Overview crest	Overview block	V/V_{ref}	$B/H_{s,d}$	$N_{s,c}$
XblocPlus top row large crest element (Reference situation)			1	2.7	2.4
XblocPlus top row small crest element			1	1.9	2.6

Table 1: XblocPlus crest armour

By application of modified XblocPlus blocks is attempted to obtain a crest configuration that meets the target stability of $N_{s,c} = 3.0$. The first version, the starting block, is a much bulkier and consequently a heavier block than the original XblocPlus block. The block shape is modified in such a way that the crest blocks on the front and rear slope can be placed back to back without the support of a crest element. Only some underlayer rock is placed between the back to back placed blocks to fill up the remaining space. As a result, the relative crest width is reduced to 1.1.

Several variants of the starting block are tested to acquire information about the stabilising effect of the applied modifications. Modified blocks with an increased permeability, an increased interlocking capacity and a relatively large resistance against rotational instability were tested. Those blocks are respectively called the permeable block, the interlocking blocks and the extended bottom block. The interlocking blocks are placed in a way that the block on the front slope is locked up by the block on the rear slope. The starting block, that has a 77% larger volume than the volume of XblocPlus ($V/V_{ref} = 1.77$), meets the target stability. The permeable block, that has an 8.5% smaller volume than the starting block, also meets the target stability. Therefore, the bulky block shape, the block's permeability, and the interlocking generated by the almost vertical back of a block, appear to be very important for the crest stability. The permeable block is the most efficient block of the preliminary research phase.


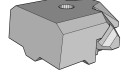

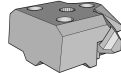
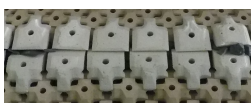
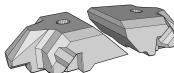


Name	Overview crest	Overview block	V/V_{ref}	$B/H_{s,d}$	$N_{s,c}$
Starting block			1.77	1.1	3.2
Permeable block			1.62	1.1	3.1
Interlocking blocks			1.72 & 1.71	1.0	2.8
Extended bottom block			1.76	1.1	2.8

Table 2: Modified XblocPlus crest armour, concept study

The acquired information of this first test series is used as a foundation for further optimisation of the permeable block. An attempt to optimise the modified block is done by reducing the volume at places that have the least impact on the block stability. Application of measures that streamline the block shape in flow direction and further increase the block's permeability were applied in this optimisation phase. Finally, a block with a 44% larger volume than the original XblocPlus block is obtained. The initial permeable block and its optimised version are shown in table 3. The measures taken were so effective that the optimised block performs better than the initial permeable block. Waves with 4% steepness appeared to be normative instead of waves with 2% steepness. Consequently, the stability value of the permeable block differs from the value that is found in the first test series.


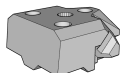
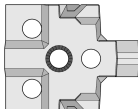

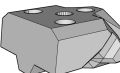
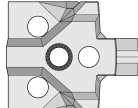
Name	Overview crest	Overview block	Bottom view	V/V_{ref}	$B/H_{s,d}$	$N_{s,c}$
Permeable block				1.62	1.1	2.8
Optimised permeable block				1.44	1.1	3.0

Table 3: Optimisation of permeable block

Contents

1	Introduction	1
1.1	Breakwaters	1
1.2	XblocPlus armour	1
1.3	Problem definition	2
1.4	Objectives	3
1.5	Approach	3
2	Theoretical framework	5
2.1	Breakwater in general	5
2.2	Failure mechanisms	6
2.3	Armour forcing	7
2.4	XblocPlus top row stability	9
2.5	General stability low crested breakwaters	11
2.6	Research into top row configurations	12
2.7	Scale effects	13
3	Target crest width	17
3.1	Wave transmission	17
3.2	Overtopping discharge	19
3.3	Construction method	20
3.4	Conclusion	21
4	Physical model setup	23
4.1	Test conditions	23
4.2	Test procedure	23
4.3	Flume configuration	24
4.4	Breakwater composition	25
5	Test information	29
5.1	Modified crest blocks	29
5.2	Definitions	29
5.3	Wall influence	30
5.4	Test program	31
5.5	Test conditions	31
5.6	Test procedure	32
6	XblocPlus crest armour	33
6.1	Reference situation	33
6.2	Stability reference situation	34
6.3	Failure mode	34
6.4	Alternative to reference situation	35
6.5	Results alternative	35
6.6	Conclusion	36
7	Modified XblocPlus crest armour	37
7.1	Starting point	37
7.2	Crest width after construction	41
7.3	Starting block test results	41
7.4	Alternatives to starting block	44
7.5	Performance of the alternatives	47
8	Comparison of alternatives	53
8.1	Stability	53
8.2	Repeated rotational movement	55
8.3	Conclusions preliminary research phase	55

9 Crest block optimisation	59
9.1 Target volume reduction	59
9.2 Foundation block optimisation	62
9.3 Design steps	63
10 Model set-up detailed research phase	67
10.1 Structure set-up.	67
10.2 Flume set-up	68
11 Performance optimised block	69
11.1 Optimised permeable block	69
11.2 Comparison blocks	72
11.3 Placement accuracy	75
11.4 Failure mode	77
11.5 Wave transmission	78
11.6 Important notes	80
12 Discussion	81
12.1 Handmade crest blocks	81
12.2 Foreshore	82
12.3 Target volume reduction	82
12.4 Wall effect.	82
13 Conclusions and recommendations	83
13.1 Conclusions.	83
13.2 Recommendations	86
Bibliography	89
A Background information	91
A.1 Rubble mound breakwaters	91
A.2 XblocPlus	92
A.3 Wave theory	92
A.4 Wave-structure interaction	95
B Scaling core material	99
C Drawings	101
C.1 Preliminary research phase	101
C.2 Detailed research phase	103
D Construction modified XblocPlus	105
D.1 Determination block density	105
E Block density	107
E.1 Blocks preliminary research phase	107
E.2 Blocks detailed research phase	111
F Test data	113
G Experiment photos	117
G.1 Preliminary research phase	117
G.2 Detailed research phase	127
H Additional test material	145
H.1 Interlocking blocks	145
H.2 Foreshore influence	146

List of symbols

Symbol	Description	Unit
A	Exposed surface area of an armour unit	m ²
B	Crest width	m
$c_{v2\%}$	A coefficient for the run-up velocity	m
C_a	Viscosity coefficient in Forchheimer equation	-
C_b	Drag coefficient in Forchheimer equation	-
C_c	Inertia coefficient in Forchheimer equation	-
C_D	Drag coefficient	-
C_I	Inertia coefficient	-
C_L	Lift coefficient	-
C_r	A reduction factor for the overtopping discharge dependent on the crest width	-
D_{50}	Rock diameter where 50% of the rock has a smaller diameter	m
D_{n50}	Characteristic rock size with 50% of the rocks of the sample being smaller than this size	m
D_n	Characteristic block size $\sqrt[3]{V}$	m
$D_{n,ref}$	Characteristic block size of model blocks XblocPlus (2.91cm)	cm
f	Frequency of wave	Hz
F_d	Drag force	N
F_l	Lift force	N
f_{peak}	Peak frequency of wave	Hz
g	Gravitational constant	m/s ²
h	Water depth	m
$H_{x\%}$	Wave height exceeded by x% of the waves	m
$H_{1/3}$	Significant wave height defined as the average of the highest one third of the waves	m
H_{m0}	Significant wave height based on the zeroth-order moment of the variance density spectrum	m
H_s	Significant wave height	m
$H_{s,d}$	Design significant wave height	m
H_{si}	Incoming significant wave height	m
$H_{s,r}$	Reflected significant wave height	m
$H_{s,t}$	Transmitted significant wave height	m
$H_{s,c}$	The critical significant wave height at the toe of the structure in test run just before failure	m
HW	high water	-
i	Hydraulic pressure gradient	-
K_D	Coefficient in the Hudson formula	-
K_r	Wave reflection coefficient (ratio between incoming and reflected wave height)	-
K_t	Wave transmission coefficient (ratio between incoming and transmitted wave height)	-
L_0	Deep water wave length	m

Symbol	Description	Unit
$L_{m-1,0}$	the deep water wave length based on $T_{m-1,0}$.	m
M	Mass of an element	kg
m_0	Zeroth-order moment of spectrum being equal to the variance of the surface elevation	m^2
n	Porosity of core material	-
N_s	Stability number	-
$N_{s,c}$	Critical stability number, just before failure, based on $H_{s,c}$	-
$N_{s,d}$	Design stability number, just before failure, based on $H_{s,d}$	-
$N_{s,overload}$	Target crest stability	-
$\frac{dp}{dx}$	Pressure gradient	N/m
q	Overtopping discharge	$m^3/s/m$
R_c	Crest elevation related to the mean water level	m
Re	Reynolds number	-
$R_{u2\%}$	Wave run-up exceeded by 2% of the waves	m
s_0	The fictitious wave steepness	-
s_{0p}	The fictitious wave steepness based on the T_p	-
SWL	Still water level	m
$T_{1/3}$	The average wave period of the highest one third of the waves	s
T_m	Mean wave period of a wave record	s
$T_{m-1,0}$	Spectral wave period	s
T_p	Peak period	s
v	Run-up velocity	m/s
$v_{A2\%}$	2%-value of run-up velocity at the seaward slope	m/s
v_f	Filter velocity	m/s
V_{ref}	Volume XblocPlus	m^3
V	Volume of armour stone	m^3
W	Weight	kg
W_{50}	Rock weight where 50% of the rock has a smaller weight	kg
Z_a	the height of a certain point on the slope related to SWL	m

Symbol	Description	Unit
α	Slope angle of a breakwater	$^\circ$
α_{PM}	Scale parameter in Pierson Moskowitz spectrum	-
α_J	Scale parameter in Jonswap spectrum	-
γ	Shape parameter for the Jonswap spectrum	-
γ_β	Influence factor for oblique wave attack	-
γ_f	Friction coefficient (0.45 for XblocPlus)	-
$\gamma_{f,surgin}$	Friction coefficient to determine run-up	-
Δ	Relative density ($\frac{\rho_c - \rho_w}{\rho_w}$)	-
λ	Scale factor between prototype and model	-
ξ	Surf similarity parameter	-
ξ_{m-1}	Surf similarity parameter based on $T_{m-1,0}$	-
ξ_p	Surf similarity parameter based on peak period	-
ρ_c	Density of concrete	kg/m^3
ρ_w	Density of fresh water	kg/m^3
σ	Shape parameter of Jonswap spectrum	-

Introduction

1.1. Breakwaters

Breakwaters are structures that are designed for protection of harbour facilities against wave action and currents. Vessels require this protection during berthing when the waves and/or currents are too heavy to sail into a port. The protection facilitated by breakwaters makes port activities less sensitive to bad weather conditions. Breakwaters also protect beaches against erosion, avoid channel siltation or protect valuable habitats that are threatened by the sea.

The dimensions of a breakwater highly depend on its function. Breakwaters near ports have other overtopping and transmission requirements than breakwaters that prevent beach erosion. Structures without or less restrictive overtopping requirements are relatively low compared to breakwaters that allow a limited amount of overtopping. The low crest height makes them financially attractive as less construction material and constructional effort is required to build them. This results in different breakwater types. These different breakwater types are expressed by the relative crest height. If the vertical distance between the design water level and the crest level is smaller than the significant wave height that acts on the structure ($R_c/H_s < 1$), the breakwater is called a low crested breakwater. A breakwater with its crest height below design water level is called a submerged breakwater. In this case, overflow is used instead of overtopping to describe the water going over the crest of the breakwater. Examples of both a low crested breakwater and a submerged breakwater are shown in figure 1.1. Breakwater properties are presented in appendix A.1.

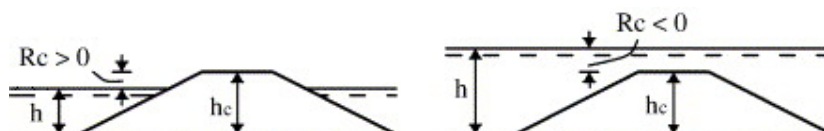


Figure 1.1: Low crested breakwater (L) and submerged breakwater (R) [2]

1.2. XblocPlus armour

The outer layer of a breakwater forms the armour layer that should be strong enough to withstand the wave loading. Rock is the classical armour type. Due to its disadvantages, concrete armour units are often used as an alternative (appendix A.2). The Xbloc, a concrete armour unit invented by BAM, was used for many years before BAM developed the XblocPlus as the successor of the Xbloc (figure 1.2). Enabling regular placement was an important objective to start with the development of XblocPlus. The biggest advantage is that regular placement reduces construction time since crane operators don't have to assess the orientation of each individual unit. Other advantages and disadvantages are described in table 1.1. The Afsluitdijk renovation project in the Netherlands is the first project where XblocPlus will be applied.

XblocPlus is a block that consists of a nose (front part), two wings and a tail (rear part which is facing towards the underlayer). There is a cone-shaped hole in the middle of the block to reduce the upward water pressure and to improve the ease of placement (figure 1.3[16]). The blocks are placed like roof tiles

Advantages	Disadvantages
Regular placement results in a very aesthetic and smooth design.	Use of XblocPlus is limited to straight or mildly curved sections.
One XblocPlus covers a larger surface area than Xbloc does. This reduces the total number of required XblocPlus blocks in a project.	Application of XblocPlus on the crest is less straightforward compared to Xbloc.
XblocPlus is less sensitive to settlements within the armour layer than other single layer armour units.	
XblocPlus has strong interlocking.	
XblocPlus makes placement with too high packing density impossible	

Table 1.1: Advantages and disadvantages for XblocPlus [16]

on a staggered grid. The stability¹ is obtained by the block weight, surface friction and interlocking between neighbouring blocks. The optimum slope to apply XblocPlus is 3V:4H [11]. More detailed information of the XblocPlus can be found in Appendix A.2.

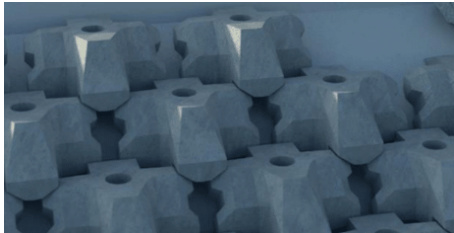


Figure 1.2: XblocPlus [23]

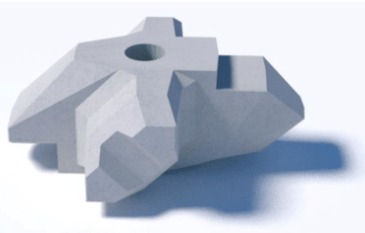


Figure 1.3: XblocPlus placement [16]

1.3. Problem definition

A disadvantage of XblocPlus is the limited block stability at the top armour rows of a low crested structure. The limited stability is caused by the reduced interlocking capacity of the blocks on the top armour row. The wave force, which is the main driving force, is maximum at the water line and slightly above the water line. For low crested breakwaters, the weakest point of the XblocPlus armour coincides with the region where the load is maximum. This causes problems for XblocPlus armoured low crested breakwaters. The top XblocPlus row is insufficiently stable to meet the target stability [17] [13].

Grigoris [13] investigated 7 methods to increase the stability of the top XblocPlus row on the front slope. After physical model tests, he proposed to place rock and an impermeable and unerodable back support behind the top XblocPlus row on the front slope (figure 1.4). The rock enhances the rotational resistance of the XblocPlus and the impermeable and unerodable back support prevents erosion of the rock. Although this structure makes the XblocPlus on the top row more stable, it is still insufficiently stable to meet the target stability at critical conditions.



Figure 1.4: Crest set-up by Grigoris [13]

The aim of this thesis is to investigate possibilities to armour low crested breakwaters with XblocPlus. In order to obtain a stable crest configuration, the method is important to consider. At first glance, the method

¹The term 'stability' refers to hydraulic stability unless otherwise stated. Structural stability is not investigated in this study.

with a supporting element seems not very attractive. As mentioned before, a supporting element does not create enough stability for the blocks on the top armour row of the front slope. Moreover, a low crested breakwater would become very wide if a supporting element would be placed between the top armour rows. For many low crested breakwaters, a smaller crest (and therefore a smaller cross-sectional area) might be preferred because it requires less construction material. Alternative methods should be investigated to obtain stable top armour rows on both the front and the rear slope.

1.4. Objectives

The main objective of this thesis is to design a stable crest configuration for low crested breakwaters armoured with XblocPlus. The main research question is:

What crest configuration(s) for low crested XblocPlus armoured breakwaters result(s) in the best hydraulic performance with respect to the economically most feasible breakwater dimensions?

The effectiveness of a breakwater is partly determined by the crest width. A wide crest requires more construction material and that might make the breakwater economically less attractive. However, a wide crest is more effective in reducing the wave height and the overtopping discharge. Prior to the preliminary research phase, the phrase 'best hydraulic performance with respect to the economically most feasible breakwater dimensions' from the main research question will be translated into a target crest width.

Two sub questions are defined to answer the main research question:

- 1. What measures positively affect the stability of the top armour row at the slope-crest transitions or are beneficial for crest width reduction?*
- 2. How should the most effective measure be employed to obtain a stable crest configuration that is efficient regarding construction material?*

1.5. Approach

A preliminary research phase and a detailed research phase are used to distinguish two research phases. The preliminary research phase functions as an exploring research phase into the effects of crest modifications on the crest stability and the crest width. The best performing solution of the preliminary research phase is further optimised in the detailed research phase. A thesis outline is given in figure 1.5. The preliminary and detailed research phase are indicated in resp. gray and blue.

1.5.1. Preliminary research phase

The first sub question will be answered in the preliminary research phase. The aim of this phase is to assess the effect of applied modifications compared to the reference situation. Each modification forms an alternative that should either enhance the stability of the crest blocks or result in crest width reduction. Two different paths will be followed. The first is based on original XblocPlus blocks on the top armour rows. The second is based on XblocPlus crest armour with a modified shape.

1.5.2. Detailed research phase

The second sub question will be answered in the detailed research phase. A stable crest configuration is designed that is efficient regarding the crest width and construction material. Stability information of the preliminary research phase is used as input. Effective principles may be optimised to enlarge their positive influence on the crest stability. In addition, aspects like the construction method are considered in the detailed research phase. Finally, the performance of the final solution is tested at different wave conditions.

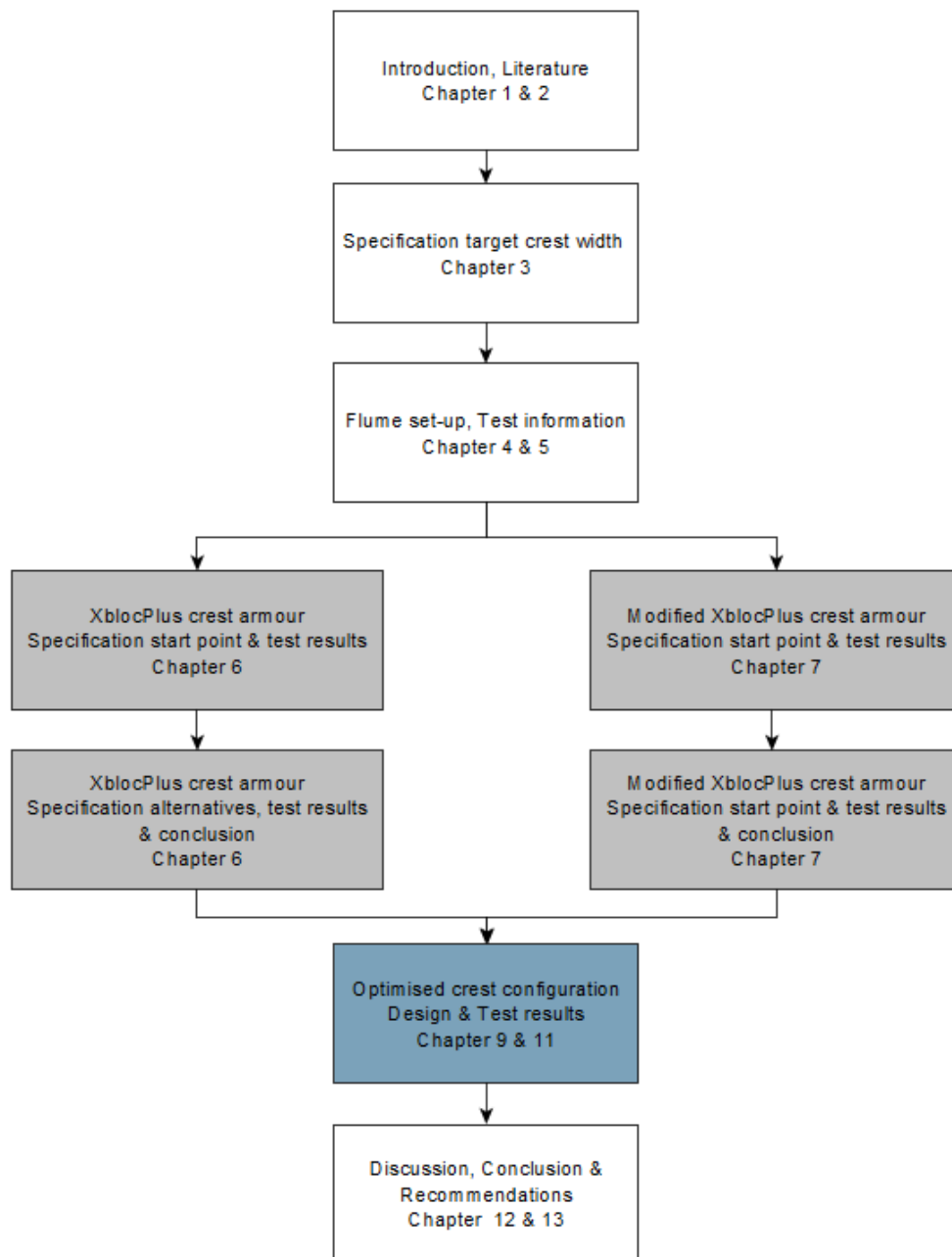


Figure 1.5: Thesis outline

1.5.3. Methodology

A model is a useful tool to find the best crest configuration for a low crested breakwater armoured with XblocPlus. Scale models of a prototype are often used with the aim to test the performance of the prototype. According to Wolters [30], physical modelling is the best method to determine effects of modifications on the stability of existing structures and wave forcing on crest elements. In addition, performing physical model tests would be in line with previously conducted research into coastal structures. An important reason to avoid a numerical model is that block specific information about drag and lift coefficients is required. Since several new block shapes will be tested, it is labour intensive to determine those values before testing. Constructing test blocks is expected to be less labour intensive. The disadvantage that facilities for physical model tests are expensive, is easy to overcome since BAM has its own wave flume. 2D physical model tests can be conducted in that flume.

2

Theoretical framework

2.1. Breakwater in general

A breakwater consists of several parts that each fulfils its own function. The armour layer is the outer layer. Depending on the armour size, one or several filter layers are used between the core and the armour layer to prevent washing out of the core material. Toe structures are applied to prevent settling in the armour layer. In some cases, a superstructure like a crown wall is placed on the crest. More information about rubble mound breakwaters and their armour is presented in appendix A.1.

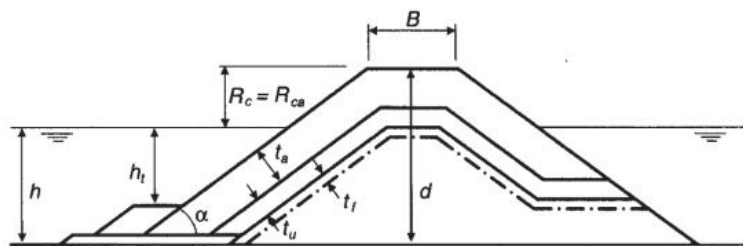


Figure 2.1: Breakwater cross-section [4]

Where:

- t_a represents the thickness of the armour layer
- t_u and t_f represent a filter layer (underlayer)
- α the slope angle
- B represents the crest width
- R_c represents the crest height
- h represents the water depth
- h_t represents the water depth above the toe

2.1.1. Crest width

The width of the crest depends on the breakwater construction method or the functional requirements after construction [4]. Without constructional limitations, the required crest width depends on the stability of the armour layer, overtopping regulations (appendix A.4.3) and transmission requirements (appendix A.4.4). For rock armoured breakwaters with a small crest, the minimum width is often defined as (3-4) D_{n50} [4]. In Delos no 43 [10] is stated that the crest should consist of at least 3 armour stones. In the Delos report is also recommended to apply a crest width that is equal or larger than the design significant wave height.

2.1.2. Crest height

The height of the crest depends, similarly to the width of the crest, on the overtopping- and transmission requirements. A small crest height is feasible since it requires less construction material. However, a small crest height results in more wave overtopping and less wave height reduction.

2.1.3. Armour stability

The armour layer frequently consists of concrete armour units like XblocPlus. The stability of XblocPlus is defined by a stability number (equation 2.1)[9]. The significant wave height (appendix A.3) in the numerator

of the expression of the stability number is a measure of the destabilising forces. The relative density¹ (Δ) and the characteristic block size (D_n) in the denominator are a measure of the stabilising forces. The design stability number ($N_{s,d}$) is a block specific stability number that guarantees stable armour blocks. No armour blocks fail if the structure is stable. Given a certain significant wave height, the required characteristic size of the armour blocks can be determined via the design stability number. The design stability number of XblocPlus is 2.5 [11]. The larger design stability number, the more effective a block is. It implies that a block of a certain size can withstand relatively larger waves than a block with lower design stability number. The critical stability number ($N_{s,c}$), which represents the stability number just before failure of the first crest block, is often much higher. Since the critical stability number for XblocPlus was between 3.5 and 4, there is a large safety margin between the obtained stability and the design stability [24].

$$N_s = \frac{H_s}{\Delta \cdot D_n} \quad (2.1)$$

The design formula used for XblocPlus is simple and is determined by performing physical model tests. However, it does not give insight into the magnitude and direction of the destabilising and stabilising forces on an XblocPlus element. Understanding the phenomena that cause failure is a prerequisite. The destabilising forces are described in the section 2.3.1 and the stabilising forces are described in section 2.3.2.

2.2. Failure mechanisms

In paragraph 2.1, a brief description of the composition of breakwaters is presented. Each section of a breakwater has failure modes that endanger the stability of the entire breakwater [14]. Hald [14] made an overview of all breakwater failure modes (figure 2.2). As stated in the problem definition, this research zooms in on the armour stability on and near the crest. Other failure mechanisms than 'Erosion, breakage of armour' will not be further elaborated.

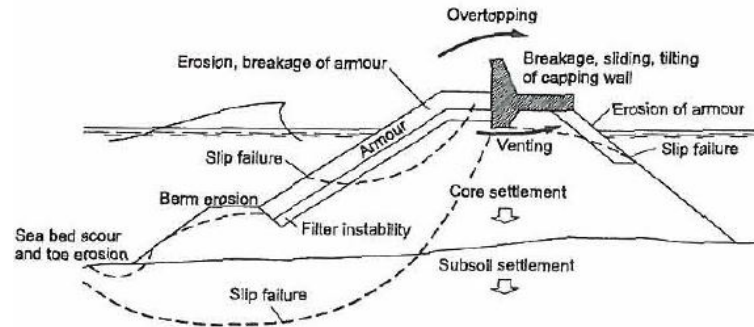


Figure 2.2: Breakwater failure mechanisms [14]

2.2.1. Erosion of armour

The stability of armour units can be formulated by using equilibrium equations. An armour unit fails when the stabilising forces are not able to balance the destabilising forces. This automatically means that equations 2.2, 2.3 and 2.4 are only satisfied for a stable block. Equation 2.2 is the vertical force balance that should prevent uplift of armour blocks. Equation 2.3 prevents a block from sliding backwards. Equation 2.4 guarantees the rotational stability of the armour.

$$\Sigma F_v = 0 \quad (2.2)$$

$$\Sigma F_h = 0 \quad (2.3)$$

$$\Sigma T = 0 \quad (2.4)$$

¹The meaning of the relative density and other parameters are explained in the list of symbols

2.2.2. Breakage of armour

Violating the rotational or vertical stability for a short moment in time does not necessarily lead to failure of armour units. If one of these requirements is not satisfied for a small moment in time, the armour unit displaces and subsequently it returns to its initial position. Rocking is the name of the phenomenon that causes a rotational movement during up-rush. The block returns to its initial position during down-rush. According to the rocking definition of BAM [7], the rotational movement should occur at more than 2% of the waves to call it rocking. Although rocking does not result in erosion of the armour blocks, it might result in mechanical failure of the blocks. Mechanical failure occurs when the non-reinforced concrete blocks break into 2 or more pieces. Provided that an armour unit breaks, it can be classified as failed. Rocking is not a failure mechanism. However, severe rocking should be prevented to minimise the probability that armour blocks break.

2.3. Armour forcing

2.3.1. Destabilising forces

External driving forces tend to destabilise the XblocPlus elements. These forces are caused by drag, lift and inertia exerted by the water. Seepage is an internal driving force that acts on the armour [14]. Figure 2.3 is used to illustrate how the destabilising forces act on the armour layer. The left image shows the forces during down-rush, the right image during up-rush.

The external forces in figure 2.3 are the drag, lift and inertia force.

- F_D is the drag force, which is the result of the run-up and the run-down (information about run-up is presented in appendix A.4.2). The drag force is directed upwards during up-rush and downwards during down-rush. The drag force mainly depends on the run-up velocity (v) and the cross-sectional area (A) of a stone/block.

$$F_D \approx C_D \cdot \rho_w \cdot A \cdot v|v| \quad (2.5)$$

- F_L is the lift force that is directed perpendicular to the flow direction of the water. It is caused by the curvature of the flow around the armour element [27]. Like the drag force, it mainly depends on the run-up velocity (v) and the cross-sectional area (A) of a stone/block.

$$F_L \approx C_L \cdot \rho_w \cdot A \cdot v|v| \quad (2.6)$$

- F_I is the inertia force caused by velocity variations in time.

$$F_I \approx C_I \cdot \rho_w \cdot v \cdot \frac{dv}{dt} \quad (2.7)$$

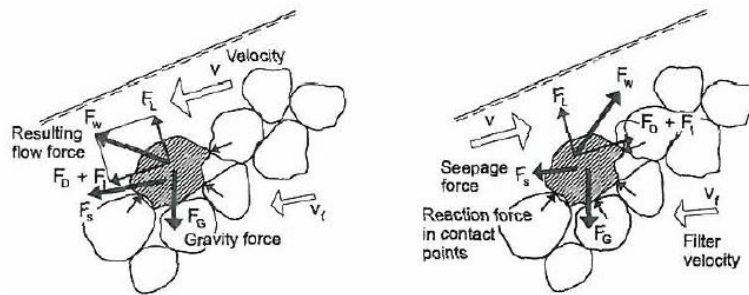


Figure 2.3: Force illustration on armour stone [14]

The vector sum of F_D , F_L and F_I forms the total external force exerted on the armour by the water. The magnitude of these forces depends on coefficients C_D , C_L and C_I . These coefficients, resp. drag, lift and inertia, are affected by:

- The Reynolds number. This number says something about the flow being laminar or turbulent. A lower Reynolds number increases the force and therefore the value of the coefficient.
- The shape of an element. Streamlined elements have a lower coefficient because the water flows easier around the element.

- The Keulegan-Carpenter number. This number says something about the lengthscale of the structure and the length scale of the orbital motion. A large KC number implies that the wave period is long. The orbital motion acts like a steady current that enhances the contribution of the drag force. Oppositely, when the wave period is short the influence of inertia increases.

The seepage force (F_s) is related to the internal flow forces. The outward directed seepage force is the vector sum of the internal flow force (F_f) and the pressure build-up in the core of the structure (F_p) [14]. The core material is the most important factor that influences the seepage force. A high hydrostatic pressure build-up (F_p) takes place if the structure's permeability is low [14]. In this case, the flow force (F_f) is small since only small internal water level fluctuations occur. For a permeable core, the opposite is the case. The equations for F_p and F_f are presented in equations 2.8 & 2.9 [14]. The extended Forchheimer equation is used for the hydraulic gradient (equation 2.10). Barends and Hölischer concluded that, in the initial failure stage, the element is lifted by the seepage force and subsequently the element is displaced by other flow mechanisms [14].

$$F_p \approx \frac{V}{1-n} \cdot \frac{dp}{dx} \quad (2.8)$$

$$F_f \approx \rho_w \cdot g \cdot \frac{V}{1-n} \cdot i \quad (2.9)$$

$$i = C_a \cdot v_f + C_b \cdot v_f |v_f| + C_c \cdot \frac{\delta v_f}{\delta t} \quad (2.10)$$

2.3.2. Stabilising forces

Figure 2.3 also indicates that the gravitational force is the main stabilising force for rock armour [14]. The stabilising forces that act on an XblocPlus block are the gravitational force, interlocking and surface friction.

- The gravitational force generates a downward directed force. The gravitational force depends on the block volume. The contribution of the gravitational force depends on the slope angle of the breakwater.
- Surface friction at the contact surfaces of an XblocPlus element impede its displacement. The magnitude of the surface friction depends on the mass of the block and the mass of the block(s) on top of it. The larger the downward directed force by the mass, the larger the surface friction. The surface friction at the armour rows near the crest is relatively small since the contribution of the weight of the blocks at higher rows is small.
- The XblocPlus shape in combination with their placement in a staggered grid results in the interlocking of the blocks on the slopes. The green circles in figure 2.4 indicate where the wings of 2 blocks are enclosed behind the block in the armour row beneath. In addition, a unit is enclosed behind the nose of the two elements in the row on top of it (orange circle). Like the surface friction, the contribution of interlocking to the total stability is relatively small for the blocks on the top armour rows. Vos [28] concluded this after conducting dry pull-out tests with the Xbloc+v1 (initial version of XblocPlus).



Figure 2.4: Interlocking mechanisms [23]

The contribution of interlocking, gravity and surface friction depends on the slope angle [13]. The single layer armour blocks are bulkier than the, on interlocking relying, slender blocks used for double layer armour (appendix A.1.2). For both the interlocking type and the bulky type holds that the contribution from interlocking and surface friction increases for increasing slope angles. The opposite holds for the contribution of the gravitational force generated by the block's weight. Therefore, the bulky single layer elements are most stable for a slope angle near 30 degrees. Complex interlocking blocks are most stable for a slope angle of 60 degrees. XblocPlus is a rather bulky single layer armour unit and it suits best on a 3V:4H slope (37 °) [11].

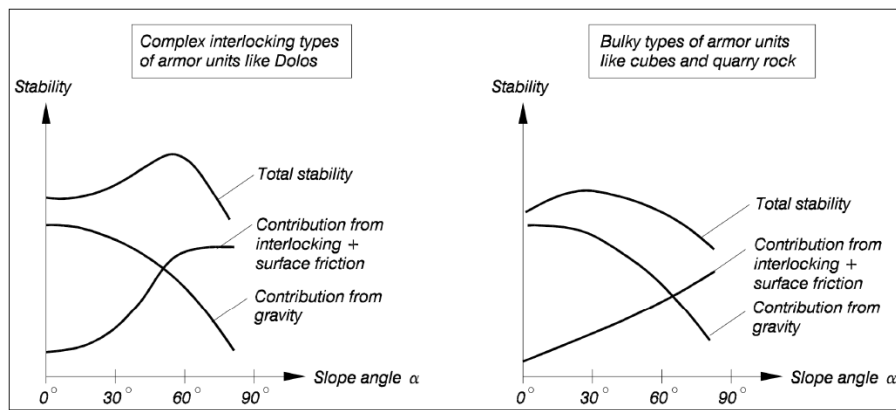


Figure 2.5: Stability concrete armour units related to slope angle [13]

2.4. XblocPlus top row stability

2.4.1. Influence relative crest height

Janssen [17] investigated the stability of XblocPlus elements placed on top of the crest (figure 2.6). He tested, by physical model tests, the stability of the crest blocks for waves with steepness $s_{0,p} = 4\%$ in combination with a relative freeboard ($R_c/H_{s,d}$) values of 0, 0.5 and 1. Janssen found that the blocks on the top row did not fail for $R_c/H_{s,d} = 1.0$. In test series with relative freeboard $R_c/H_{s,d} = 0.5$ and $R_c/H_{s,d} = 0.0$, the blocks on the top row quickly failed. For these conditions, the block stability was far lower than the design stability number of 2.5 (table 2.1).

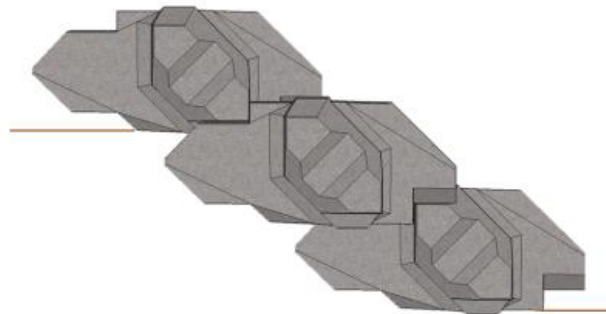


Figure 2.6: Schematic model set-up [17]

Rel. freeboard ($R_c/H_{s,d}$)	N_s at failure
0.0	≥ 3.75
0.5	≤ 1.5
1.0	≤ 1.3

Table 2.1: Start of damage as percentage of target conditions [17]

2.4.2. Combined influence rel. crest height and wave steepness

Grigoris [13] investigated the combined influence of the relative crest freeboard and the wave steepness on the stability of XblocPlus blocks on the crest. He performed physical model tests with a wave steepness $s_{0,p}$ of 2% and 4% in combination with $R_c/H_{s,d}$ of 0.0, 0.5, 1.0 and 1.5. The relation between the wave steepness and the armour stability is explained in A.4.

Grigoris concluded that the stability at failure is lowest for conditions $R_c/H_{s,d} \leq 0.5$. For both $R_c/H_{s,d} = 0.0$ and $R_c/H_{s,d} = 0.5$, waves with steepness $s_{0,p} = 2\%$ caused first block failure at $N_s \approx 1.5$. Waves with steepness $s_{0,p} = 4\%$ caused first block failure at $N_s \approx 1.3$. Higher stability numbers were achieved for $R_c/H_{s,d} > 0.5$. For $R_c/H_{s,d} > 0.5$, waves with steepness $s_{0,p} = 2\%$ caused more damage than waves with steepness $s_{0,p} = 4\%$.

Grigoris concluded that stability differences between 2% and 4% wave steepness are related to run-up and wave breaking. The run-up of waves with 2% steepness is larger than the run-up of waves with 4% steepness. This is caused by the larger wave period of waves with 2% steepness. Although the run-up velocity for waves with 4% steepness is smaller, their impact on the crest is larger due to more energetic collapsing waves. As a result, waves with steepness 4% appeared to be critical for $R_c/H_{s,d} = 0.0$.

2.4.3. Normative failure mode

Besides stability tests, Janssen [17] performed numerical model tests as well to assess the block failure of the top armour row. Janssen found the lowest factor of safety for the rotational stability (0.16) followed by the vertical stability (0.81) and the horizontal stability (4.76). Therefore, the rotational stability is normative for XblocPlus blocks on the top armour row of the front slope.

2.4.4. Rocking

Besides stability tests, Grigoris [13] investigated the influence of rocking on failure. He found that units were rocking before and after failure. Rocking was observed most frequently in the test series with conditions $R_c/H_{s,d} = 0$ & $s_{0,p} = 4\%$, $R_c/H_{s,d} = 0$ & $s_{0,p} = 2\%$ and $R_c/H_{s,d} = 0.5$ & $s_{0,p} = 2\%$. A larger relative crest height resulted in a smaller number of rocking elements. The decay went faster for waves with steepness $s_{0,p} = 2\%$ compared to $s_{0,p} = 4\%$. More rocking was observed after units have failed. He argued that the units were subjected to more severe wave action. This was caused by the non-idealised new place of the blocks that resulted in a larger exposed surface area of the block. Grigoris concluded that rocking cannot be characterised as a reliable indicator of failure since most units did not rock before failure.

2.4.5. Visual failure

Janssen [17] observed that failure of the armour units happened frequently as a combination of two processes. These processes are horizontal displacement (figure 2.8) and rotation (figure 2.7). During horizontal displacement, the element slides backwards due to the horizontal directed load. During up-rush, the resultant wave load (blue arrow) results in an anticlockwise rotation of the unit around the red dot (rotation point). The above-mentioned events did often happen as a combination of those events. Janssen explained this by the changed area that becomes exposed to wave impact after rotation. In rest, the wave load acts on a small part of the block. The contact surface that is exposed to the wave load enlarges after rotational movement (figure 2.9).

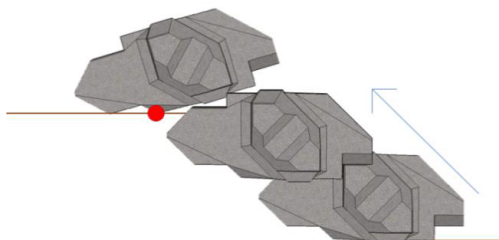


Figure 2.7: Rotational failure Janssen([17])

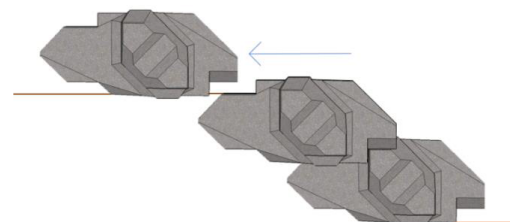


Figure 2.8: Horizontal displacement [17]

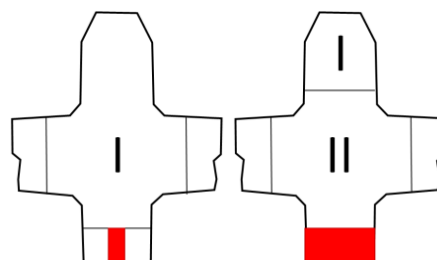


Figure 2.9: Impact area in rest (L) and during rocking (R) [17]

Grigoris [13] also concluded that failure often happened as a combination of rotation and translation. He stated that the front part of a block is subjected to the wave action first, followed by the rest of the unit as the wave is passing. Initially, a unit makes a rotational movement. After the rotation has started, the unit

does return to its initial position or it doesn't. In the latter case, the rotating unit moves slightly upwards due to uplift. An instant later it moves downward during down-rush. In the end, the unit made a combined motion of rotation, horizontal and vertical translation.

2.5. General stability low crested breakwaters

2.5.1. Interlocking concrete armour

Muttray [21] and Van den Bosch [24] investigated the stability of single layer armour units (Xbloc) on a low crested breakwater. Both reanalysed the tests performed by Peter van der Linde.

2.5.1.1. Wave steepness

The wave steepness appeared to be an important parameter for the armour stability. After comparison of the armour stability for waves with 2% and 4%, the armour stability appeared to be approximately 20% smaller for waves with 2% steepness. This applies to both emerged and submerged structures.

2.5.1.2. Relative crest height

Both Muttray and Van den Bosch concluded that the location of damage depends on the relative freeboard. The stability numbers were determined based on the start of damage (the test condition where the first armour unit has been displaced). The lowest stability number was found for a crest with zero freeboard ($N_s = 3.0$). The front slope and the rear slope were least stable for $R_c/H_{s,d} = 0.4$ (Resp. $N_s = 3.1$ and $N_s = 3.2$). An overview of the stability related to the freeboard can be found in figure 2.10 and table 2.2. The orange band forms the safety margin that is used for design with concrete armour units. The safety margin is approximately 25% of the design stability number. In general, the rear slope is the most stable part of a breakwater armoured with interlocking armour units.

The interlocking mechanism of Xbloc armour units performs similar to other interlocking single layer armour units (Coreloc®, Accropode™, etc.). Therefore, the results of this study can also be applied to other single layer armour types.

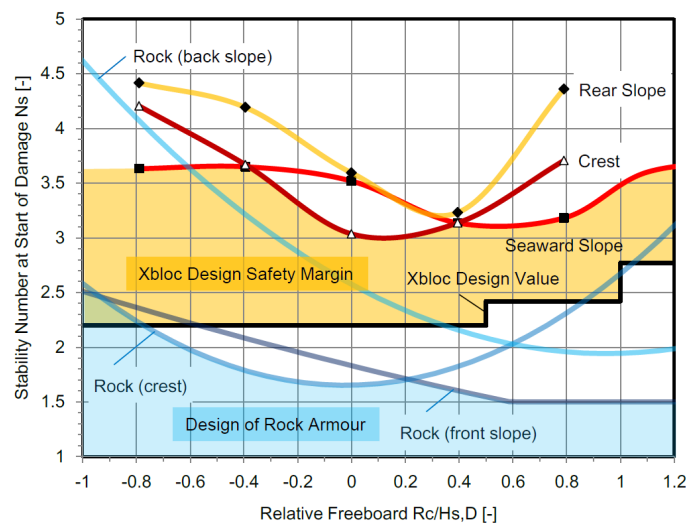


Figure 2.10: Xbloc armour stability [24]

Structure	Rel. freeboard ($R_c/H_{s,d}$)	Reduced stability	N_s at SoD [-]
Emerged	+ 0.8	Seaward slope	3.2
	+ 0.4	Seaward slope, crest, rear slope	3.1
Zero freeboard	+/- 0.0	Crest	3.0
Submerged	-0.4	No reduction	3.5
	-0.8		3.5

Table 2.2: Reduced armour stability at low crested and submerged breakwaters [24]

2.5.2. Rock

Non-interlocking armour (rock) and interlocking armour (Xbloc) behave very different as a result of the interlocking [24]. The initiation of damage for rock starts at much lower stability numbers than is the case for interlocking armour blocks (figure 2.10). The crest stability of rock armoured structures has, just like a crest armoured interlocking armour units, a minimum at zero freeboard. In contrast to interlocking armour units, the lowest stability numbers are achieved on the front slope for relative freeboard $R_c/H_{s,d} \geq 0.6$.

2.5.3. Influence of crest width

Van der Linde [25] investigated the influence of the crest width on the stability of Xbloccs. He performed tests with both a narrow crested and a wide crested breakwater. The narrow crest had a width of 3 armour units and the wide crest had a width of 9 armour units. For $R_c/H_{s,d}$ close to zero in combination with long waves ($S_{0,p} = 2\%$), the wide crest was slightly less stable than the small crest. However, stability differences were very small. For emerged structures ($R_c/H_{s,d} > 0.6$) and submerged structures ($R_c/H_{s,d} < -1.7$), the small crest was less stable (figure 2.11).

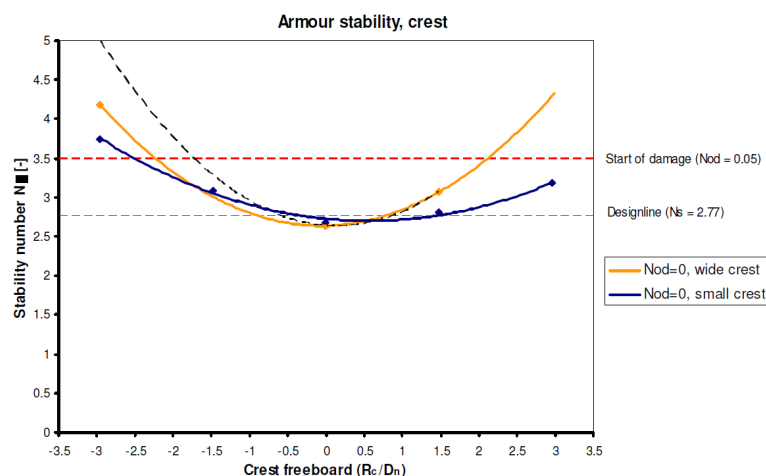


Figure 2.11: Stability of crest [25]

2.6. Research into top row configurations

2.6.1. XblocPlus armour with back support

Janssen [17] proposed to enlarge the rotational stability of XblocPlus blocks on the top armour row by applying rock behind it. The rock should cause a backwards shift of the rotation point of the XblocPlus. This is indicated by point 1 and point 3 in figure 2.12. The stabilising moment of the XblocPlus units should increase due to the backwards shifted rotation point.

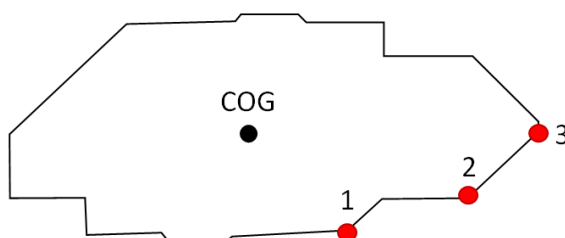


Figure 2.12: Rotation point with and without supporting rock [17]

Grigoris [13] tested a structure with an XblocPlus top armour row supported by underlayer rock. He applied a stiff element behind the rock to prevent erosion of the rock. Figure 2.13 shows an overview of Grigoris' structure in the wave flume.



Figure 2.13: XblocPlus, rock fill and stiff element [13]

Grigoris tested the crest configuration with 4 different wave conditions (all possible combinations with 2% and 4% wave steepness and $R_c/H_{s,d}$ of 0.0 and 0.5). It turned out that 2% wave steepness combined with zero freeboard was normative. At $N_s = 2.5$, rather abrupt failure occurred. The abrupt failure was caused by displacement of the stiff element. The abrupt displacement created more space for the filling material to spread. As a result, the XblocPlus units displaced. For all other conditions, the crest configuration appeared to be stable till the end of the test series ($N_s \approx 3.5$). To summarise, the proposed crest configuration is stable up to the design stability. However, there is no safety margin between the design stability and the stability obtained in the model tests.

2.6.2. Modified XblocPlus armour

The renovation project of the Afsluitdijk in the Netherlands is the first project where XblocPlus will be applied. The outer slope of the dam has a berm that subdivides the slope in 2 sections. The lower section is covered with XblocPlus (figure 2.14). The design water level equals the berm level. As a result, the relative berm height is zero. Since the top XblocPlus row is unstable at zero freeboard, a modified XblocPlus block is designed for the transition from the slope toe to the berm (figures 2.15). The modified block is 92% heavier than an XblocPlus block. Drawings of the final berm block are provided in appendix C. In a test in the Delta flume, the berm blocks were stable until $N_s = 2.95$.



Figure 2.14: Overview Afsluitdijk [5]

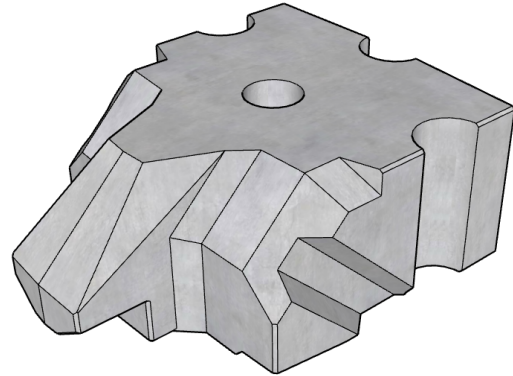


Figure 2.15: Berm block

2.7. Scale effects

Scaling rules for physical model tests rely on geometric, kinematic and dynamic similarity. Kinematic similarity means that the time-related processes in the model have a constant time relation to the processes in nature. According to Wolters [29], a correct kinematic similarity in a geometrically similar model can only be achieved by a correct representation of the dynamic similarity.

2.7.1. Geometric similarity

Scaling the dimensions of a rubble mound breakwater is rather straightforward. The dimensions of a prototype (L_p) are transferred into the model dimensions (L_m) by a constant scale factor (λ).

$$\lambda = \frac{L_p}{L_m} \quad (2.11)$$

2.7.2. Dynamic similarity

Dynamic similarity entails that there is a constant relation between the forcing in the model and the prototype. Constants like the Froude, Reynolds, Cauchy and Weber number are important for dynamic similarity. Figure 2.16 shows for which forces these scale numbers are important.

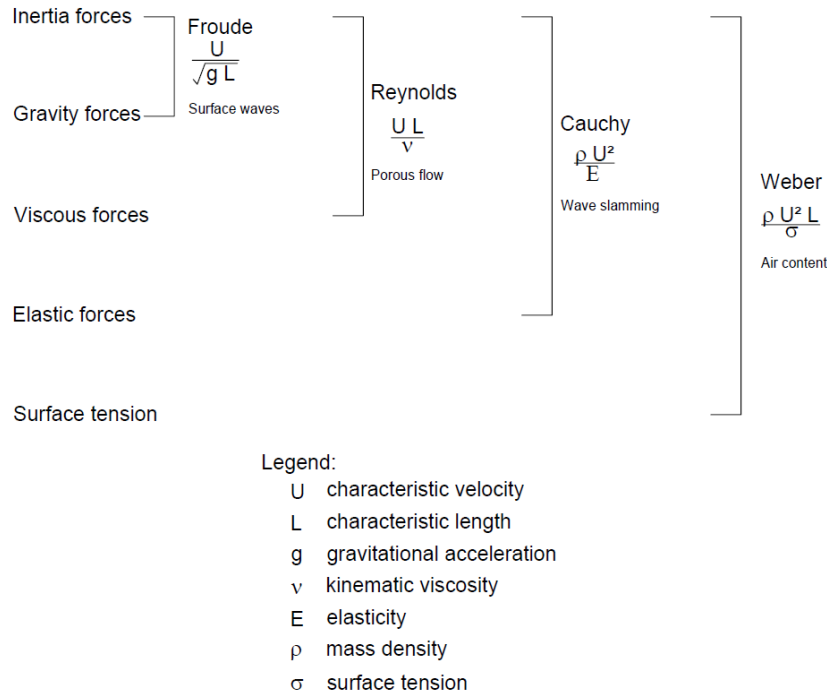


Figure 2.16: Scale effects [1]

Perfect dynamic similarity is impossible because some of the constants in figure 2.16 contradict each other. For example, the length scale is in the denominator of the Froude expression and in the numerator of the Reynolds expression. This makes perfect scaling of both the Froude number and Reynolds number impossible. In this thesis is dealt with surface waves. Therefore, Froude scaling is applied to obtain an accurate wave model with acceptable errors. As a result, viscosity, elasticity and surface tension are not correctly scaled [30]. To make errors negligible, limits are set to the Reynolds and Weber number. By the limits is assured that their values in the model are in the same range as in the prototype. For the Reynolds number, condition 2.12 should be met to assure that the flow in the primary armour layer remains turbulent [30].

$$Re_{armour} = \frac{\sqrt{g \cdot H_s} \cdot D_n}{\nu} > 30.000 \quad (2.12)$$

Surface tension effects are negligible if the Weber number is large enough. Conditions 2.13 to 2.16 are specified in the Overtopping Manual 2018 [12].

$$h > 2cm \quad (2.13)$$

$$H_s > 5cm \quad (2.14)$$

$$L \gg 2cm \quad (2.15)$$

$$T > 0.35s \quad (2.16)$$

2.7.3. Stability scaling

Stability scaling is an important link between dynamic similarity and the geometric similarity. The stability number (N_s) of the prototype should be equal to the stability number of the model. It is important to take the difference in relative density between the prototype and the model units into account.

2.7.4. Permeability scaling

Breakwater dimensions in physical models must be scaled geometrically. This might cause difficulties for the underlayer and the core of the breakwater. If the grading becomes too small, the flow becomes laminar due to the limited permeability. The inflow and outflow in the underlayer and/or core decrease. As a result, the run-up height increases, the run-up velocity increases and the armour stability reduces [26]. To minimise those errors caused by scale effects, the filter velocities in the prototype and the model can be scaled by Froudian similitude. Scaling by Froudian similitude results in equal hydraulic gradients in model and prototype. The flow in the core is considered as turbulent when the Reynolds number in the core exceeds 300 [3].

3

Target crest width

The aim of this thesis is to find a crest configuration with the best hydraulic performance. Furthermore, the costs are also important to consider. The financially most attractive solution regarding construction material has the smallest possible cross-sectional area. However, wave transmission and overtopping requirements should not be violated. To obtain a target crest width, the effect of the crest height and the crest width on wave transmission and overtopping is investigated. For $R_c/H_s = 0.0$, crest stability differences between narrow crested structures and wide crested structures armoured with interlocking armour units are negligible (paragraph 2.5.3). Therefore, the optimum crest width regarding the crest stability is not assessed.

3.1. Wave transmission

The wave transmission formula for rubble mound small crested breakwaters (appendix A.4.4.1) is used to assess the effect of crest height and crest width modifications. The effect of crest width and crest height adjustments on the wave transmission coefficient are related to changes in cross-sectional area. For example, an increased crest width compared to a certain reference situation reduces the wave transmission. However, the cross-sectional area of the structure increases. A structure with an increased crest height compared to the same reference situation also results in a reduced wave transmission coefficient and an increased cross-sectional area. The most effective measure is the one with the largest wave transmission reduction and the smallest increase in cross-sectional area.

3.1.1. Applicability wave transmission equation

An important note is that equation A.14 is proposed for permeable breakwaters armoured with rock. An XblocPlus armoured breakwater is also a permeable structure. The behaviour of XblocPlus and rock armour should be more or less equal to apply equation A.14 in the assessment. The reflected, transmitted and absorbed wave energy should be similar if XblocPlus behaves similar to rock. The friction factor plays an important role in the absorption of wave energy. Assuming that the core of the rock armoured structure and the XblocPlus armoured structure are equally permeable, the energy absorption will be comparable if the friction factors are similar. Therefore, both the friction and reflection coefficient of rock armour and XblocPlus should have similar values.

The friction factors and the reflection coefficients of rock and XblocPlus are compared:

- The friction factor for XblocPlus is slightly smaller than for rough armour stone ($\gamma_{f,XblocPlus} = 0.45$ and $\gamma_{f,rock} = 0.55$ [4]). This indicates that the absorbed wave energy is slightly larger for XblocPlus.
- The value of the reflection coefficient depends on the surf similarity parameter. Based on the reflection equation for rock (appendix A.4.4.2) and the XblocPlus reflection results found by Jimenez [18], it can be concluded that the reflection coefficients are comparable. A 3V:4H slope in combination with $s_{0,p} = 2\%$ gives K_r values of 0.47 and 0.50 for respectively rock and XblocPlus. For $s_{0,p} = 4\%$, the K_r values for rock and XblocPlus are respectively 0.37 and 0.4.

The reflection coefficients of rock and XblocPlus are comparable. The friction factor for XblocPlus is slightly smaller than the friction factor of rock. Therefore, the wave transmission of XblocPlus is expected to be slightly smaller than the wave transmission of rock. Hence, making use of equation A.14 to assess the effect of the dimensions of an XblocPlus armoured breakwater on the wave transmission seems valid.

3.1.2. Reference structure

A fictional reference structure is used to assess the impact of adjustments of crest height and crest width. This reference structure has the minimum crest width of $1 \cdot H_s$ (paragraph 2.1.1). The crest level equals the water level. Furthermore, a breakwater height of $3.5 \cdot H_s$ (0.35m) is assumed. This reference structure is solely used in this assessment. For the values of the significant wave height and the wave steepness is referred to chapter 4.

Parameter	Value
$H_{s,i}$	9.9 cm
$s_{0,p}$	2%
B	9.9 cm
h	35 cm

Table 3.1: Input parameters fictional reference structure

3.1.3. Results

Figure 3.1 shows the effect of height and width modifications relative to the reference situation. The X-axis represents the ratio between the cross-sectional area after crest modification and the cross-sectional area of the reference structure. The Y-axis represents the ratio between the reduced transmission coefficient and the transmission coefficient of the reference structure. Small modifications in crest width and crest height result in small differences in wave transmission reduction. When larger modifications are needed to meet transmission requirements, increasing the breakwater height is more effective than increasing the crest width. This pattern is independent of the initial freeboard.

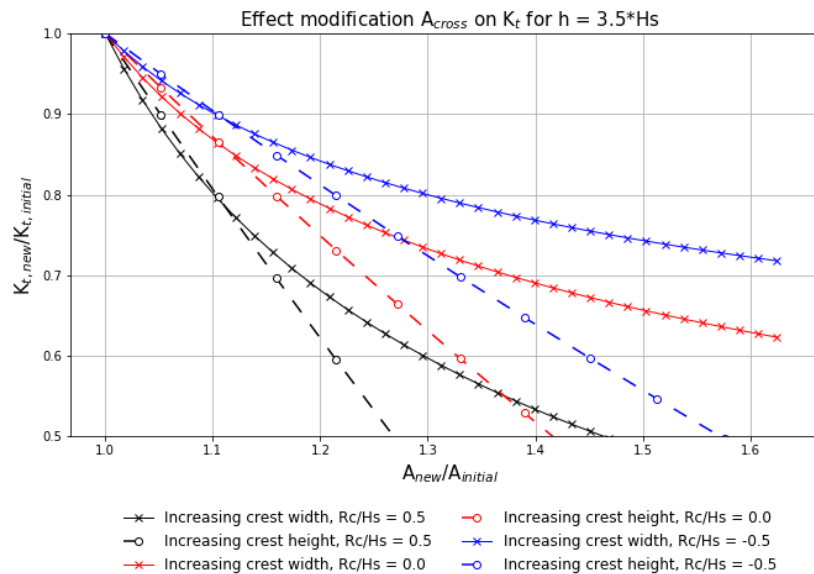


Figure 3.1: Effect of width and height modifications on wave transmission

The growth of the cross-sectional area highly depends on the water depth near the structure. Initially, the water depth was set at $h = 3.5 \cdot H_s$. Varying the water depth at the toe shows that the effect of the water depth on crest modifications is rather small (figure 3.2). In very shallow water ($h = 2 \cdot H_s$), increasing the crest width is slightly more effective than increasing the crest height. However, the obtained differences are negligible. Height modifications are always more effective for a breakwater situated in relatively deep water ($h = 5 \cdot H_s$).

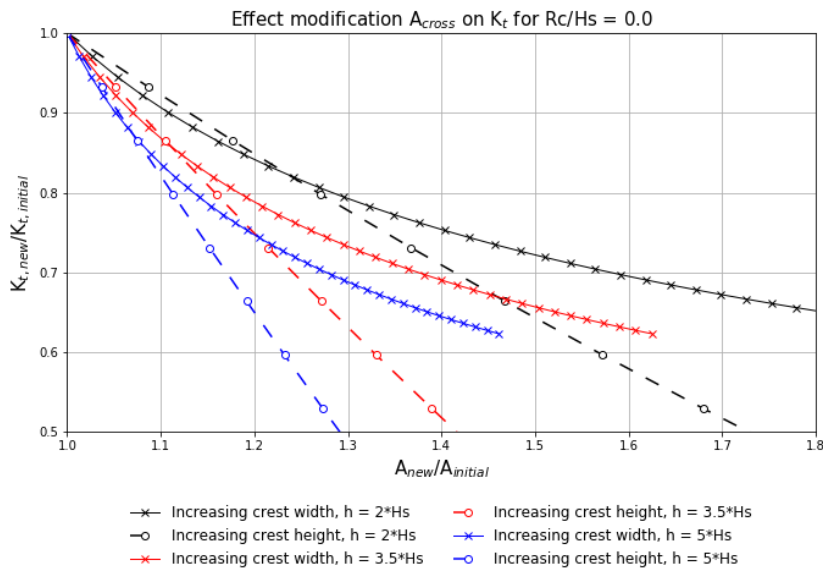


Figure 3.2: Effectiveness width and height modifications on wave transmission with varying depth

A larger initial crest width than the minimum of $b/H_s = 1.0$ shows that increasing the crest level is always more effective than increasing the crest width (figure 3.3).

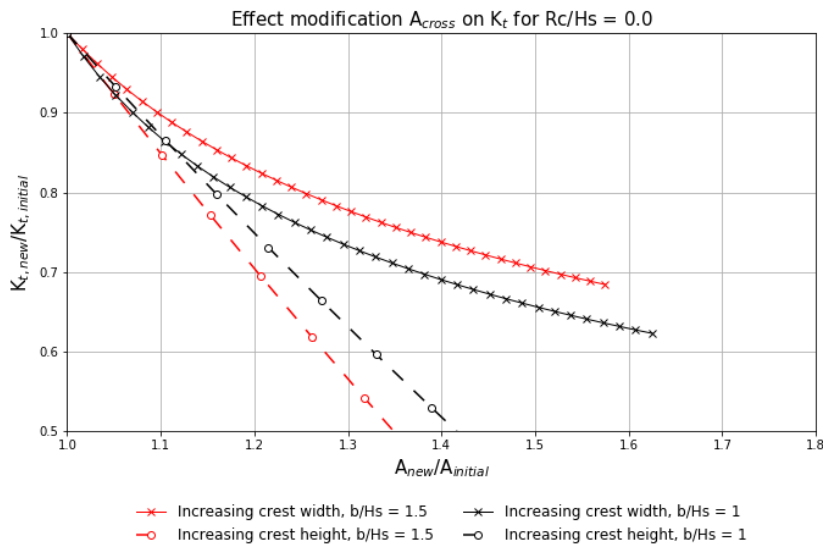


Figure 3.3: Effectiveness width and height modifications on wave transmission with varying crest width

To conclude, increasing the crest height is most effective to reduce the wave transmission. Therefore, small crested structures are preferred above wide crested structures.

3.2. Overtopping discharge

Just like the wave transmission, the effect of crest height and crest width modifications on the overtopping discharge is assessed. Standard overtopping formulas for rubble mound breakwaters are used (appendix A.4.3). However, implementing the roughness coefficient for a concrete armour unit gives an adequate estimation of the overtopping discharge of that specific concrete armour unit [12]. The results are shown in figure 3.4. Again, the X-axis represents the ratio between the cross-sectional area after crest modification and the cross-sectional area of the reference structure. The Y-axis represents the ratio between the overtopping discharge after crest modifications and the overtopping discharge of the reference structure. The initial crest height appears to be important. For $R_c/H_s = 0.1$, increasing the crest width is more effective than increasing the crest height. The opposite holds for $R_c/H_s = 0.5$. The transition is at $R_c/H_s = 0.25$.

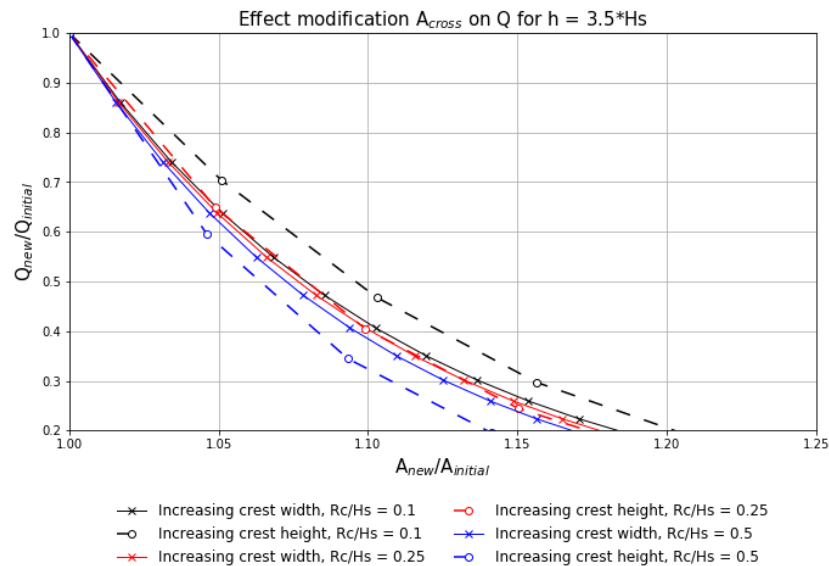


Figure 3.4: Effectiveness width and height modifications on overtopping

Changing the initial crest width from $b/H_s = 1.0$ to $b/H_s = 1.5$ does not affect the previously found overtopping pattern.

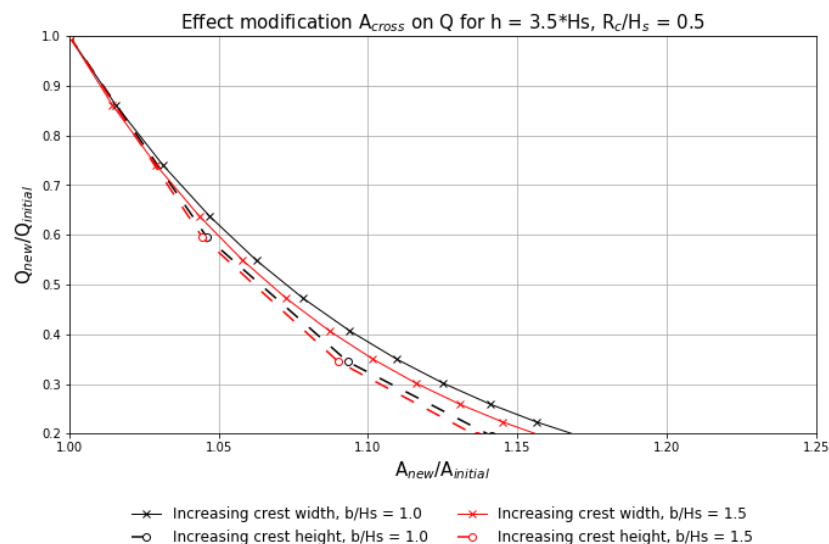


Figure 3.5: Effectiveness width and height modifications on overtopping with varying initial crest width

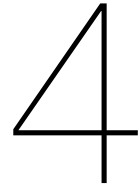
Based on overtopping requirements, it can be concluded that the most effective measure to meet overtopping requirements depends on the relative freeboard of the reference situation. Widening the crest is more effective for $R_c/H_s < 0.25$ whereas increasing the crest height is more effective for $R_c/H_s > 0.25$.

3.3. Construction method

The construction method is important to consider during breakwater design since it may influence the crest width. Both rolling and floating equipment can be used for construction. The choice depends on the breakwater location. Construction with land-based equipment is preferred if quarries are nearby. During construction, land-based equipment drives over the core to the dumping place. Consequently, at least a 7m wide core for two-lane traffic and a 4m wide core for one-lane traffic is required to drive with trucks. Moreover, the core level at the crest must be higher than the high water level to guarantee the safety of equipment and personnel. This is usually not a problem for regular breakwaters. For low crested breakwaters, the core width above high water is usually limited. Therefore, floating equipment is often required for construction [9]. There might be exceptions where land-based equipment is preferred above floating equipment.

3.4. Conclusion

Regarding the wave transmission, small crested structures are preferred. Regarding the overtopping discharge, a small crested structure is preferred for $R_c/H_s > 0.25$. Wide crested structures are preferred for $R_c/H_s < 0.25$. However, overtopping requirements are usually not too strict for low crested breakwaters. As a result, the overtopping requirements are probably not normative for low crested breakwaters. This makes it still reasonable to strive for a small crested structure. The construction method does usually not require a minimum crest width. Therefore, the target crest width is set at the smallest possible crest width of $1 \cdot H_s$ (paragraph 2.1.1). Since H_s varies in the test series, the design significant wave height $H_{s,d}$ is implemented as target crest width. The design significant wave height is based on the design stability number of 2.5. The phrase 'best hydraulic performance with respect to the economically most feasible breakwater dimensions' in the main research question can be defined as 'the structure with a crest width as close as possible to the minimum width of $1 \cdot H_{s,d}$ '.



Physical model setup

4.1. Test conditions

The flume set-up is a very important part of the physical model because it determines the loading behaviour on the structure. The test conditions are specified before designing the flume set-up. The standard XblocPlus model units of BAM are used as a starting point for both the flume set-up and the breakwater composition. The D_n value of the model units is 2.91cm.

4.1.1. Wave height

The density of the model units (2360 kg/m³) combined with the design stability number of 2.5 (paragraph 2.1) and the density of fresh water gives the design wave height ($H_{s,d}$) of 9.9cm. The wave generation is based on a standard Jonswap spectrum with $\gamma = 3.3$, $\sigma_a = 0.07$, $\sigma_b = 0.09$, $\alpha = 0.0081$ [15].

4.1.2. Wave steepness

Initially, the physical model tests are performed with 2% wave steepness ($s_{0,p}$). This steepness value is chosen based on several arguments. According to Muttray [21], $s_{0,p} = 2\%$ causes more intense failure compared to waves with $s_{0,p} = 4\%$ (paragraph 2.5.1). In addition, it aligns with the wave theory (paragraph A.3) about the lift and drag force. Both forces are larger for waves with $s_{0,p} = 2\%$ due to their dependency on the run-up velocity. Using $s_{0,p} = 2\%$ is not exactly in line with the normative steepness Grigoris [13] found ($s_{0,p} = 4\%$) for XblocPlus blocks on the top row without back support (section 2.4.2). Probably, the low stability of the blocks and the absence of interlocking resulted in slightly different results than expected. However, wave steepness $s_{0,p} = 2\%$ appeared to be normative for his best performing set-up.

4.1.3. Relative freeboard

The stability of interlocking armour units on the crest also depends on the relative freeboard (paragraph 2.4). The final solution found by Grigoris [13] was least stable for $R_c/H_{s,d} = 0.0$. Consequently, it seems straightforward to test crest configurations with original XblocPlus crest armour with zero relative freeboard.

According to Muttray [21], interlocking armour units are least stable at the crest ($N_s = 3.1$). This minimum stability was obtained for a relative freeboard of $R_c/H_{s,d} = 0.0$. At $R_c/H_{s,d} = 0.4$, the stability value of both the front and rear slope reached a minimum value of $N_s = 3.1$. The stability number of the crest also has a value of 3.1 for $R_c/H_{s,d} = 0.4$. This suggests that the transitions from the crest to the slopes are least stable for freeboard $R_c/H_{s,d} = 0.4$. In contrast to Grigoris' results, it is not directly clear whether $R_c/H_{s,d} = 0.0$ or $R_c/H_{s,d} = 0.4$ is normative. For the crest configurations with modified XblocPlus blocks will be assessed which freeboard is normative. $R_c/H_{s,d} = 0.5$ instead of $R_c/H_{s,d} = 0.4$ will be used because it corresponds better to Grigoris' results.

4.2. Test procedure

Each test session of the physical model tests is subdivided in runs. The duration of the runs is specified in such a way that each run contains approximately 1000 waves. This number of waves is required to obtain a good representation of the Jonswap spectrum. The design wave height $H_{s,d}$ specified in paragraph 4.1.1 is set at 100%. A test session is started with a run having a significant wave height equal to 60% of $H_{s,d}$. This

is the minimum wave height to satisfy the dynamic similarity conditions (paragraph 2.7.2). The increments in wave height are 20% for $H_s < H_{s,d}$. For $H_s > H_{s,d}$ the significant wave height increases 10% per run. The test sessions are stopped after:

- failure of more than 2 crest blocks. The test procedure is continued after failure of the first block with the aim to diminish the effect of one bad placed block. In addition, knowledge about the residual strength of the blocks can be obtained.
- succession of the run with $H_s = 140\% \cdot H_{s,d}$. Succeeding this test session implies that the crest stability is equal to the blocks the slopes.

4.3. Flume configuration

4.3.1. Wave flume BAM

The wave flume of BAM in Utrecht will be used to perform physical model tests (figure 4.1). The flume has a length of 25m, a width of 0.6m and its height is 1m. The maximum allowable water depth 0.7m. In length direction, the flume is subdivided in 10 sections of 2.5m each. Observing wave attack on structures is easy since the flume walls are made of glass. The flume is equipped with an Edinburgh Designs piston wave generator. This generator makes it possible to generate regular and irregular waves. In addition, the generator damps the reflected waves. Wave gauges are used to measure the generated waves.



Figure 4.1: Wave flume BAM[13]

4.3.2. Water level

4.3.2.1. Depth requirements

The general dimensions of the breakwater depend on depth requirements. A minimum water depth is determined for the deep-water section near the wave generator [30]. In addition, a minimum water depth at the breakwater toe is set to prevent heavy wave breaking on the foreshore [15]. The largest significant wave height in the test program ($H_{s,max} = 140\% \cdot H_{s,d}$) is used to determine both minimum water depths. An overview of those values is presented in table 4.1.

Parameter	Definition	Value (cm)
Significant wave height	$H_{s,d}$	9.9
Deep water depth (h_0)	$3 \cdot H_{s,max}$	41.6
Water depth at toe ($h_{toe,min}$)	$\frac{H_{s,max}}{0.45}$	30.8

Table 4.1: Hydrodynamic requirements

4.3.3. Foreshore

The foreshore is important for the breakwater stability since it determines the wave height development over the decreasing water depth before the structure (appendix A.3.5). Both shoaling and wave breaking occur. In general, dissipation due to wave breaking is more dominant than shoaling. Consequently, applying no foreshore represents the most conservative condition to test the stability of crest configurations. However, it is not very realistic. Most tests with Xbloc and XblocPlus were performed with a seabed slope of 1:30. An important argument for the application of this slope is that it is slightly steeper and therefore slightly more conservative than frequently found foreshores. For this research is chosen to apply a 1:30 foreshore to make easy comparison with other tests possible.

In the flume, foreshore panels must be placed in the sections that are each 2.5m long. To meet the requirements for the minimum water depth at the toe and the maximum water depth in the flume, the length of the foreshore is restricted to 7.5m. The minimum spacing between the wave generator and the foreshore is $(3-5)h_0$ to reduce the effect of errors near the wave paddle (table 4.2) [30].

4.3.4. Measuring equipment

Wave gauges are used to measure the surface elevation of the water in the flume. Making use of wave gauges is necessary to obtain the incoming wave height. The incoming and reflected waves are separated by the reflection analysis method of Mansard & Funke. One set of wave gauges is placed just before the breakwater toe. Also, a set of wave gauges is placed in the deep-water section relatively close to the wave generator. Each set has 3 wave gauges to measure the surface elevation properly. The required distance between the gauges depends on wavelength L_p . Requirements for the wave gauges are presented in equations 4.1a to 4.1d [20]. L_p for the deep-water section is 3.7m and it shortens to 3m in the shallow section.

$$L_p/6 < X_{1,3} < L_p/3 \quad (4.1a) \quad X_{1,3} \neq L_p/5 \quad (4.1b) \quad X_{1,3} \neq 3L_p/10 \quad (4.1c) \quad X_{1,2} = L_p/10 \quad (4.1d)$$

The same gauge spacing is used for both sets of gauges. The distance between the first and second gauge is 0.3m. The distance between the first and the third gauge is 0.7m. All gauges measure the surface elevation at a frequency of 32 Hz. The wave gauges are placed at $0.4 \cdot L_p$ from the structure to improve the assessment of the incident waves near the breakwater toe (table 4.2).

Parameter	Definition	Value (m)
Wave gauge distance from structure	$0.4 \cdot L_p$	1.2
Minimum foreshore distance from wave paddle	$(3-5) h_0$	2.1 - 3.5

Table 4.2: Other requirements

Three cameras are used to film the crest to make failure assessment easier. One camera faces the front slope, one faces the rear slope and one camera is placed next to the flume to observe the structure from the side. The cameras at the front and at the side film at a rate of 60 frames per second. The camera that faces the rear slope films at a rate of 25 frames per second due to camera limitations.

4.3.5. Cross-section flume

Figure 4.2 shows an overview of the flume set-up. All dimensions are given in metres.

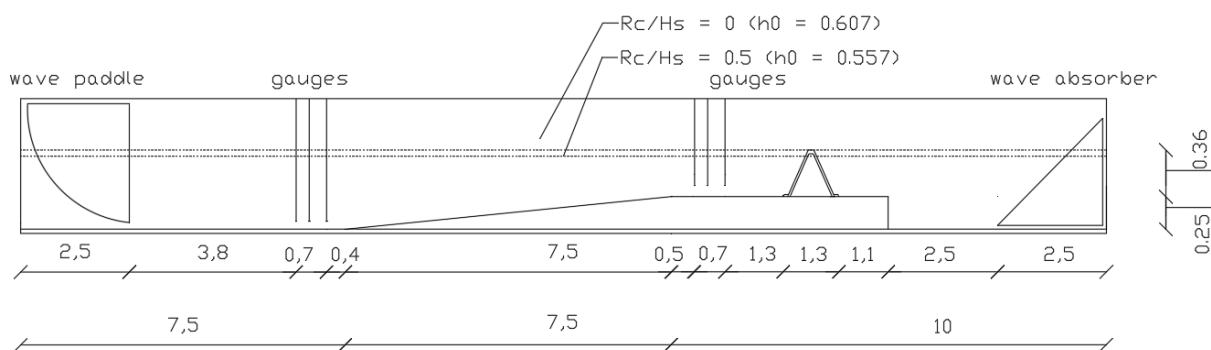


Figure 4.2: Flume configuration

4.4. Breakwater composition

4.4.1. Armour layer

The composition of the breakwater model is based on a fictitious prototype with armour units of 3 m^3 ($D_n=1.44\text{m}$) and a standard 3H:4V slope. The geometric scale factor between the XblocPlus prototype units and the model units is 1:49. The Reynolds number in the armour layer should be larger than 30.000 to satisfy the criterion for dynamic similarity (paragraph 2.7.2). For the design wave height $H_{s,d}$, a value

of 28.670 is obtained. Although the criterion is not satisfied for $H_{s,d}$, the scale effects are expected to be negligible because the Reynolds number in the armour layer is close to the specified criterion. In addition, the wave height that determines the stability of the crest is expected to be larger than the design wave height. Consequently, Reynolds numbers are expected that are even closer to 30.000.

4.4.2. Underlayer

The underlayer grading of the model is based on the underlayer of the prototype given in the XblocPlus guidelines [11]. The $D_{n50,underlayer}$ used in the prototype is 0.65cm. Scaling geometrically by factor 1:49, gives a $D_{n50,underlayer}$ in the model of 1.3 cm.

4.4.3. Core

Quarry run is typically used as core material for breakwaters. Defining a D_{n50} is hard since quarry run is residual rock material of the quarry. The size of quarry run differs in size per quarry and per blast. This makes scaling of core material not unambiguous. However, expression 4.2 can be applied to find the D_{n50} of the core [9].

$$\frac{D_{n50,underlayer}}{D_{n50,core}} = 2 - 3 \quad (4.2)$$

Application of this guideline results in a 15-300 kg core grading for the prototype ($D_{n50} = 0.31\text{m}$). Geometrical scaling of the prototype core material results in very fine model core material with a D_{n50} between 4 and 6mm. With such a fine grading the flow in the core will probably be laminar. To obtain a better representation of the prototype in the model, Burcharth's permeability scaling method is applied (paragraph 2.7.4) [26].

The computed D_{n50} of the core grading with Burcharth's permeability scaling method depends on the structure geometry itself. Consequently, the D_{n50} for a structure with the target crest width ($B/H_{s,d} = 1.0$) differs from the D_{n50} found for the reference situation (chapter 6). The computed D_{n50} values by Burcharth's method are presented in table 4.3. The D_{n50} for a structure with $B/H_{s,d} = 1.1$ is also presented in the table. The D_{n50} values for small crested structures indicate that the D_{n50} is sensitive to small crest width variations if the crest width is close to the target crest width. More details about the computations are explained in appendix B.

Structure	D_{n50} (mm)	Re	Grading (mm)
Small crested structure ($B/H_{s,d} = 1.0$)	8.1	331	8-11
Small crested structure ($B/H_{s,d} = 1.1$)	8.8	377	8-11
Reference - wide crest ($B/H_{s,d} = 2.7$)	10.6	439	8-11

Table 4.3: Core grading

All D_{n50} values are between 8 and 11mm (values of a common core grading). For this grading, the flow remains turbulent because the Reynolds number is larger than 300 2.7.4. This makes the 8-11mm grading a suitable core grading. In addition, Grigoris [13] did crest stability tests with a core grading of 8-11mm. Consequently, all tests in this study are performed with an 8-11mm grading.

4.4.4. Toe structure

The applied toe structure depends on the subsoil below the breakwater. On a rocky seabed, the armour units are directly placed on the seabed. On a sandy seabed, a foundation layer made of rock is placed between the seabed and the armour units (figure 4.3). Both induce height deviations of the armour blocks on the seabed. These height deviations affect the height of crest blocks. The effect of those irregularities must be incorporated in a flume where a wooden plank of the foreshore functions as seabed. Therefore, a foundation layer is placed below the bottom armour row like it is done on a sandy seabed.

The W_{50} of the foundation layer below the bottom XblocPlus ($W_{50,foundation}$) row is approximately equal to the weight of the armour layer divided by 30. Since the W_{50} of the underlayer at the slope ($W_{50,underlayer}$) is between 1/8 and 1/20 of armour unit's weight, the foundation layer below the toe is in general slightly smaller than the underlayer at the slope. However, in some cases, the difference between $W_{50,foundation}$ and $W_{50,underlayer}$ is relatively small. That results in the same grading for the underlayer and the foundation

layer. In the model, the foundation layer has the same grading as the underlayer.

The grading of the rock toe (figure 4.3) is not very important for this research. The only requirement is that the toe is stable enough to prevent settlements in the armour layer. Therefore, 18cm long gabions filled with rock are placed next to the bottom XblocPlus row to prevent toe failure.

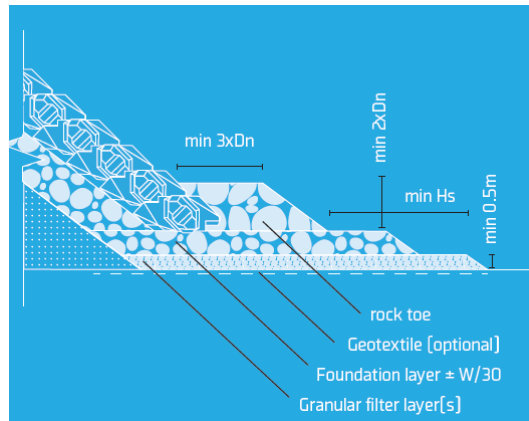


Figure 4.3: Standard toe structure 1[11])

4.4.5. Cross-section

The breakwater cross-section, with its crest width equal to the target crest width of $1 \cdot H_{s,d}$ (9.9cm), is presented in figure 4.4. An overview of the applied rock gradings is given in table 4.4. All dimensions are given in centimetres and the slope of the armour layer is 3V:4H.

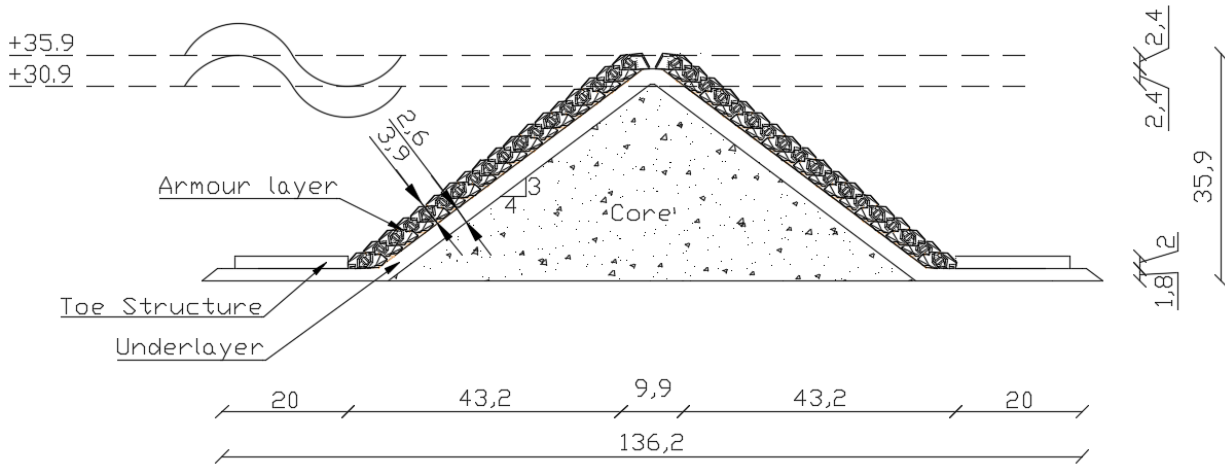


Figure 4.4: Breakwater cross-section block based

Parameter	Prototype		Scale model	
	Grading	$D_{n.50}$ (m)	Grading (mm)	$D_{n.50}$ (cm)
Armour	-	1.44	-	2.91
Underlayer & foundation layer	300-1000 kg	0.65	11-16	1.3
Core	15-300 kg	0.31	8-11	0.95

Table 4.4: Rock gradings in model structure

5

Test information

5.1. Modified crest blocks

The modified XblocPlus crest armour is handmade. Details about the construction method are explained in appendix D. Acrystal Aqua is the construction material that is used for the crest blocks. The density of the construction blocks is lower than the density of the XblocPlus test blocks. The density of the XblocPlus is 2360 kg/m^3 . The density of the modified crest blocks is close to 2200 kg/m^3 . Detailed density information per block is presented in appendix E.

5.2. Definitions

5.2.1. Failure

Failure is defined as the situation where at least one wing of a crest block lost contact with the horizontal part of the armour blocks beneath. Two failure examples for a modified XblocPlus block are given in figures 5.1 and 5.2.



Figure 5.1: Example 1 of failure

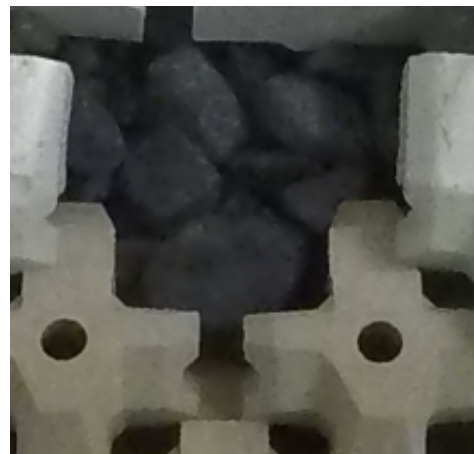


Figure 5.2: Example 2 of failure

5.2.2. Displacement

Displacements of crest blocks are important to assess because the interlocking capacity of displaced blocks is reduced. In addition, crest blocks might damage other blocks due to excessive displacement. The impact of a displacement depends on the degree of displacement. Three categories of displacement were defined to assess the degree of displacement. The displacement categories are based on the red line in figure 5.3. This line represents the length of the horizontal contact surface between the crest blocks and the XblocPlus beneath the crest blocks. Its length is $0.36 \cdot D_n$, which is 1cm for the test blocks. The displacement categories are presented in table 5.1.

Overlay photos are used to measure the degree of displacement. By using overlay photos, displacements

of 1mm are visible but hard to measure. Therefore, displacement category 1 can better be described by ' $< 0.09 \cdot D_n$ ' with exclusion of the smallest displacements.

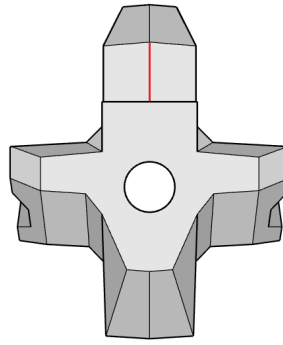


Figure 5.3: Displacement definition

Category	Displacement (D_n)	Displacement (mm)	Percentage of support length
1	$> 0.036 \cdot D_n$	> 1	10
2	$> 0.09 \cdot D_n$	> 2.5	25
3	$> 0.18 \cdot D_n$	> 5	50

Table 5.1: Displacement categories

5.2.3. Rocking

BAM defined rocking as a repeated rotational movement occurring at more than 2% of the waves [7] (>20 times in a wave series of 1000 waves). During the up-rush the block makes a rotational movement and it returns to its initial position during down-rush (figure 5.4). The rotational movement is called repeated rotational movement instead of rocking if it is observed less than 20 times in a wave series of 1000 waves.



Figure 5.4: Example of a rotational movement

5.2.4. Stability number

In the theoretical framework is already mentioned that the design stability number ($N_{s,d}$) for XblocPlus equals 2.5. In a design process, a safety margin of 20% is used to keep up with uncertainties. This means that the structure should remain stable till the overload stability value of 3.0 ($N_{s,overload}$). Sometimes the target stability is used to refer to the overload condition. The critical stability number ($N_{s,c}$) is based on the test run with the highest significant wave height without failure of a single crest block.

5.3. Wall influence

The crest blocks next to the wall are not taken out of the assessment. However, there is a possibility that the outer blocks have experienced some wall influence. The wave loading on the crest blocks might be slightly different due to influence of the wall. In one test series, the 2 leftmost blocks were influenced by the wall. Taking 2 blocks next to each wall out of the assessment reduces the number of crest blocks by 6 blocks per slope. Given that small number of crest blocks, all crest blocks are taken into account because

it is expected to give a better picture of the crest performance. It is considered that it is better to mention the influence of the wall mentioned if it appeared.

5.4. Test program

An overview of all executed test series is presented in table 5.2. The test results of the preliminary research phase are presented in chapters 6 & 7. The results of the detailed research phase are presented in chapter 11.

Phase	Test nr.	Crest configuration	$R_s/H_{s,d}$	$s_{0,p}$ (-)
Preliminary	1.1.1	Reference non-modified XblocPlus	0.0	0.02
Preliminary	1.1.2	Small crest block	0.0	0.02
Preliminary	1.2.1	starting block	0.0	0.02
Preliminary	1.2.2	starting block	0.5	0.02
Preliminary	1.3.1	Permeable block	0.0	0.02
Preliminary	1.4.1	Extended bottom block	0.0	0.02
Preliminary	1.5.1	Interlocking block attempt 1	0.0	0.02
Preliminary	1.5.2	Interlocking block attempt 2	0.0	0.02
Preliminary	1.6.1	Reversed interlocking block	0.0	0.02
Detailed	2.1.1.	Optimised permeable block	0.0	0.02
Detailed	2.1.2.	Optimised permeable block	0.0	0.04
Detailed	2.1.3.	Optimised permeable block	0.5	0.02
Detailed	2.1.4.	Optimised permeable block	0.5	0.04
Detailed	2.1.5.	Optimised permeable block - repetition	0.0	0.02
Detailed	2.1.6.	Optimised permeable block - repetition	0.0	0.04
Detailed	2.2.1.	Berm bloc Afsluitdijk	0.0	0.04
Detailed	2.3.1.	Initial permeable block - attempt 1	0.0	0.02
Detailed	2.3.2.	Initial permeable block - attempt 2	0.0	0.02
Detailed	2.3.3.	Initial permeable block - attempt 3	0.0	0.02
Detailed	2.3.4.	Initial permeable block	0.0	0.04

Table 5.2: Overview test series

5.5. Test conditions

A design significant wave height of $H_{s,d} = 9.9\text{cm}$ is determined in the model set-up chapter. This value is based on $\rho_{block} = 2360 \text{ kg/m}^3$ and $D_{n,ref} = 2.91\text{cm}$. The nominal diameter of the original XblocPlus blocks ($D_{n,ref} = 2.91\text{cm}$) is also used for the modified XblocPlus crest armour as input to determine $H_{s,d}$. The reason is that the stability of the modified XblocPlus crest blocks should be related to the stability of the original XblocPlus armour on the slopes. Implementing the D_n value of XblocPlus yields equal $H_{s,d}$ values for both the crest blocks and the slope blocks. However, a prerequisite is that both blocks should have equal density. This is not the case for the modified XblocPlus test blocks. The mean block density of the modified XblocPlus crest armour is 2200 kg/m^3 instead of 2360 kg/m^3 for the original XblocPlus. Consequently, the relative density becomes 1.2 instead of 1.36. $H_{s,d}$ of 8.7cm is obtained after implementing a mean block density of 2200 kg/m^3 and $D_{n,ref} = 2.91\text{cm}$.

A test series consists of several test runs. The wave conditions per test run depend on the density of the crest blocks. H_s and T_p values for a crest armoured with original XblocPlus blocks are presented in table 5.3. The 100% condition is based on $H_{s,d}$. The waved period depends on the wave height via the wave steepness. Each test run contains approximately 1000 waves.

Parameter	60%	80%	100%	110%	120%	130%	140%
H_s (cm)	5.9	7.9	9.9	10.9	11.9	12.9	13.9
T_p (s)	1.38	1.59	1.78	1.87	1.95	2.03	2.11

Table 5.3: Wave conditions for XblocPlus crest armour, $s_{0,p} = 2\%$

The test conditions for crest configurations with modified XblocPlus crest blocks are different due to their lower block density compared to the XblocPlus test blocks. Table 5.4 shows the theoretical wave parameters for $s_{0,p} = 2\%$. In the detailed research phase, several tests are performed with waves of steepness $s_{0,p} = 4\%$. The test conditions for those tests are shown in table 5.5. A 150% test run is added to both tables because it is performed in several test series in the detailed research phase.

Parameter	60%	80%	100%	110%	120%	130%	140%	150%
H_s (cm)	5.2	7.0	8.7	9.6	10.5	11.3	12.2	13.1
T_p (s)	1.30	1.50	1.67	1.75	1.83	1.91	1.98	2.05

Table 5.4: Wave conditions for modified XblocPlus crest armour, $s_{0,p} = 2\%$

Parameter	60%	80%	100%	110%	120%	130%	140%	150%
H_s (cm)	5.2	7.0	8.7	9.6	10.5	11.3	12.2	13.1
T_p (s)	0.92	1.06	1.18	1.24	1.30	1.35	1.40	1.45

Table 5.5: Wave conditions for modified XblocPlus crest armour, $s_{0,p} = 4\%$

5.6. Test procedure

The test procedure is explained in 8 steps:

1. In the wave flume, the structure is constructed accurately by making use of a drawing on both walls of the glass flume. A spatula is used to minimise deviations in the core and under layer.
2. The flume is filled with water.
3. Photos of the initial situation were taken with the cameras facing the front slope, rear slope and side of the structure. The photos of the front camera are shown in Appendix G.
4. The wave gauges were calibrated.
5. The test is started. Every test run is filmed from start to end.
6. New photos were taken after each test run. Test photos of the camera that faces the front slope are given in appendix G.
7. The incoming significant wave height is generated by performing reflection analysis (paragraph 4.3.4). The test data of every test are given in appendix F.
8. The test series is stopped if 3 or more crest blocks failed. The next run is started if less than 3 crest blocks failed after the test run. Step 4 to 7 are repeated.

XblocPlus crest armour

This chapter forms part 1 of the preliminary research phase. The central question is the first sub question of this research (paragraph 1.5). This chapter contains the test results of the reference situation and the test results of an alternative based on the reference situation. Crest configurations with modified XblocPlus blocks are treated in chapter 7.

6.1. Reference situation

Grigoris proposed to support the top XblocPlus row with underlayer rock and a stiff element to prevent erosion of the rock (paragraph 2.6.1). Figure 6.1 shows an overview of his set-up. The reference situation is obtained by extending Grigoris' structure with a rear slope (figure 6.2). The dimensions of the stiff element are 48 x 2 x 15 cm and it weighs 3 kg. The space between the stiff element and the armour blocks on the top rows is approximately 2 cm. Underlayer rock is applied at both sides of the stiff element to fill that space. The crest width of the structure extended with a rear slope becomes 26.6 cm ($2.7 \cdot H_{s,d}$). Different to Grigoris' structure, the 16-22mm rock placed at the crest and next to the walls is not glued. A cross-section of the reference situation is shown in figure 6.3.



Figure 6.1: Crest set-up proposed by Grigoris [13]



Figure 6.2: Crest-set up Grigoris with rear slope

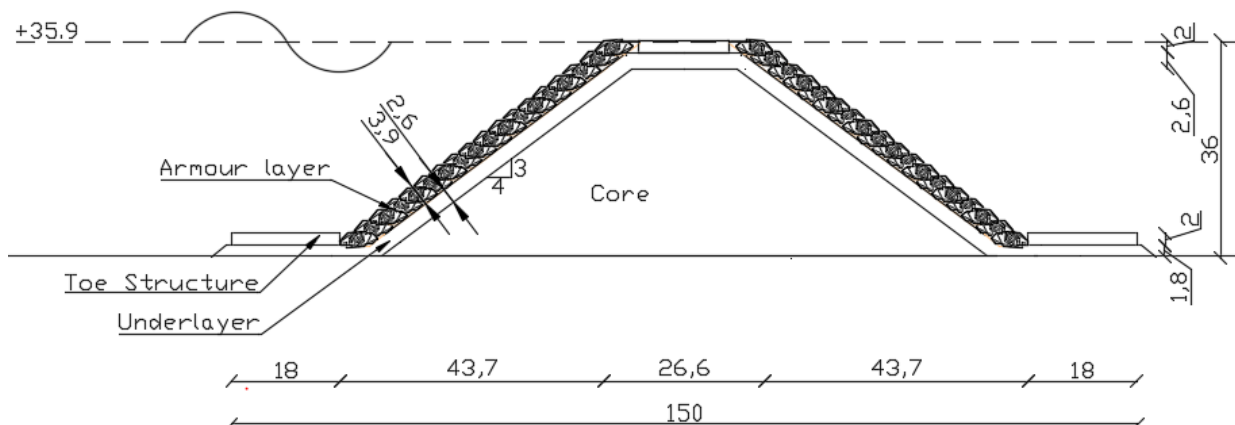


Figure 6.3: Breakwater cross-section non block based

6.2. Stability reference situation

Figure 6.4 shows the test results of the reference situation. The percentage on the Y-axis shows the percentage of failed/displaced crest blocks related to the total number of crest blocks on the front slope. The X-axis represents the test runs expressed by the stability number. The structure remained stable until $N_{s,c} = 2.4$ whereas Grigoris found that the structure remained stable up to $N_{s,c}$ equal to 2.5. Displacements of category 1 started approximately at $N_s = 2.0$. Erosion of filling material also started at $N_s = 2$. None of the crest armour blocks at the rear slope failed. In fact, no displacements were observed at the rear slope (figure 6.5). The crest blocks on the rear slope suffer less as a result of the wave load.

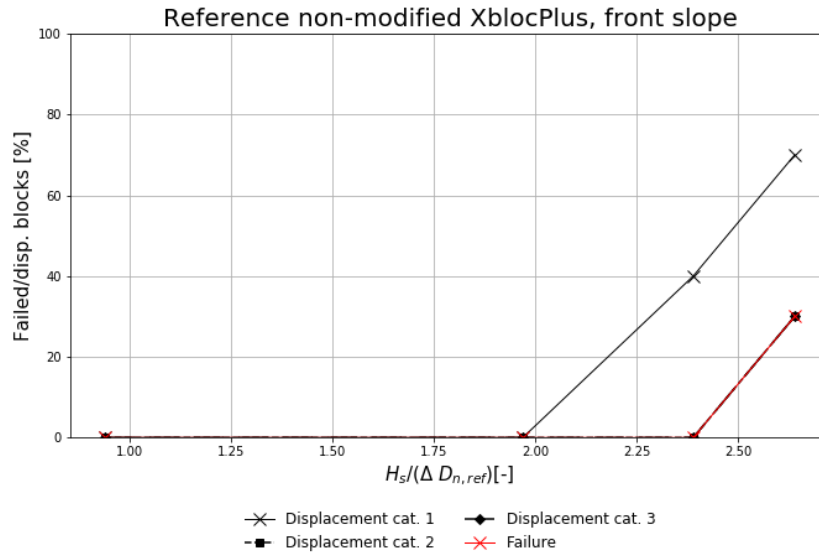


Figure 6.4: Failure progression front slope reference situation

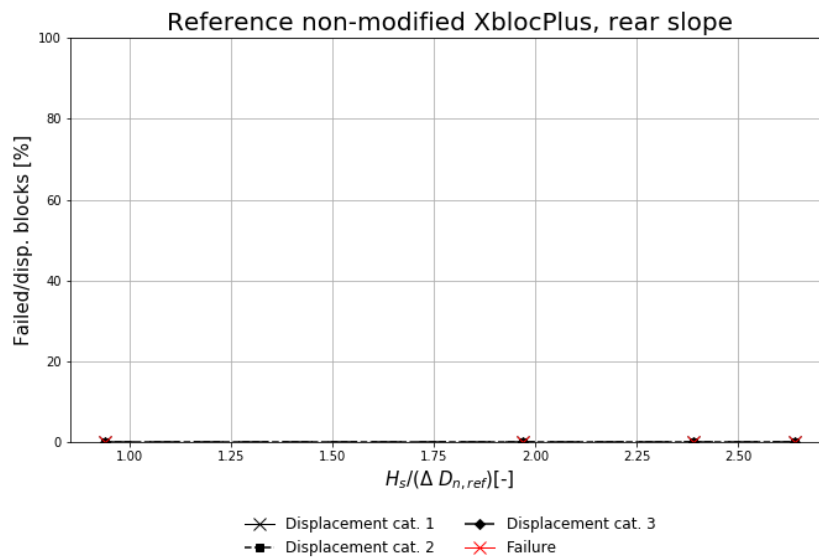


Figure 6.5: Failure progression rear slope reference situation

6.3. Failure mode

Grigoris found a critical stability number (stability number based on the test run with the highest significant wave height without failure of a single crest block) of $N_{s,c} = 2.5$. This value is similar to the critical stability number of $N_{s,c} = 2.4$ found for the reference structure. However, the failure mode of the armour blocks differed. In the reference situation, 3 armour units failed on the top row of the front slope. One armour unit directly rolled over, whereas the other 2 mainly lifted up and displaced in a way that caused failure. In contrast, Grigoris attributed the failure due to the uplift of the stiff element. Due to the uplift, the element

also moved slightly backwards allowing the underlayer material to spread. The armour blocks on the front slope excessively displaced with failure as a result.

6.4. Alternative to reference situation

As mentioned before, Grigoris [13] investigated many possibilities to reinforce the top armour row. However, none of them were able to reach the overload stability for $R_c/H_{s,d} = 0$ and $s_{0,p} = 2\%$ [13]. Based on Grigoris' effort to stabilise the top row without block shape modifications, no further attention is paid to the stability of the top armour row on the front slope. Instead, the width of the stiff element is reduced to assess the effect of the wave load on the top armour row of the rear slope.

A new stiff element is constructed that has half the width of the stiff element in the reference situation. The dimensions of the block are $48 \times 2 \times 7.5$ cm and it weighs 1.5 kg. The crest width reduced by 29% to 19 cm ($1.9 \cdot H_{s,d}$). Figure 6.6 shows the crest configuration with a small stiff element. The stiff element is packed in plastic foil to prevent dust formation near the structure. It does not affect the top row stability. The cross-section of the structure with small stiff element is presented in figure 6.7.



Figure 6.6: Small stiff element

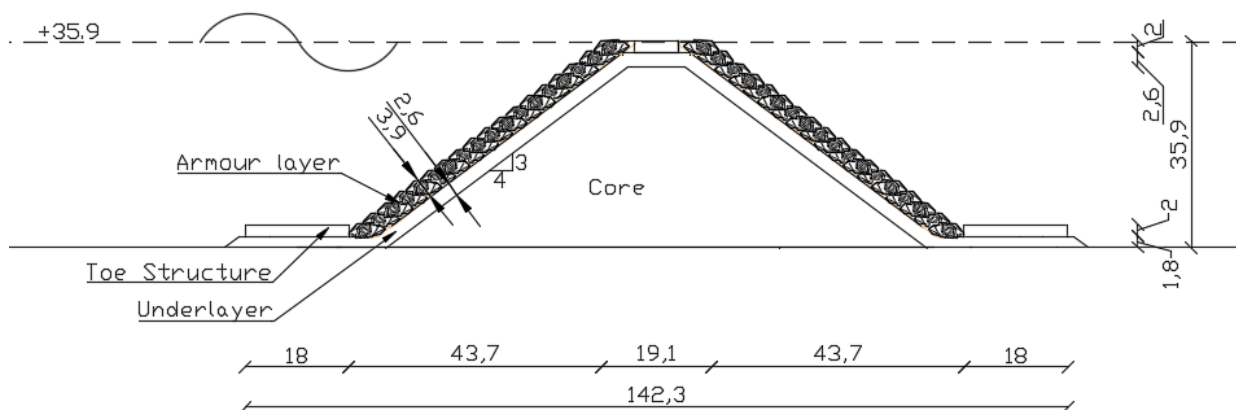


Figure 6.7: Breakwater cross-section small stiff element

6.5. Results alternative

Figure 6.8 presents the failure and displacement development over time. The critical stability number $N_{s,c} = 2.6$ is obtained. A strong increase in failure and displacements of the crest blocks on the front slope is visible at $N_s = 3.1$. This is caused by the displacement of the stiff element. The stiff element mainly displaced at the right part of the structure. The displaced stiff element resulted in filling material erosion failure of armour blocks mainly on the right part of the test setup. Without displacement of the stiff element, the number of failed armour blocks might be smaller. However, one crest block already failed before the displacement of the stiff element. This indicates that the displaced stiff element did not influence the critical stability of the crest. Just like the crest armour blocks on the rear slope of the reference structure, no armour units failed at the rear slope of the structure with the small crest block (figure 6.9). Only one block at the top row of the rear slope displaced.

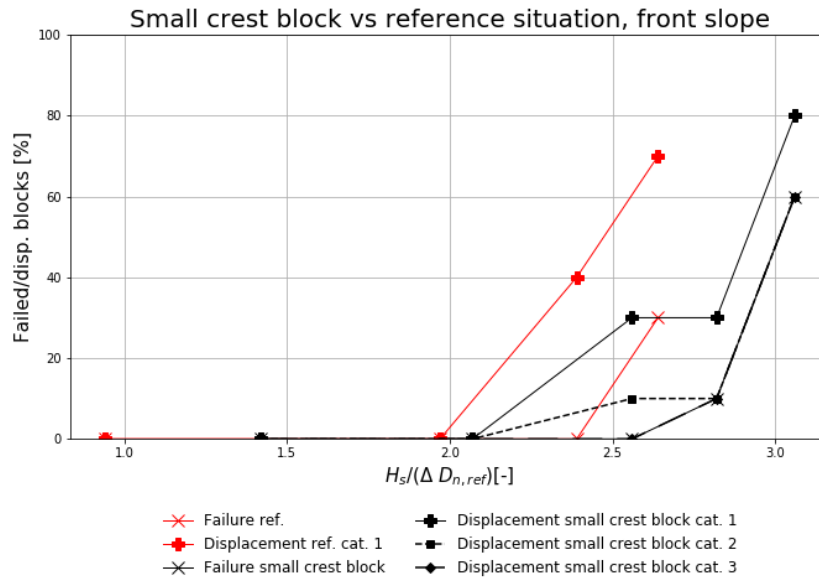


Figure 6.8: Failure development of front slope small stiff element

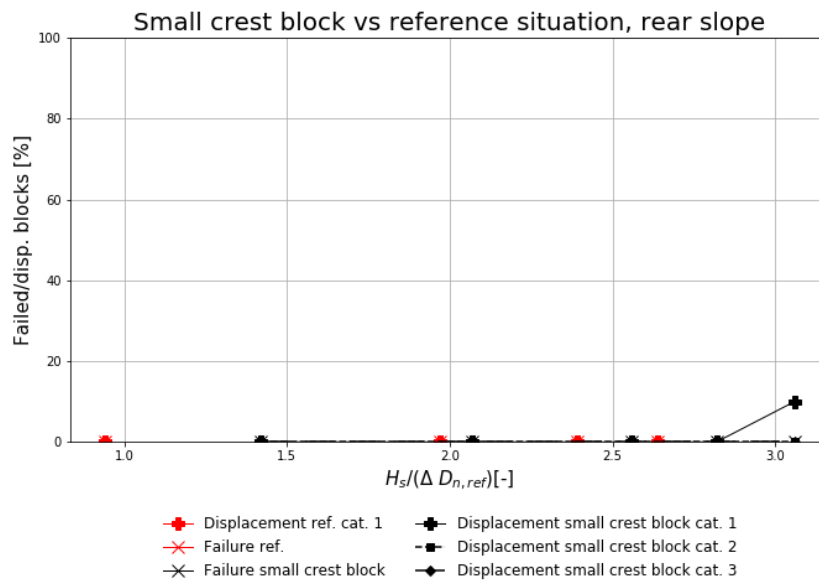


Figure 6.9: Failure development rear slope with small stiff element

6.6. Conclusion

After testing crest configurations with XblocPlus blocks placed on the top armour row, it can be concluded that the stability of the crest armour blocks on the front slope is insufficient at normative conditions $R_c/H_{s,d} = 0$ and $s_{0,p} = 2\%$. Failure of the front top row armour units cannot be avoided. This indicates that the weight of the crest blocks on the front slope is too small to withstand the wave load at the target stability. A combination of vertical and rotational instability results in failure. The armour units at the top row of the rear slope remain stable. Reducing the crest width hardly affects the stability of the blocks at the rear top row.

Modified XblocPlus crest armour

This chapter contains part 2 of the preliminary research phase. Crest configurations with modified XblocPlus armour blocks form the content of this chapter. The chapter starts with the design and the test results of the starting block. Afterwards, the designs and test results of alternatives to the starting block are presented.

7.1. Starting point

A low crested breakwater with original XblocPlus crest armour is insufficiently stable to meet the target stability. Therefore, the XblocPlus shape is modified in a way that its weight increases. Three targets are defined to design the modified blocks:

- The crest blocks must be placed back to back.
- The crest blocks must be designed in a way that the crest width is as close as possible to the target crest width of $1 \cdot H_{s,d}$
- The volume of the crest blocks should be at most twice the volume of original XblocPlus blocks ($V_{modified-block} < 2 V_{ref}$). Too large crest blocks destabilise the blocks on the second armour row.

Grigoris [13] already concluded that the stiff element and the rock fill have a positive impact on the XblocPlus stability on the top row. The rock caused a backwards shift of the rotation point of the XblocPlus. Therefore, compared to XblocPlus, the crest blocks with a modified block shape should at least have a backwards shifted rotation point (figure 7.2). However, it is not expected that this block meets the target stability since its additional mass compared to an original block is limited. Therefore, more mass is added to the original block to obtain the block used as a starting point (figure 7.3). The length of the starting block is extended by 1.7%. As a result, a crest width of $1 \cdot H_{s,d}$ is obtained with 2 back to back placed blocks.

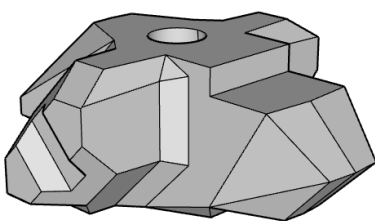


Figure 7.1: Normal XblocPlus

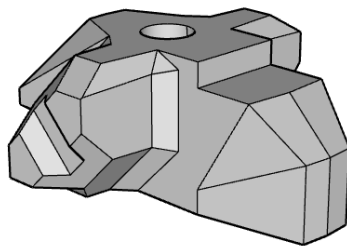


Figure 7.2: Shift rotation point only

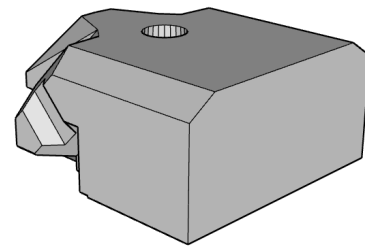


Figure 7.3: Starting block v1

7.1.1. Underlayer tolerances

Height deviations in the underlayer affect the position of armour units. Therefore, tolerances of the underlayer are important to consider. The crest blocks should have, similar to the original XblocPlus blocks, sufficient flexibility to fit them in the structure. Theoretically, insufficient flexibility of the crest blocks might lead to interference of neighbouring blocks. In practice, it obstructs the construction process due to the required replacement of crest blocks and underlayer rock. The tolerance criteria used by BAM are [6]:

- The underlayer tolerance around the design profile is $\pm 0.5 D_{n50}$.

- The underlayer shall not deviate more than $0.3 D_{n50}$ between 2 points within a distance of D_{n50} from each other.

Important to mention is that $0.5 D_{n50}$ of the underlayer is almost 30% of the crest block height.

7.1.1.1. Longshore underlayer deviations

In this section, the effect of underlayer irregularities is assessed for 2 neighbouring crest blocks with its nose facing in the same direction. The width of one crest block is 48mm and the D_{n50} and D_{50} of the underlayer rock are respectively 13mm and 15.5mm. Therefore, a crest block rests on approximately 3 to 4 underlayer stones. With a maximum deviation of $0.3 D_{n50}$ between 2 points with D_{n50} in-between spacing, the maximum underlayer level difference below one crest element is approximately $1 \cdot D_{n50}$. The interlocking capacity for tilted crest blocks is smaller than the interlocking capacity for horizontal positioned crest blocks. As a result, the stability of the crest blocks decreases.

A disadvantageous example is shown in figure 7.4. Here, an underlayer stone that is located approximately in the middle of the crest element is close to the upper tolerance bound of the underlayer (red dot). When the neighbouring underlayer stones are located $0.3 D_{50}$ lower (green dot), the crest block tilts to one side. Theoretically, it might interfere with a neighbouring block. This case seems quite extreme. In many cases, the crest blocks are less skewed due to the support of 2 normal XblocPlus units in the underlying armour row (figure 7.5). Therefore, the height difference between two neighbouring supporting XblocPlus blocks on the second armour row also affects the crest block position.

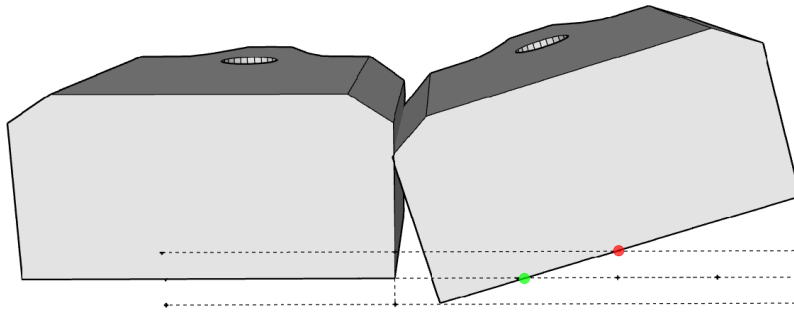


Figure 7.4: Max sideways rotation

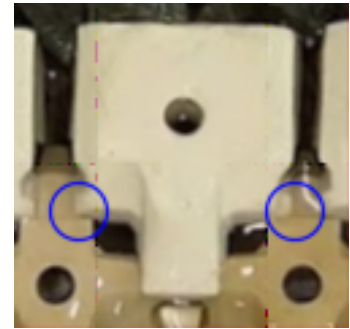


Figure 7.5: Support by XblocPlus

To make it easier for the crest blocks to cope with underlayer deviations, the bottom of a crest block is subdivided in 3 equal sections (figure 7.6). The bottom level of the 2 outer sections is raised by $0.3 D_{n50,underlayer}$. This quantity is chosen because it equals the maximum underlayer deviation between 2 points within a distance of D_{n50} . The transition zones between the sections have a 1:1 slope. The height of the cutouts is 17% of the crest element's height ($0.15 D_{n,ref}$). The length of the cutouts in cross-shore direction is long enough to reach further than the slope-crest transition of the underlayer. For the test blocks, this is 19.9 mm ($0.68 D_{n,ref}$).

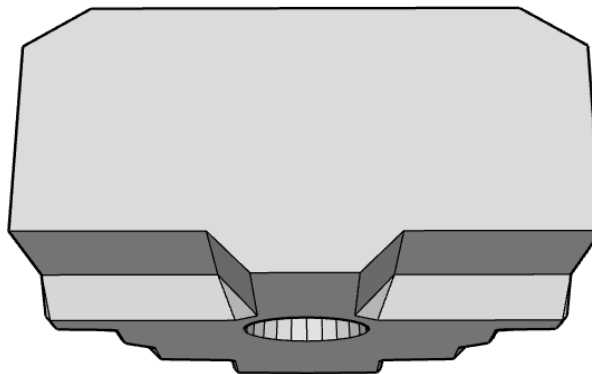


Figure 7.6: Solution to handle longshore tolerances

Figure 7.7 indicates that the taken measures theoretically make placement of the crest blocks easier. In the figure, the middle dashed line is the theoretical underlayer level. The upper and lower dashed lines

indicate the underlayer levels that deviate $0.3 D_{n50}$ from the theoretical level. The effect of the measure in practice is shown in figure 7.8. Only the second block from the right is tilted to one side. All the other blocks remained horizontal.

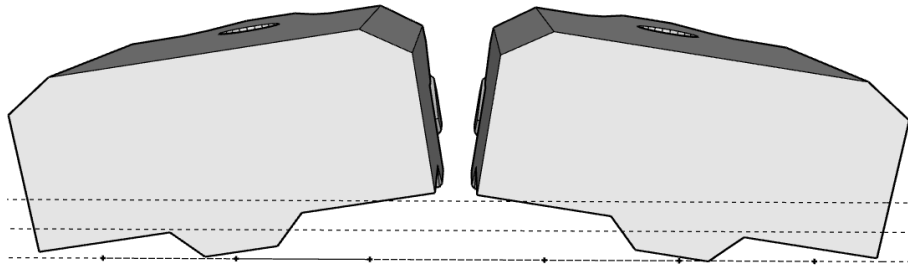


Figure 7.7: Effect of block modification to deal with longshore tolerances



Figure 7.8: Theoretical solutions applied in practice

7.1.1.2. Cross-shore underlayer deviations

Height deviations over the entire structure are analysed to implement the consequences for back to back placed crest blocks. The reason is that height deviations at the breakwater toe affect the position of slope armour units and so the position of crest armour units. This is visualised by figures 7.9 and 7.10. The red line in the figures represent the top of the underlayer in the theoretical profile. Figure 7.10 also shows the bandwidth of $0.5 D_{n50}$. Besides vertical margins, also horizontal margins of $1/6 * D_{n50}$ should be implemented for breakwaters with a 3V:4H slope. The green line represents an example of the underlayer profile in practice.

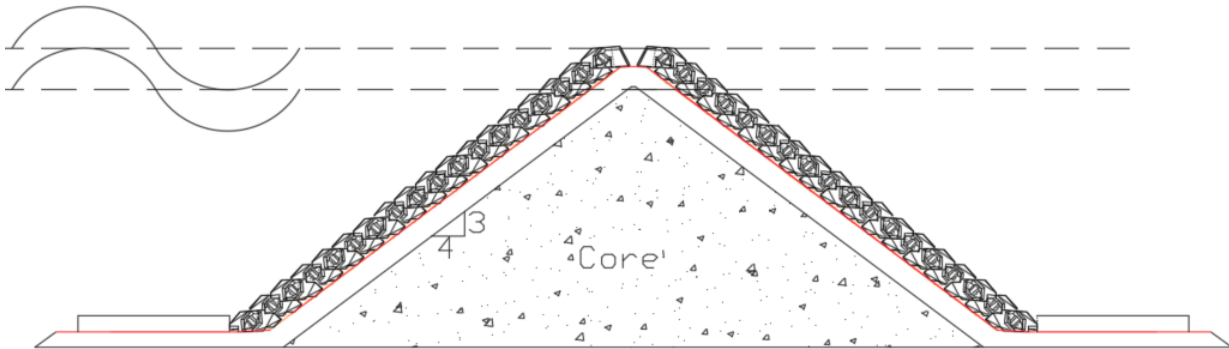


Figure 7.9: Top underlayer

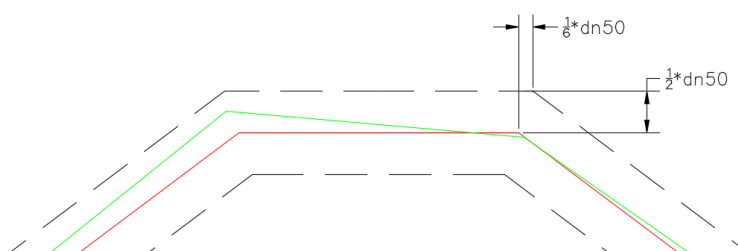


Figure 7.10: Underlayer bandwidth

Due to the underlayer deviations specified in figure 7.10, the position of crest armour units might differ horizontally and vertically. When the crest blocks are positioned higher than in the design profile while the underlayer is not, the crest blocks are tilted forwards (figure 7.11). The opposite might also happen (figure 7.12). The coloured dots indicate the rotation point of the blocks.

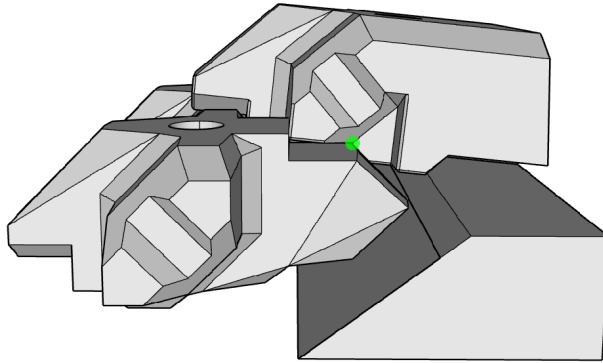


Figure 7.11: Crest blocks tilted forwards

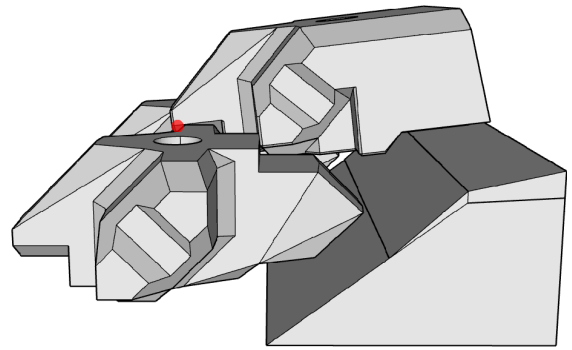


Figure 7.12: Crest blocks tilted backwards

Tilted crest blocks affect the shape of directly back to back placed crest blocks. They might theoretically interfere with each other due to underlayer tolerances. Figure 7.13 shows what theoretically would happen to the crest blocks when the underlayer at the crest is close to the lower tolerance bound. Figure 7.14 shows what happens to the crest blocks when the crest width is at both slope-crest transitions $1/6 * D_{n50,under-layer}$ smaller than the theoretical crest width.

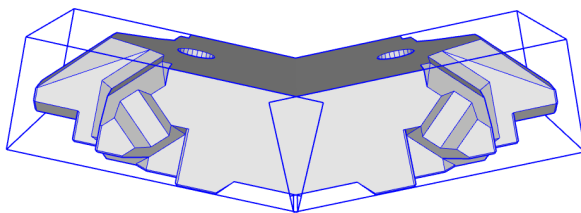


Figure 7.13: Block interference case 1

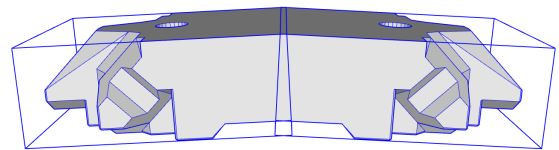


Figure 7.14: Block interference case 2

Both figures indicate that the back to back placed blocks would interfere with each other if block shape remains unaltered. Based on the interference analysis, the block length is slightly shortened. The length at the top of the block is reduced by $0.25 D_n$ and the length at the bottom is reduced by $0.17 D_n$ (resp. 7 and 4.5mm for the test block). This means that the back of the block becomes slightly skewed. The smaller length reduction at the bottom has a favourable impact on the stabilising moment because the length between the rotation point and the block's centre of mass remains larger. Figure 7.15 shows the final starting block after implementation of the underlayer tolerance effects.

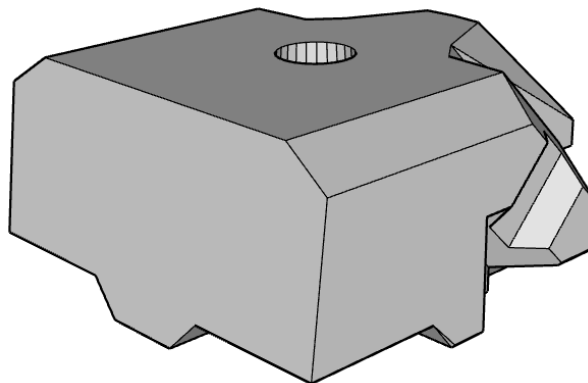


Figure 7.15: starting block for modified XblocPlus solutions

7.1.2. Hole

The rear part of the block is much bulkier than an original XblocPlus block. As a result, its centre of mass is located further backwards compared to the original XblocPlus. The centre of mass of an original XblocPlus block is in the middle of the hole. As a result, the block position remains horizontal when it is lifted by a crane. Hence, the hole in the starting block is moved backwards to the centre of mass.

7.1.3. Final shape starting block

The dimensions of the starting block are given in table 7.1. In general, the dimensions are comparable with the dimensions of an original XblocPlus block. However, the starting block is bulkier shaped than an original XblocPlus block. This makes the volume of the starting block 77% larger than the volume of the original XblocPlus block. Detailed information about the block dimensions is given in appendix C.1.1.

Parameter	XblocPlus	Modified XblocPlus
Length	61mm	60mm
Width	48mm	48mm
Height	24mm	24mm
Volume	24700 mm ³	43465 mm ³

Table 7.1: Block properties normal and modified XblocPlus

7.2. Crest width after construction

The slightly sloped back of the starting block makes direct back to back placement impossible. Initially, the intention was to place rock between the blocks at places where the space between the blocks is large. Excessive crest block displacements should be prevented by the rock. However, during the construction process in the lab, it was concluded that it is better to place rock between all back to back placed crest blocks. The reason is that the rock fill generates interlocking between the crest blocks. The crest width in the lab setup varied between 10.5 and 11.3cm. The average width of 10.9 cm is equal to $b/H_{s,d} = 1.1$. Figure 7.16 shows the final crest set-up with rock fill between all crest blocks.



Figure 7.16: Crest armoured with starting blocks

For construction purposes, it is favourable to fill the space between the crest blocks with rock of a grading that is already present in the structure. Therefore, underlayer rock is chosen as filling material. Its suits better than core material due to its larger size. Toe rock might also have been an option.

7.3. Starting block test results

7.3.1. Normative freeboard

To start, the normative freeboard for modified XblocPlus solutions was investigated since it was not directly clear whether $R_c/H_{s,d} = 0.0$ or $R_c/H_{s,d} = 0.5$ is normative (paragraph 4.1.3). Figure 7.17 contains the failure development for both conditions. The percentage on the Y-axis shows the percentage of failed crest blocks related to the total number of crest blocks on both the front and rear slope. The total number of crest blocks in the test set-up is 20. The X-axis represents the test runs expressed by the stability number. Surprisingly,

the starting block met the target condition of $N_s = 3.0$ for both conditions. Failure started at a lower stability number for $R_c/H_{s,d} = 0.0$ than for $R_c/H_{s,d} = 0.5$.

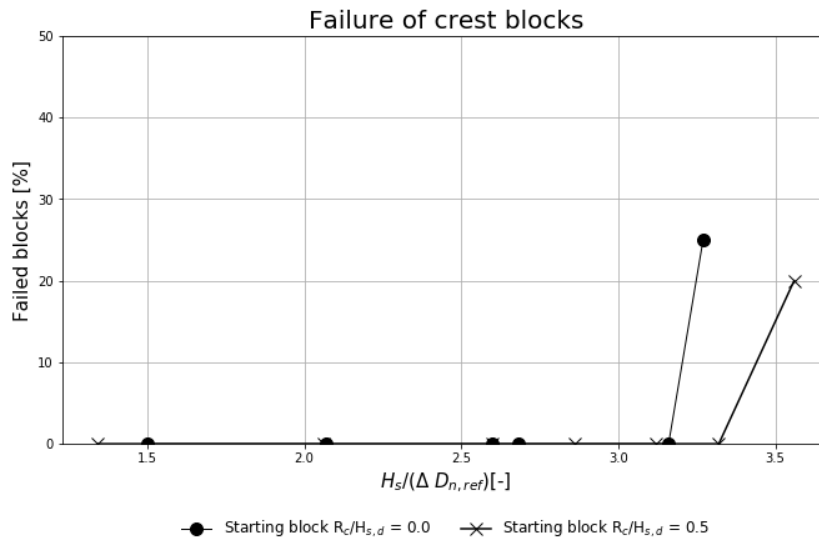


Figure 7.17: Normative freeboard for starting blocks

Important to mention is that the effect of the relative freeboard was assessed by lowering the water level instead of heightening the structure. Performing tests with a lower water level makes it necessary to assess whether the depth change influenced the wave distribution. If the depth becomes too limited, the largest waves in the wave distribution break. Since the block stability is determined by the largest wave in the wave distribution, it could also be different due to the changed boundary conditions. This makes the comparison unfair.

The armour stability in shallow water is usually described by $H_{2\%}$ due to the changed wave height distribution [4]. This makes it straightforward to compare H_s with $H_{2\%}$. If differences in depth influence were too large, the test series with $R_c/H_{s,d} = 0.5$ had smaller $H_{2\%}/H_s$ ratios than the test series with $R_c/H_{s,d} = 0.0$. The results are shown in figure 7.18. The test series with $R_c/H_{s,d} = 0.0$ and $R_c/H_{s,d} = 0.5$ gave almost equal $H_{2\%}/H_s$ values. Also differences for $H_{1\%}/H_s$ were negligible. No large errors were made by lowering the water level instead of changing the structure dimensions. Therefore, it can be concluded that relative freeboard $R_c/H_{s,d} = 0.0$ is normative for structures with modified XblocPlus crest armour.

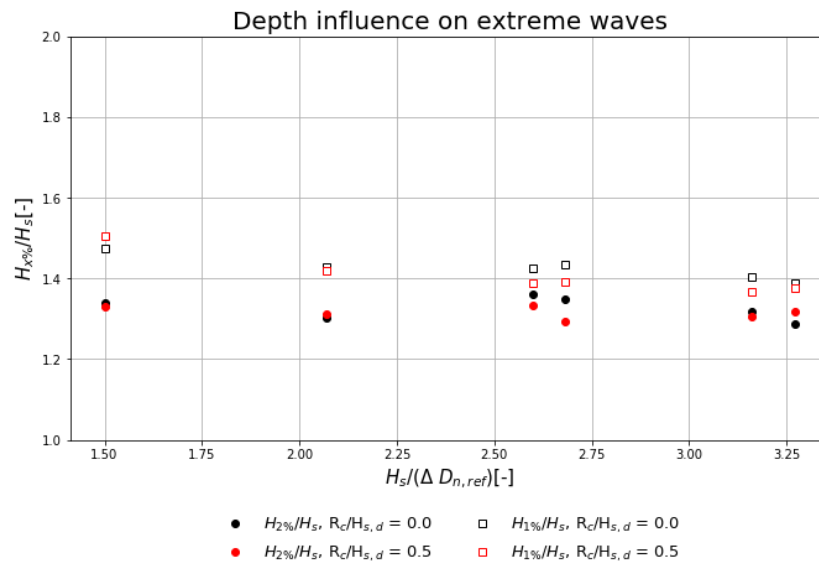


Figure 7.18: Relation between H_s , $H_{2\%}$ and $H_{1\%}$

7.3.2. Failure development

Figure 7.17 in paragraph 7.3.1 already showed that the starting block remained stable till $N_s = 3.2$. Figure 7.19 represents the development of failure and displacements. The percentage on the Y-axis shows the percentage of failed crest blocks related to the total number of crest blocks on the front slope. Very small displacements are visually observed. However, those displacements were smaller than the smallest displacement category defined in section 5.2.2. The negligible displacements were caused by the interlocking generated by the rock fill between the crest blocks. Failure and displacements at the rear slope were not observed (figure 7.20).

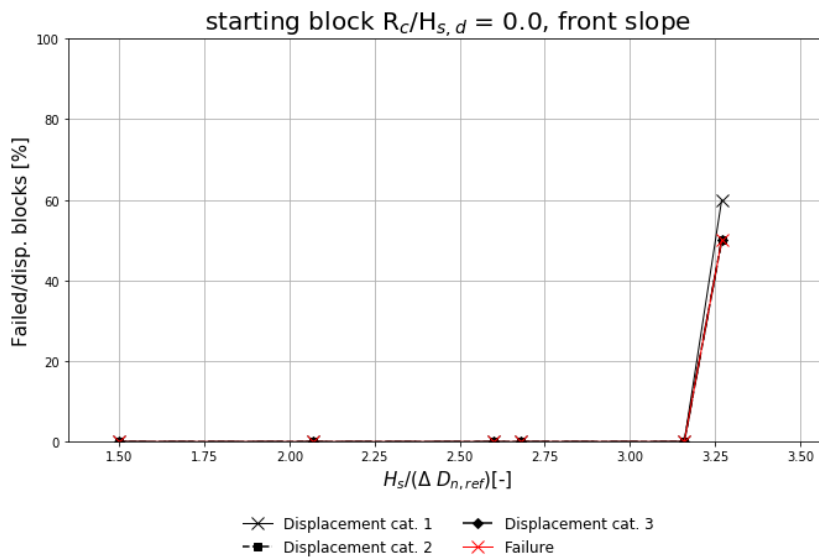


Figure 7.19: Results crest armoured with starting blocks

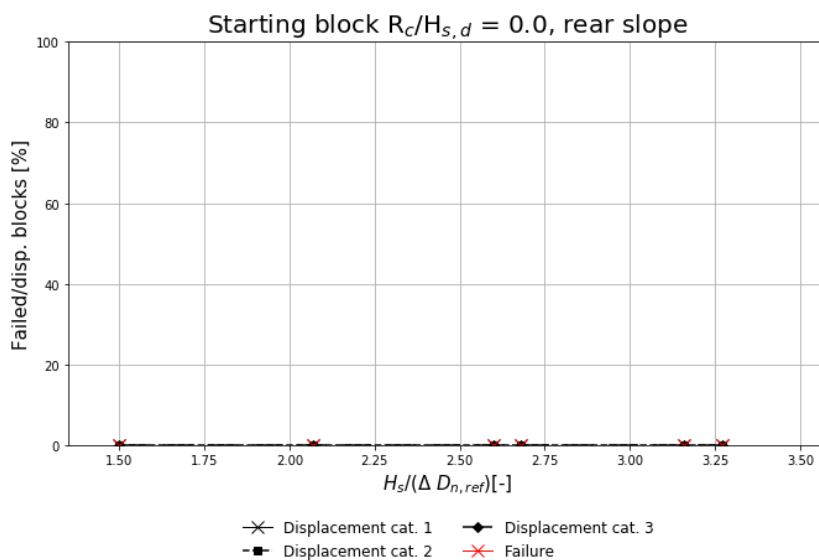


Figure 7.20: Results crest rear slope armoured with starting blocks

7.3.3. Visual failure

In comparison to the original XblocPlus without back support, a combination of vertical and rotational instability results in failure. However, the rotational movement dominates the failure of the starting blocks. Failing crest blocks roll over to the back of the structure (one block excepted). The rotation point is located at the green dot in figure 7.21. Figure 7.22 shows a few shots of a crest block that fails due to rotational instability.

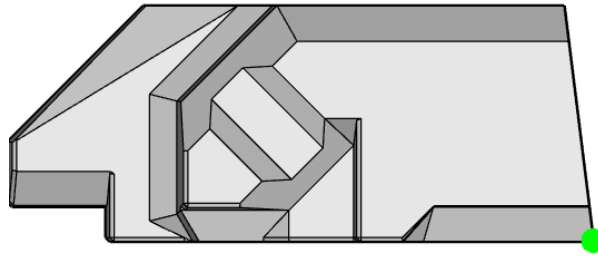


Figure 7.21: Rotation point starting block

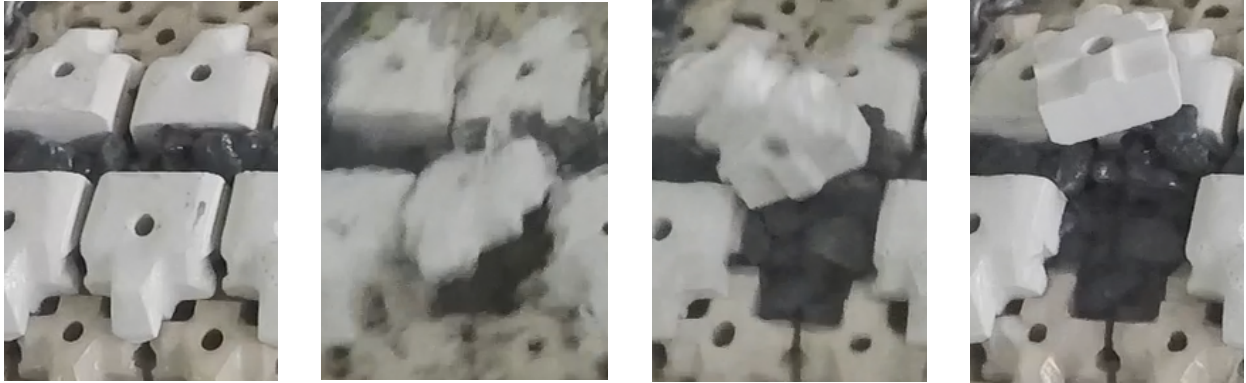


Figure 7.22: Four stages of failure

7.4. Alternatives to starting block

In this section, alternatives to the starting block are presented. The rotational stability of the crest blocks on the front slope proved to be normative for a crest armoured with starting blocks. Therefore, all alternatives are designed with the aim to increase the rotational stability. To make the comparison of the alternatives with the starting block easier, the alternatives are designed in a way that their volume is approximately equal to the volume of the starting block. Appendix C contains drawings including dimensions of each alternative.

7.4.1. Permeable block

The rotational and the vertical instability can be increased by increasing the permeability of a crest block. During up-rush, the increased permeability reduces the upward water pressure under the block. Theoretically, the increased permeability reduces the values of the drag and lift coefficients. As a result, both the lift and the drag force on a crest block become smaller.

Increasing the permeability of a block is most effective if the upward water pressure is reduced at places where it is highest. For the original XblocPlus, the upward water pressure was highest below the centre of the block where the distance to the sides is largest. Therefore, the block permeability is enlarged by creating a hole in the middle of the block. Inspection of the starting block directly shows that it is much bulkier and less permeable than the original XblocPlus. To make it more permeable, 3 additional holes are applied at locations where probably most water pressure reduction can be gained. The permeable block and the starting block have equal dimensions. Due to the 3 holes, the permeable block volume is 9% smaller than the volume of the starting block. A top view and a bottom view of the permeable block are shown in figures 7.23 and 7.24. Figure 7.25 shows the lab structure armoured with permeable blocks.

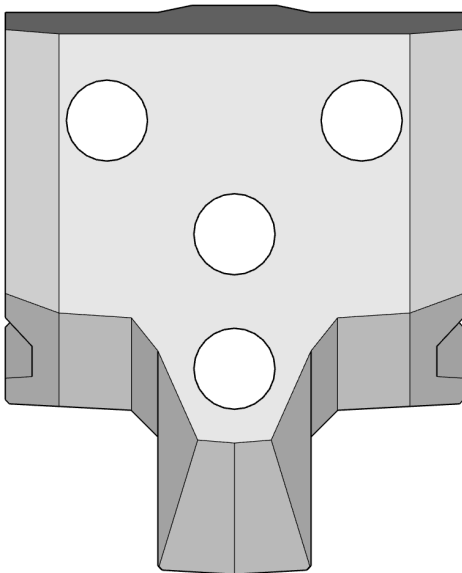


Figure 7.23: Top view permeable block

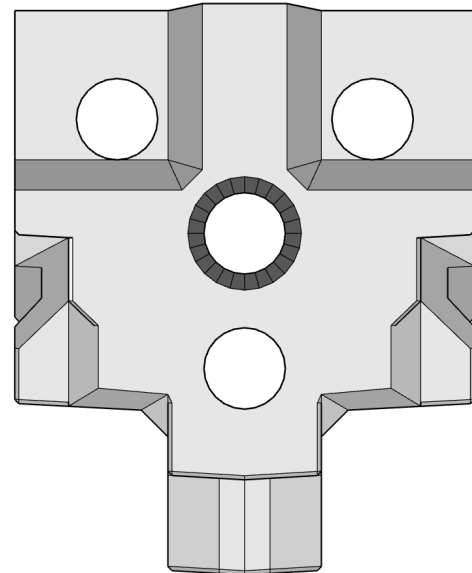


Figure 7.24: Bottom view permeable block

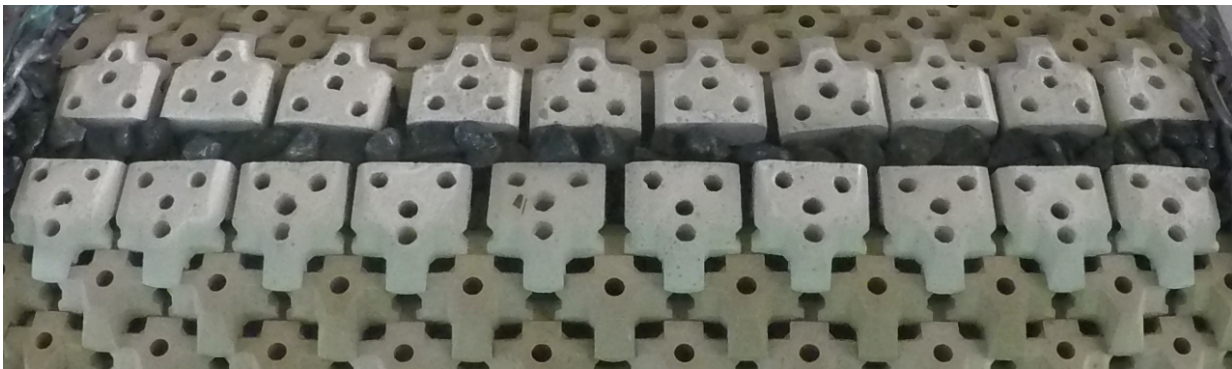


Figure 7.25: Crest armoured with permeable blocks

7.4.2. Extended bottom block

A backwards shift of the rotation point increases the distance between the rotation point and the point of application of the wave force. Therefore, the stabilising moment increases and that would theoretically enhance the rotational stability. A counter-argument is that the bottom area of the block increases. Therefore, both the drag and lift force become slightly larger.

The top of the block is shortened and the bottom is extended. In this way, a block with a sloped back is obtained that has the same volume as the starting block. The shape of the block is depicted in figure 7.26. The back slope of the block is approximately 2V:1H. The block volume is 99.3% of the starting block. Although the block length increased, the crest width remains $B/H_{s,d} = 1.1$. Figure 7.27 shows a crest armoured with the extended bottom blocks. The space between the blocks is filled with underlayer rock. Compared to the starting blocks, more filling material is required to fill the space between the extended bottom blocks.

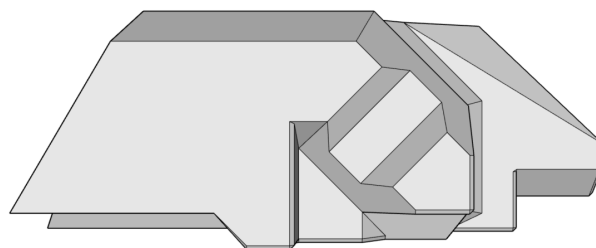


Figure 7.26: Extended bottom block



Figure 7.27: Crest armoured with 'Extended bottom blocks'

7.4.3. Interlocking blocks

A possibility to lock up the crest blocks on the front slope is investigated. The interlocking should increase the stabilising moment. Measures to increase the interlocking capacity of crest blocks can be incorporated in many ways. However, some are easier to implement than others. Sideways interlocking with neighbouring blocks is expected to be cumbersome due to underlayer irregularities and the relatively large space between the blocks. On the contrary, interlocking between the crest blocks on the front and the rear slope seems easier to establish. Here, the weight of the crest block on the rear slope should enhance the rotational stability of the crest block on the front slope.

The degree of interlocking depends on the angle of the back slope of a block. The milder the slope of block's back, the stronger the expected interlocking effect. However, it becomes more difficult to deal with underlayer tolerances. For this reason, the blocks are designed with a 1:1 slope. After implementation of underlayer tolerance effects, the block combination in figure 7.28 is obtained. The arrow indicates the wave direction. The space between the blocks is filled with underlayer rock. This alternative has a relative crest width of $B/H_{s,d} = 1.0$. This is slightly smaller than the relative crest width of the other alternatives. However, this is required to make the interlocking possible. As a result, rock cannot be placed between all blocks. A photo of the test setup in the lab is shown in figure 7.29.

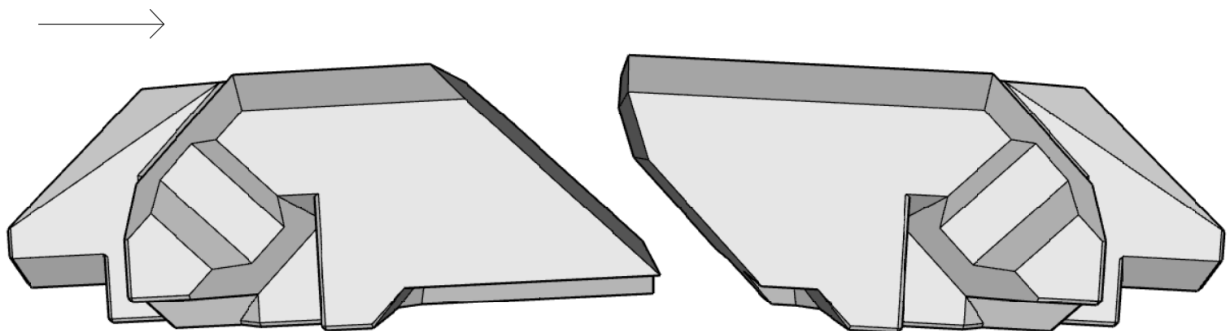


Figure 7.28: Interlocking block 1 (L) and interlocking block 2 (R)

7.4.4. Dimensions modified XblocPlus blocks

An overview of several block properties of modified XblocPlus blocks is presented in table 7.2.

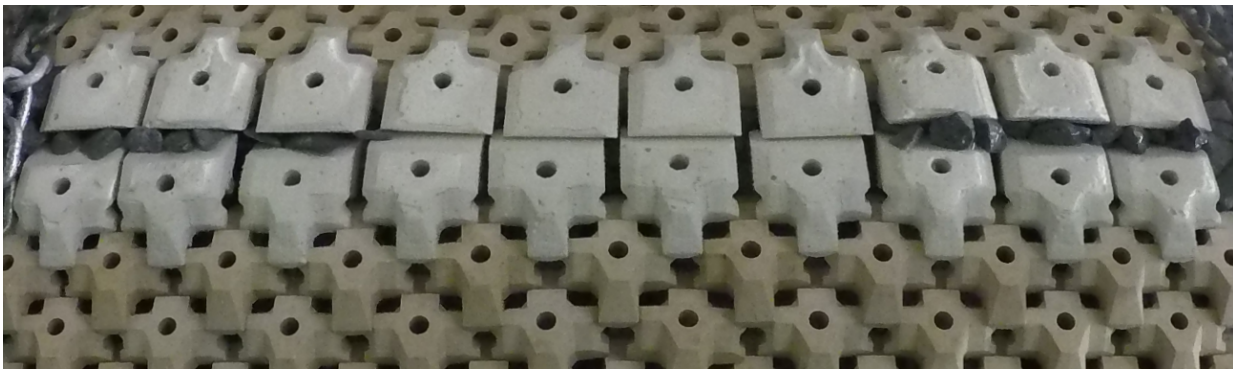


Figure 7.29: Crest armoured with interlocking blocks

Block	Length (mm)	Volume (mm ³)	D_n (mm)	V/V_{ref}
XblocPlus	61	24575	29.1	1
Starting block	60	43465	35.2	1.77
Permeable block	60	39781	34.1	1.62
Extended bottom block	65.7	43171	35.1	1.76
Interlocking block 1	66.8	42360	34.7	1.72
Interlocking block 2	61.5	41823	34.9	1.71

Table 7.2: Modified XblocPlus properties

7.5. Performance of the alternatives

7.5.1. Permeable block

Progression of failure and displacements of the permeable block on the front slope is shown in figure 7.31. Failure and displacement category 1 of the starting block are also presented in the graph. Displacement categories 2 and 3 ($>0.09 \cdot D_n$ and $>0.18 \cdot D_n$) are left out because their trajectory equals the trajectory of the failure line. The critical stability number (paragraph 5.2.4) of the permeable block is $N_{s,c} = 3.1$. From the graph can be obtained that the permeable blocks behave similar to the starting blocks. Its critical stability number of $N_{s,c} = 3.1$ is close to that of the starting block ($N_{s,c} = 3.2$). However, for the permeable blocks, the failure progression went slower than the failure progression of the starting blocks. Displacements of the permeable blocks were small due to the interlocking generated by the rock fill. Only one block displaced in an early test run. It is plausible to assume that it wasn't completely locked up since the experiment photos show that the block displaces without displacement of the filling material. At the rear slope, 1 block displaced and eventually failed (figure 7.32). However, it failed after it became more exposed to the wave load due to failure of its neighbouring block on the front row.

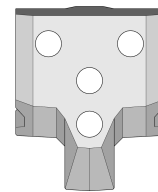


Figure 7.30: Permeable block

7.5.1.1. Wall effect

Important to mention is that the test results of the permeable block stability are affected by the wall. The leftmost block of the second armour row displaced during the test session. This resulted in a reduction of the interlocking capacity of the leftmost crest block. Consequently, the leftmost crest block displaced to the right and the space between the left most block its neighbouring block reduced. The pressure build-up below the blocks increased. Eventually, the 2 leftmost permeable blocks were the first crest blocks that failed. In the subsequent test run, the block at the rear slope failed after it became more exposed. As a result, the failure of 3 crest blocks is affected by the wall. Probably, without the wall effect, the crest armoured with permeable blocks would have been stable up to $N_s = 3.3$.

7.5.1.2. Failure mode

One block on the front slope failed due to uplift. However, also a weak rotational movement was observed. Two other crest blocks failed due to rotational instability. These blocks directly rolled over to the rear slope. The rotational movement seemed to be slower compared to the starting block. As a result, the angular velocity, and therefore the rotational instability, may be lower than is the case for the starting block.

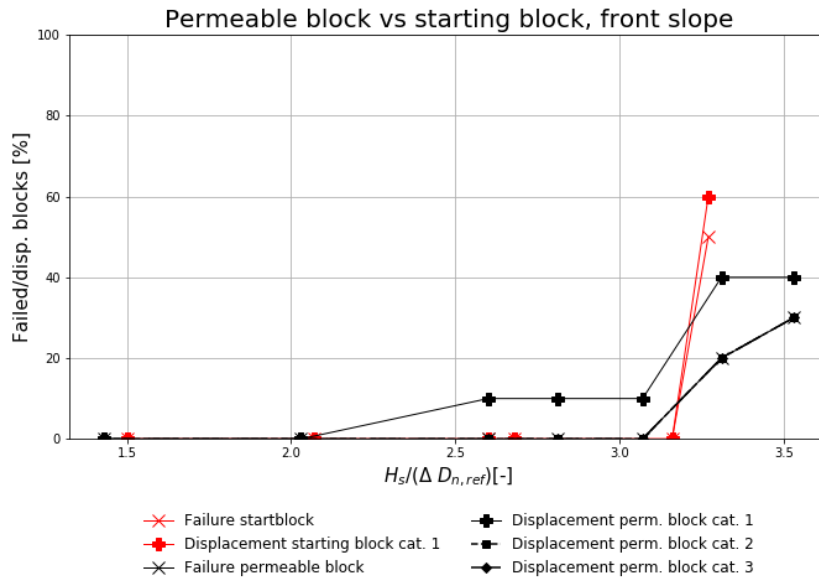


Figure 7.31: Failure development front slope armoured with permeable blocks

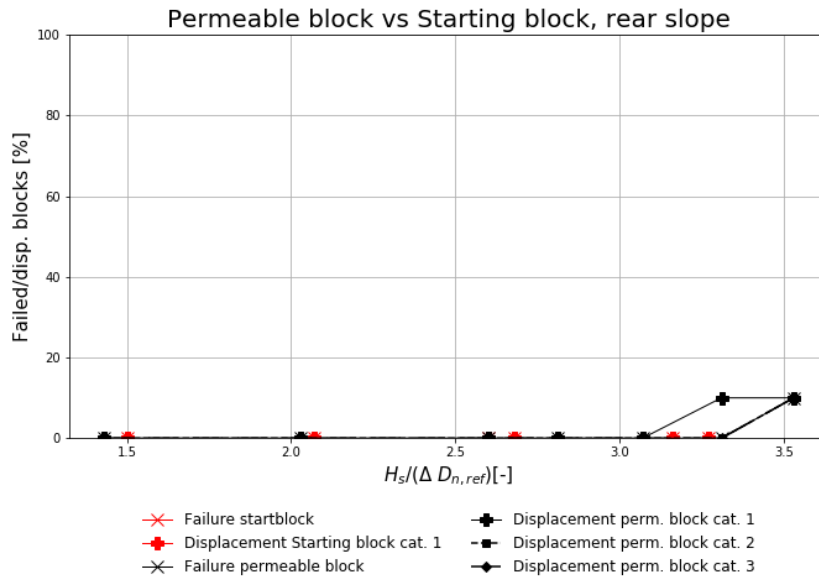


Figure 7.32: Failure development rear slope armoured with permeable blocks

Possibly, the permeable block is slightly less dominated by the rotational instability. This might be due to the lower pressure build-up below the nose of the block.

7.5.2. Extended bottom block

The failure progression of the extended bottom block is depicted in figures 7.34 and 7.35. Due to the inclined back, the filling material is less effective in locking up the crest blocks. This can be observed from the test results. Displacements of all categories occur more frequently before failure than the case is for the starting blocks. The extended bottom blocks remained stable till $N_{s,c} = 2.8$ whereas the starting block remained stable till $N_{s,c} = 3.2$. It can be concluded that the crest armoured with extended bottom blocks is less stable than a crest armoured with starting blocks. This is caused by the reduced interlocking capacity of the extended bottom blocks.

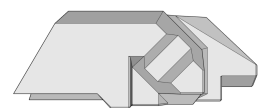


Figure 7.33: Extended bottom block

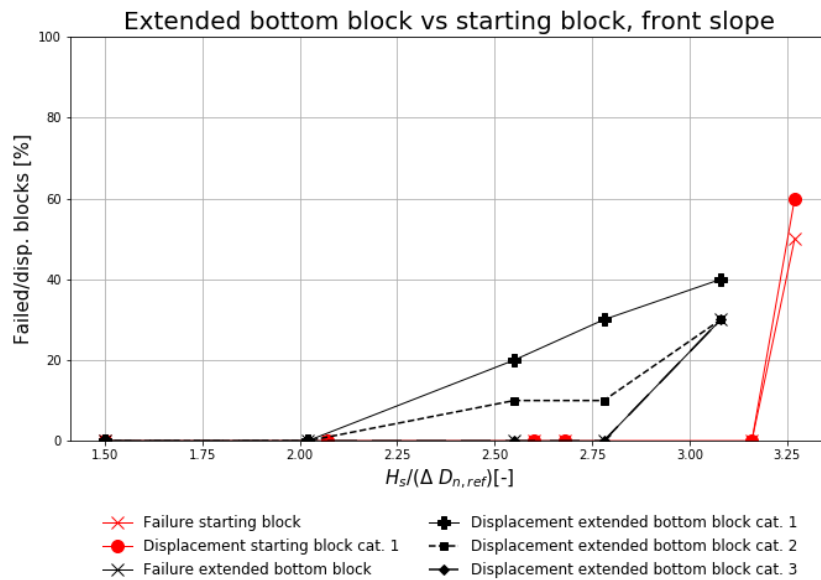


Figure 7.34: Results front slope armoured with extended bottom block

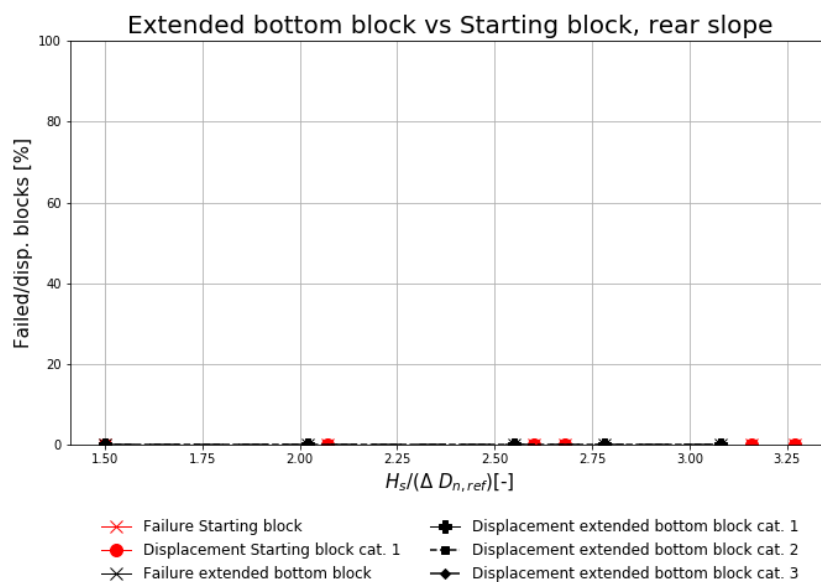


Figure 7.35: Results rear slope armoured with extended bottom block

7.5.2.1. Failure mode

In contrast to the starting blocks, the extended bottom blocks that failed due to rotational instability did not directly roll over. These observations may indicate that the rotational stability of the extended bottom block was indeed slightly larger than the rotational stability of the starting block.

7.5.3. Interlocking blocks

The failure and displacement progression of the interlocking blocks are depicted in figure 7.37 and figure 7.38. The structure remained stable till $N_{s,c} = 2.8$ whereas the starting block remained stable till $N_{s,c} = 3.2$. The interlocking blocks displaced even more than the extended bottom blocks did. These two observations indicate that the interlocking between the crest blocks is ineffective. Another disadvantage is that the interlocking blocks require a high placement accuracy to benefit from the interlocking. Moreover, 80% of the crest blocks failed at $N_s = 3.1$. This indicates that the residual strength after failure of the first crest block is very marginal. Appendix H.1 contains more information about the placement accuracy of the interlocking blocks.

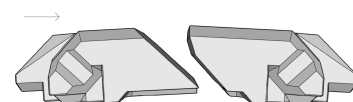


Figure 7.36: Interlocking blocks

Moreover, 80% of the crest blocks failed at $N_s = 3.1$. This indicates that the residual strength after failure of the first crest block is very marginal. Appendix H.1 contains more information about the placement accuracy of the interlocking blocks.

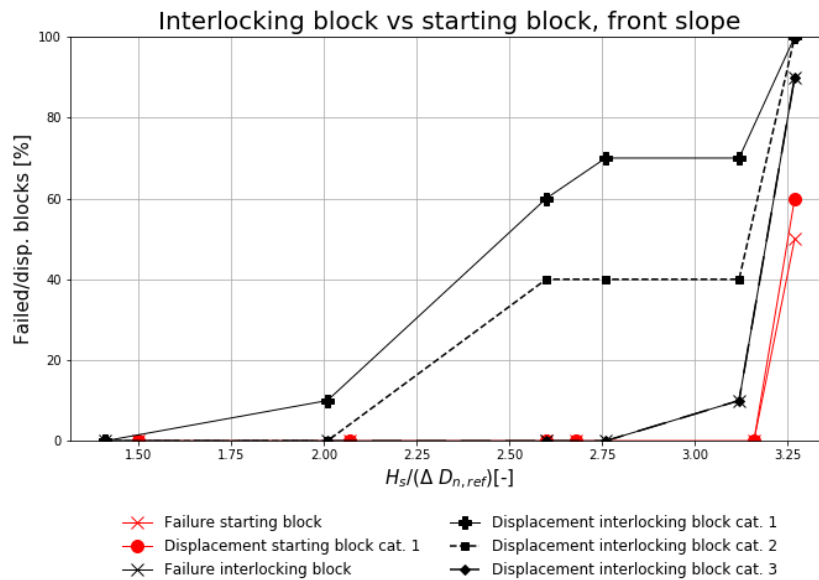


Figure 7.37: Results front slope armoured with interlocking blocks

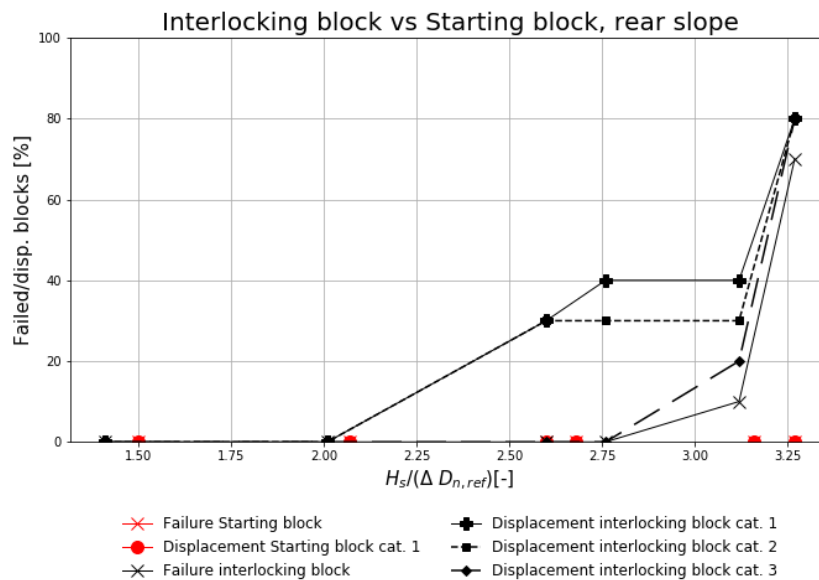


Figure 7.38: Results rear slope armoured with interlocking blocks

7.5.3.1. Failure mode

Observations clarify why so many crest blocks failed. The crest blocks on the front slope displaced early in the test series. As a result, the backwards displaced blocks pushed the blocks at the rear crest row upwards (figure 7.40). Consequently, the crest blocks on the rear slope became more exposed to the wave action and eventually they failed (figure 7.41). After failure of the crest blocks on the rear slope, the blocks at the front row failed due to excessive displacement (figure 7.42).

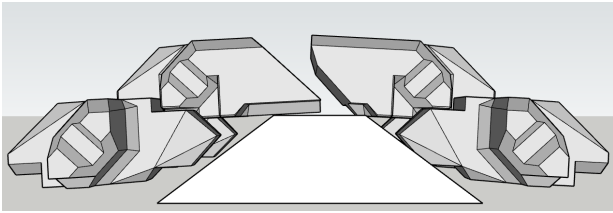


Figure 7.39: Initial position

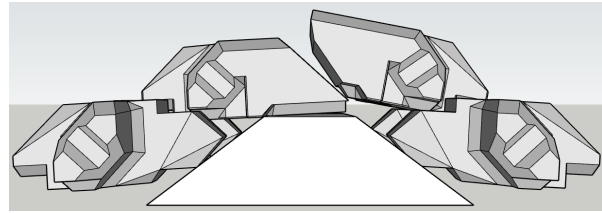


Figure 7.40: Failure stage 1

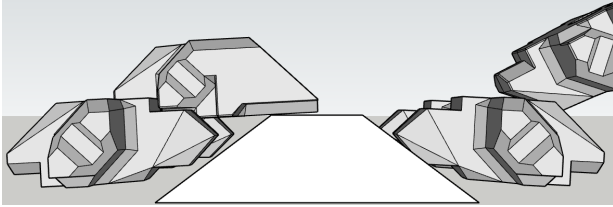


Figure 7.41: Failure stage 2

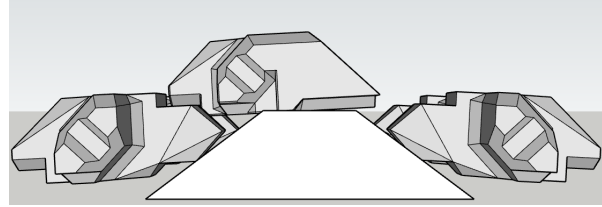
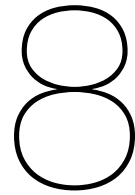


Figure 7.42: Failure stage 3

The failure observations indicate that the blocks at the back slope are normative for the crest stability. The effect of reversed placement of the interlocking blocks is also investigated. This appeared to be not the case. The test results are shown in appendix H.1.



Comparison of alternatives

An overview of all tested alternatives of the preliminary research phase is presented in table 8.1. It contains stability information about crest configurations with original XblocPlus crest armour and modified XblocPlus crest armour.






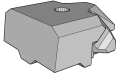

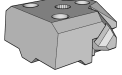

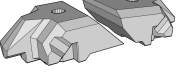


Name	Overview crest	Overview block	V/V_{ref}	$B/H_{s,d}$	$N_{s,c}$
XblocPlus top row, large crest element (Reference situation)			1	2.7	2.4
XblocPlus top row, small crest element			1	1.9	2.6
Starting block			1.77	1.1	3.2
Permeable block			1.62	1.1	3.1
Interlocking blocks			1.72 & 1.71	1.0	2.8
Extended bottom block			1.76	1.1	2.8

Table 8.1: Overview alternatives preliminary research phase

8.1. Stability

The critical stability number ($N_{s,c}$), which is based on the test run with the highest significant wave height without failure of a single crest block, is used to determine the crest stability. From the critical stability numbers in table 8.1 can be concluded that the alternatives with original XblocPlus blocks on the top rows are

least stable. Despite the positive effect of the back support, the original XblocPlus blocks are insufficiently stable to meet the target stability. The obtained stability values with modified XblocPlus crest armour are much higher. The highest stability number is obtained for the starting block. However, the permeable block could have been more stable without influence of the wall. It is expected that, without the wall effect, the crest armoured with permeable blocks could have been stable up to $N_s = 3.3$ (paragraph 7.5.1). Stability differences between the alternatives are mainly caused by differences in permeability and interlocking. The effectiveness of the interlocking is explained in section 8.1.2.

8.1.1. Block efficiency

The volume of the starting block is 9% larger than the volume of the permeable block. Therefore, a gain factor is used to make a fair comparison between the alternatives possible. The gain factor, which is described by equation 8.1, is used as a measure for the efficiency of a crest block. The gain factor is the ratio between the gained stability and the gained block volume.

$$G = \frac{N_{s,c}/N_{s,ref}}{V/V_{ref}} \quad (8.1)$$

In equation 8.1, $N_{s,ref}$ is the critical stability number of XblocPlus blocks on the top armour row without back support. According to Grigoris [13], $N_{s,ref} = 1.0$ for conditions $R_c/H_{s,d} = 0$ and $s_{0,p} = 2\%$. V/V_{ref} is the ratio between the crest block volume and the volume of an original XblocPlus block. These ratios are presented in table 8.1. Table 8.2 shows the gain factor per block type.

Block	Gain factor (G)
Starting block	1.89
Permeable block	1.97
Extended bottom block	1.65
Interlocking blocks	1.67

Table 8.2: Block efficiency

From the gain factor results can be concluded that the gain factor of the permeable block is the largest of all crest blocks. This makes the permeable block, independently of the wall effect, the most efficient crest block.

8.1.2. Interlocking

Rock is placed between the modified XblocPlus crest blocks to generate interlocking. The effectiveness of the interlocking varies per alternative. Crest blocks displacements indicate how effective the interlocking is. The more crest blocks displace, the less effective is the interlocking. Figure 8.1 shows the crest block displacements of each category just before failure. The failure categories are defined in paragraph 5.2.2.

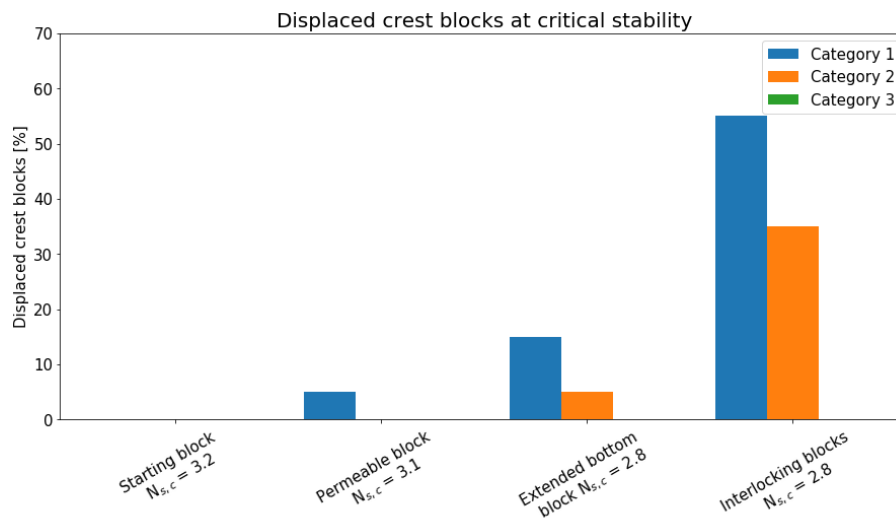


Figure 8.1: Displaced crest blocks at critical stability

From figure 8.1 can be obtained that displacements are negligible for starting blocks and permeable blocks. These block types are most stable of all alternatives with modified XblocPlus armour. This indicates that the almost vertical back of both block types makes the interlocking very effective.

The extended bottom blocks are less stable than the starting blocks and the permeable blocks. Moreover, displacements are larger. It can be concluded that the interlocking capacity of extended bottom blocks is smaller due to its sloped back. The same applies to the set of interlocking blocks.

8.2. Repeated rotational movement

Rocking may lead to breakage of armour blocks (paragraph 2.2.2). Relatively slender armour units like Xbloc are more sensitive for breaking than the rather bulky XblocPlus. The crest blocks used in this research are even bulkier than XblocPlus. Nevertheless, rocking is important to assess. BAM defined rocking as a repeated rotational motion that occurs at more than 2% of the waves (>20 times in a wave series of 1000 waves)[7]. Each crest block at the front slope rotated at most 5 times during the entire test session. Consequently, the term 'repeated rotational movement' is used to distinguish the rotational movement from rocking.

The bulky crest block shape makes it unlikely that a block breaks in two or more pieces as a result of repeated rotational movement. However, repeated rotational movement can be related to the failure of crest blocks. Rotational movement before failure was most observed for the starting blocks, permeable blocks and the extended bottom blocks. No rotational movements were observed for crest configurations with original XblocPlus crest armour. The results are shown in figure 8.2. The rotational movement of a crest block indicates that it is close to failure. Failure of crest blocks is almost guaranteed after rotational movement was observed (figure 8.3).

8.3. Conclusions preliminary research phase

The following general conclusions can be drawn about the results of the preliminary research phase:

- Crest configurations with modified XblocPlus armour are more effective than crest configurations with original XblocPlus blocks and a supporting crest element. Two arguments confirm this conclusion. First, higher stability numbers can be achieved with modified XblocPlus crest blocks. Second, the width of a crest that is armoured with modified XblocPlus blocks is much smaller than the width of a crest with original XblocPlus blocks and a supporting crest element.
- Crest configurations with modified XblocPlus blocks are necessary to meet the target stability number of 3.0 at conditions $R_c/H_{s,d} = 0$ and $s_{0,p} = 2\%$.
- The crest blocks on the front slope are most exposed to the wave load. Consequently, damage to

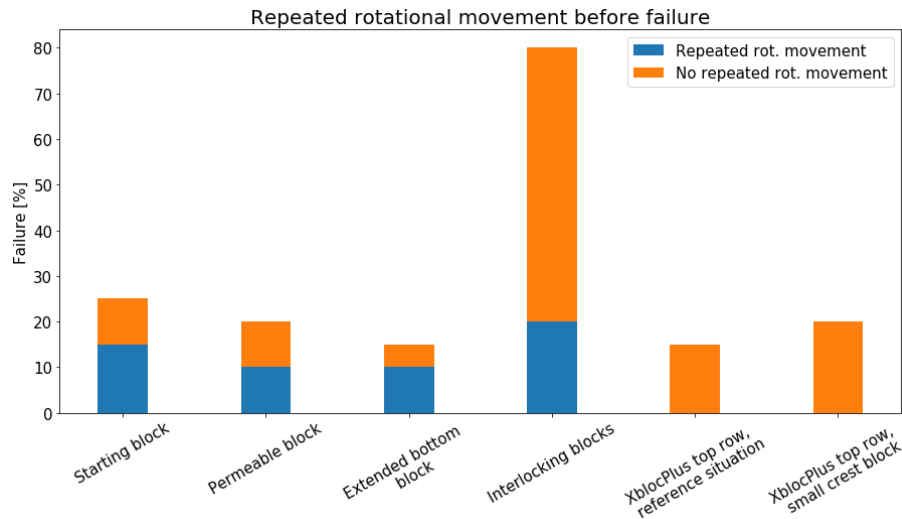


Figure 8.2: Repeated rotational movement before failure

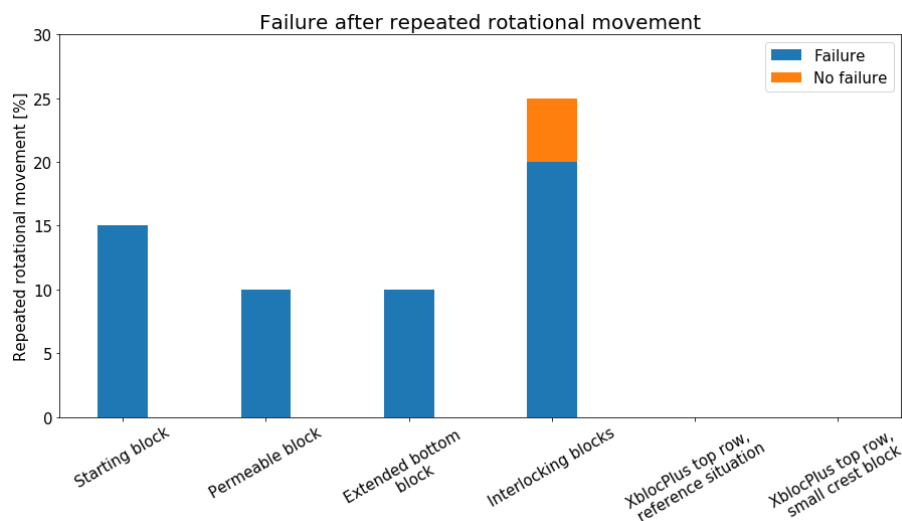


Figure 8.3: Failure after repeated rotational movement

the crest starts on the front slope. For the interlocking blocks holds that excessive displacement of the block on the front slope results in failure of the crest block on the rear slope. For all other tested alternatives, failure of crest blocks starts at the front slope where crest blocks fail due to rotational instability. Crest blocks on the rear slope barely fail.

The following conclusions can be drawn about properties of the modified XblocPlus crest blocks:

- Underlayer rock between back to back placed crest blocks is effective to lock up the crest blocks. The interlocking enhances the crest stability. The almost vertical back of the starting block and the permeable block makes the interlocking very effective.
- Application of a sloped back to a crest block is not an effective measure to increase the block stability. The sloped back should enhance the resistance against rotation because of the backwards shifted rotation pint. However, the interlocking capacity between two back to back placed crest blocks is reduced due to the sloped back. The enlarged resistance against rotation does not compensate the reduced interlocking capacity.
- A set of interlocking blocks is ineffective. Locking up the crest blocks on the front slope below the crest blocks on the rear slope turned out to be an ineffective measure to increase the crest stability. The crest blocks on the rear slope (block with long top) should enlarge the resistance against rotation of the crest blocks on the front slope (block with short top). However, the crest blocks on the front slope push the crest blocks on the rear slope to a less favourable position. This less favourable position

causes failure of the crest blocks on the rear slope. Moreover, the interlocking capacity is smaller compared to the starting blocks. Therefore, a crest armoured with interlocking blocks is not effective.

- Increasing the permeability of a crest block by applying 3 additional holes is an effective measure to reduce the block weight without reduction of the crest stability. Taking the appeared wall effect in consideration, the stability of the permeable block could have been higher than the stability of the starting blocks. Consequently, it is likely that higher stability values can be achieved with a smaller block volume.

A crest configuration with permeable blocks can be considered as the best performing crest configuration of the preliminary research phase. The target stability is met with a relatively small block volume. In the next chapter, the permeable block is further optimised. The aim is to meet the target stability with a block that has a smaller volume than the existing permeable block.

9

Crest block optimisation

This chapter forms part 1 of the detailed research phase. The design of the permeable block, which is considered to be the most efficient block of the preliminary research phase, is optimised to answer the second sub research question. Chapter 11 contains the test results of the optimised block. From this chapter on, the permeable block of the preliminary research phase is called the 'initial permeable block' and the optimised version designed in this chapter is called the 'optimised permeable block'.

9.1. Target volume reduction

Without the influence of the wall, the initial permeable block would probably have been stable up to $N_s = 3.3$. This means that the target stability $N_{s,target}$ of 3.0 is exceeded by 9.4%. The initial permeable block can be considered as slightly oversized. Reduction of the block volume is required to obtain a block with its stability close to the target stability. Two methods were assessed to define the target volume reduction. The first method was based on the vertical stability. This method, explained in paragraph 9.1.1, appeared to be an inadequate method. Therefore, a method based on the rotational stability number is applied. This method is explained in paragraph 9.1.2.

9.1.1. Vertical stability

The stability number, which is based on a vertical force balance, can be used to define the target volume reduction. The stability number gives an indication of volume reduction that is required to obtain a new block with its critical stability at $N_{s,c} \approx 3$ instead of $N_{s,c} \approx 3.3$. D_n in the stability expression refers to the nominal diameter of the original XblocPlus. Therefore, D_n in the stability expression is constant. As a result, the $N_{s,c}$ reduction of 9.4% can only be achieved if the critical significant wave height ($H_{s,c}$) reduces 9.4%. Effectively, stability of the the crest block should remain the same before and after volume reduction. Therefore, the nominal diameter of the crest block ($D_{n,crest-block}$) should be reduced by 9.4% as well.

Given that $V_{crest-block}$ is equal to $D_{n,crest-block}$ to the third power, the block volume must be reduced by 25.6%. The V/V_{ref} ratio would reduce from 1.62 for the initial permeable block to 1.20 for the optimised permeable block. Original XblocPlus blocks without back support were far from stable on the crest. Consequently, this measure is expected to be too rigorous to get stable crest blocks with $N_{s,c} = 3.0$. More support can be given to this idea by the fact that D_n represents just a scaling factor for the block size while it doesn't give a good representation of the block size. In addition, the stability number is based on a vertical force balance whereas the failure of the crest blocks is caused by rotational instability. Although the rotation is also affected by vertical forces, an expression based on a rotational balance is expected to be more adequate to determine the target volume reduction.

9.1.2. Rotational stability

Failure of crest blocks is caused by rotational instability of crest blocks on the front slope. Consequently, the moment balance around the rotation point of a crest block on the front slope is used to obtain a rotational stability expression. Figure 9.1 schematically shows the forces acting on a crest block¹. The orange dot indicates the centre of gravity and the green dot indicates the rotation point. Equations 9.1, 9.2 and 9.3 present how the drag (F_d), lift (F_l) and gravitational force (F_g) are related to important parameters like H_s and D_n . Compared to the expressions for F_d and F_l in paragraph 2.3, v is replaced by \sqrt{gH} . This is permitted because the velocity in a breaking wave on a slope is proportional to the celerity in shallow water with the wave height as a representative measure for the water depth [27].

Expressions 9.5, 9.6 and 9.7 give the derivation for the rotational stability number. Important to note is that the exact values of both the lift force and the drag force are unknown. The dependency in equation 9.4 is used to express the drag force in the lift force.

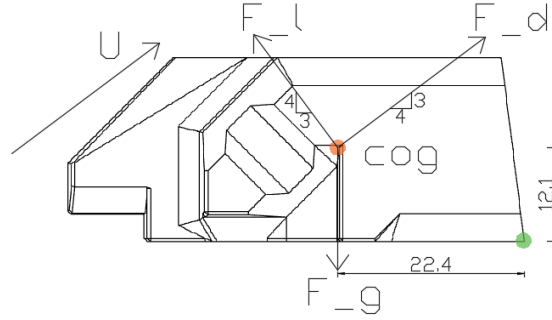


Figure 9.1: Force schematisation XblocPlus

$$F_d \propto \rho_w g H_s D_n^2 \quad (9.1)$$

$$F_l \propto \rho_w g H_s D_n^2 \quad (9.2)$$

$$F_g \propto (\rho_c - \rho_w) g D_n^3 \quad (9.3)$$

$$F_d = x F_l \quad (9.4)$$

$$\Sigma T_{rot} = \frac{3}{5} \cdot 22.4 \cdot x F_l + \frac{4}{5} \cdot 12.1 \cdot x F_l + \frac{4}{5} \cdot 22.4 \cdot F_l - \frac{3}{5} \cdot 12.1 \cdot F_l - 22.4 F_g = 0 \quad (9.5)$$

$$\Sigma T_{rot} = (23.1x + 10.7) F_l - 22.4 F_g = 0 \quad (9.6)$$

$$N_{s,rot} = \frac{23.1x + 10.7}{22.4} \frac{H_s}{\Delta D_n} \quad (9.7)$$

Reduction of the rotational stability number by 9.4% yields a reduction of $H_{s,c}$ by $9.4\% \cdot 22.4 / (23.1x + 10.7)$. Again, the effective stability number should have equal values before and after reduction of $H_{s,c}$. D_n should be reduced by that same factor to achieve this. The value of x must be determined first to obtain the D_n reduction.

The fraction $(23.1x+10.7)/22.4$ becomes larger than 1 for $x > 0.5$. If $x > 0.5$, the percentage of volume reduction with the rotational stability number is smaller than the percentage obtained with the vertical stability number. The larger the x value in the rotational stability number, the smaller the volume reduction becomes. For example, $F_d/F_l = 5$ results in just 5% volume reduction. This reduction percentage is within the margin of errors that is acquired by physical model tests. Consequently, such a small volume reduction makes it

¹In reality, the point of application of the lift force and the drag force is located leftward of the centre of gravity. However, the load distribution below the block is unknown. As a result, the point of application is unknown. Assuming that the point of application coincides with the centre of gravity causes errors. However, the obtained volume reduction by using this assumption is slightly larger than the volume reduction that would be obtained with the real point of application. Therefore, it can be considered as a conservative assumption.

hard to observe differences in block performance. In addition, the volume reduction that is achieved with this method is small. Roughly estimated, the value of x should be between 0.5 and 5 to make the rotational stability number a beneficial method to define the target volume reduction.

9.1.2.1. Relation between drag and lift

The lift and drag force both contribute to a clockwise rotation of the crest block. Therefore, the direction of rotation makes it impossible to conclude which of the two forces is the largest. The vertical force balance provides more clarity. If F_d/F_l equals 1, the resultant force of F_d and F_l would be directed nearly vertically upwards. In that case, an upward movement of the crest block would be expected at failure. However, a rotational movement is observed. Consequently, F_d must be larger than F_l .

The question that arises is how much larger F_d is compared to F_l . Janssen [17] did numerical model tests to investigate the effect of the XblocPlus orientation on the drag and lift forces acting on a block. Figure 9.2 shows his model set-up. The block is exposed to a flow that is comparable to the up-rush velocity. The angle $\alpha = 37^\circ$ of a 3V:4H slope in combination with the blocks on the slope being 3° tilted backwards gives $\alpha = 34^\circ$ to investigate. Janssen investigated the drag and lift forces for $\alpha = 33^\circ$ and $\alpha = 38^\circ$. He found $F_d/F_l \approx -13$ for $\alpha = 33^\circ$. This result indicates that the resultant vertical force is directed downwards. Apparently, the downward directed force that acts on the orange planes is larger than the upward directed force that acts on the green planes (figure 9.3). Angle $\alpha = 38^\circ$ results in a very small positive directed lift force since F_d/F_l became equal to 60. Figure 9.4 shows the block orientation for an angle of 38 degrees between the block and the flow direction. Compared to a block with an angle of 33 degrees, differences are hardly visible. However, the F_d/F_l ratio is very different. This is mainly caused by the small resultant lift force. Consequently, the F_d/F_l ratio is very sensitive to small changes in angle α .

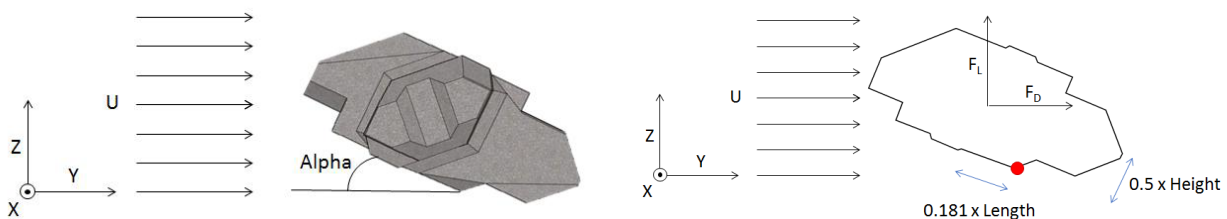


Figure 9.2: Schematisation Janssen's numerical model [17]

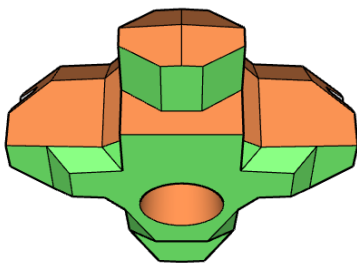


Figure 9.3: 33 degrees

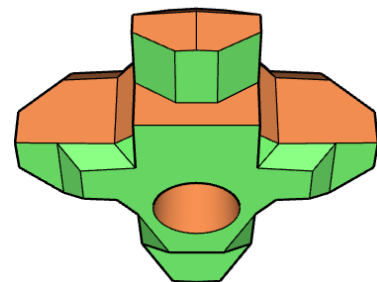


Figure 9.4: 38 degrees

For the initial permeable block, the cumulative area of the green planes is much larger than for XblocPlus (figure 9.5). On the contrary, the cumulative area of the orange planes remains approximately the same. As a result, the upward directed force is expected to be much larger. The magnitude of the drag force is expected to be larger as well. However, the $|F_d/F_l|$ ratio for the crest block is expected to be much smaller since the large ratio for XblocPlus is mainly caused by a very small lift force. By taking the failure mode of the permeable blocks into account, more support can be given to the expectation that F_d is not much larger than F_l . One of the three initial permeable blocks failed due to a combination of uplift and rotational instability whereas rotational instability dominated failure of the other two blocks. If $F_d \gg F_l$, all blocks would have failed due to rotational instability. To conclude, it is expected that F_d is larger than F_l . However, F_d is not much larger than F_l .

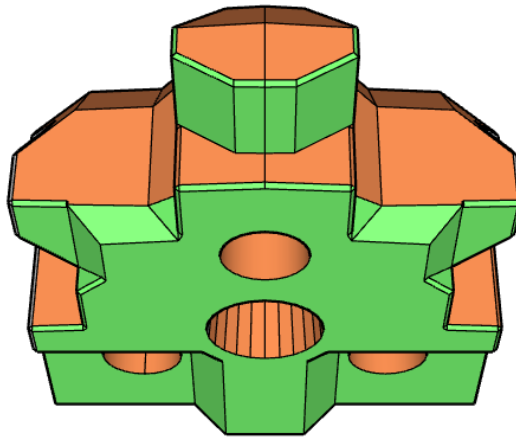


Figure 9.5: Planes initial permeable block contributing to lift force

9.1.2.2. Final target

An x value of 2 is chosen to define the target volume reduction. This value for x fulfils the criterion that F_d must be larger than F_l ($F_d/F_l > 1$). The criterion that F_d is not much larger than F_l is also fulfilled. A larger x value, for example $x = 3$, would also have been an option. However, a slightly lower value is chosen to prevent too conservative volume reduction. Implementing an x value equal to 2 gives a target volume reduction of 10.7%.

9.2. Foundation block optimisation

To obtain an efficient block, the volume should be reduced at places that have least impact on the block stability. Background theory and test results of the preliminary research phase are used to specify restrictions and priorities for effective volume reduction. The restrictions are subdivided in general and constructional restrictions.

9.2.1. General restrictions

Three general requirements are specified:

- The block width should be equal to the original XblocPlus width. This makes placement on the original XblocPlus row beneath possible.
- The distance from the 3 additional holes to the edges of the block should be enough to prevent concrete parts breaking off. The hole in the nose of the block is most important to consider since the part between the hole and the orange hatched planes is relatively slender (figure 9.6). Based on engineering experience, it is determined that the distance between the hole and the edge of an orange hatched plane should be at least 25% of the hole diameter. No structural analysis is performed to assess this criterion.

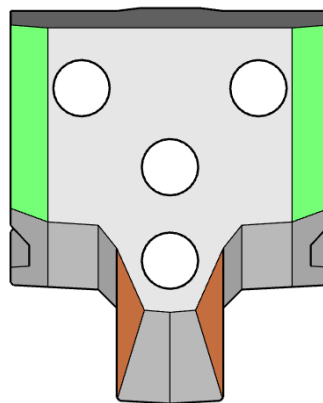


Figure 9.6: Concrete thickness between holes and boundaries

9.2.2. Constructional requirements

Constructional requirements are:

- The 3 additional holes in the crest block should all have the same diameter to facilitate the construction process. In a block construction factory, the easiest method to construct the holes is to place cardboard tubes or PVC tubes in the mould. Making use of tubes that all have the same diameter is desirable for an efficient construction process since individual assessment of the tube size is not required.
- The centre of the middle hole should preferably coincide with the block's centre of mass. It facilitates the construction process since a block should remain horizontal when it is lifted by the crane with a clamp. Small deviations are possible. For example, the length between the centre of the middle hole and the block's centre of mass is approximately 1.3% of the berm block length. Deviations of this magnitude are allowed.
- The dimensions of the middle hole should remain unchanged to make placement with a clamp possible. This automatically means that the block height modifications are not allowed since it requires to modify the cone size.

9.2.3. Stability priorities

The block volume should be reduced in a way that it has the least impact on the block stability. The following priorities are specified to achieve this requirement:

- The distance between the block's centre of mass and rotation point should remain as large as possible. Therefore:
 - Reducing the block length should preferably be avoided. It reduces the block volume and the distance between the centre of mass and the rotation point. Both harm the stabilising moment.
 - Mass should preferably be removed close to the rotation point while the block length remains unaffected. This enlarges the distance between the rotation point and the centre of mass. Consequently, the reduction of the stabilising moment is relatively small.
- Removing weight while making the block more permeable is an effective measure to reduce the block volume.
- Slope modifications of the block's back should be avoided. A sloped back of the block makes the interlocking less effective.

9.3. Design steps

In five steps, the block volume of the initial permeable block is reduced by 10.7%. The specified restrictions and stability priorities are used as a guideline.

9.3.1. Tolerance margins

In the preliminary research phase, a varying bottom level is applied to deal with underlayer deviations in the width direction of the block (figure 9.7). The height difference is $0.3 D_{n50}$ of the underlayer. This margin is enlarged to $0.5 D_{n50}$ to reduce the block volume (figure 9.8). The idea behind it is that underlayer height deviations are allowed up to $0.5 D_{n50}$. This measure reduces the block volume by 3.1%. The distance between the centre of mass and the rotation point slightly increases.

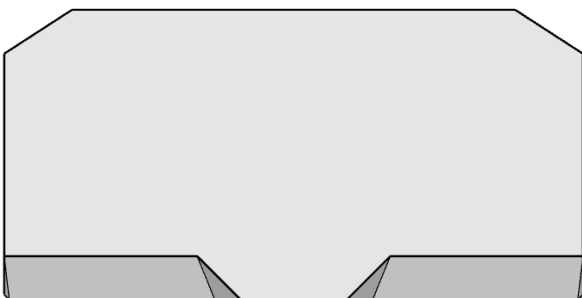


Figure 9.7: $0.3 D_{n50}$ tolerance margin initial perm. block

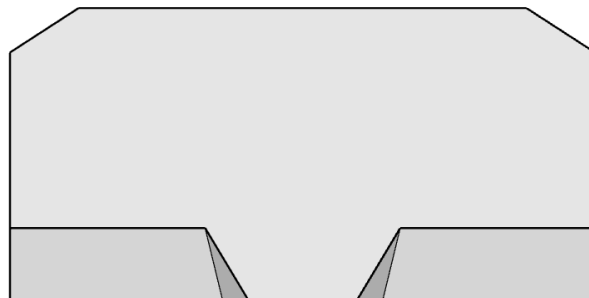


Figure 9.8: Enlarged tolerance margin to $0.5 D_{n50}$

9.3.2. Bottom profile

The bottom profile is streamlined to reduce the load exerted by the water. This measure facilitates the water flow from the block wings to the holes at the rear part of the block. In addition, the block volume reduces by 3.3%. The total volume reduction becomes 6.4%.



Figure 9.9: Modified bottom profile

9.3.3. Streamlined wings

The sections between the wings and the rear holes are streamlined to further facilitate the flow from the wings to the 2 holes at the rear part of the block. Consequently, the pressure build-up below the block is expected to be smaller. The result is shown in figure 9.10. The obtained volume reduction of 0.1% is negligible.

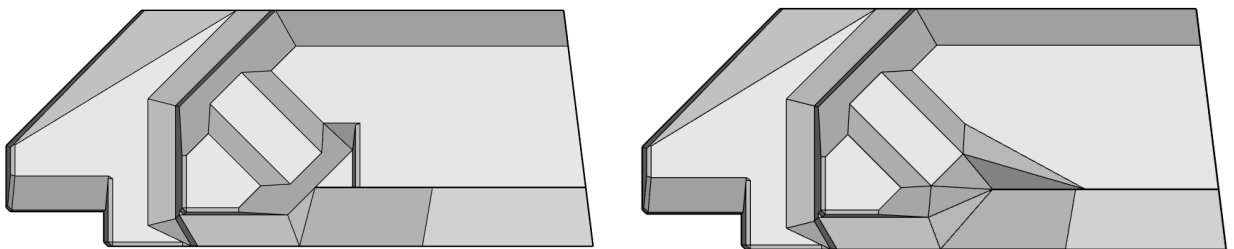


Figure 9.10: Streamlined wings

9.3.4. Diameter additional holes

The diameter of the 3 additional holes is enlarged by 8%. The obtained diameter is the maximum diameter that can be applied without violating the general requirements specified in paragraph 9.2.1. The result is shown in figure 9.11. The block volume is further reduced by 1.3%. The total volume reduction becomes 7.8%.



Figure 9.11: Enlarged holes

9.3.5. Block length

Up to this point, the block volume is reduced by 7.8%. The block length is reduced as a last measure to achieve the target for volume reduction. A length reduction of 2% reduces the block volume by 3.2%. As a result, the volume of the optimised permeable block becomes 89% of the initial permeable block volume.

9.3.6. Final block shape

The designed optimised permeable block is 44% larger than the original XblocPlus blocks. Some important numbers of the optimised permeable block are given in table 9.1. The table also contains information about XblocPlus and the initial permeable block to make it easier to compare the blocks. More information about the dimensions of the optimised permeable block is given in appendix C.2.1.

Block	Length (mm)	Volume (mm ³)	D_n (mm)	V/V_{ref}
XblocPlus	61.1 (2.10 $D_{n,ref}$)	24575	29.1	1
Initial permeable block	60.0 (2.06 $D_{n,ref}$)	39781	34.1	1.62
Optimised permeable block	58.6 (2.01 $D_{n,ref}$)	35423	32.8	1.44

Table 9.1: Block information optimised permeable block

10

Model set-up detailed research phase

The model set-up in the detailed research phase differed to the set-up that is used in the preliminary research phase. The flume was just partly available. Therefore, it became impossible to apply a foreshore.

10.1. Structure set-up

10.1.1. Water level requirements

Absence of the foreshore requires careful assessment of the depth requirements. Using $H_{s,max} = 1.4 \cdot H_{s,d}$ for the significant wave height in the last run of a test series, gives the minimum depth requirements specified in table 4.1.

Parameter	Definition	Value (cm)
Significant wave height	$H_{s,d}$	8.7
Deep water depth (h_0)	$3 \cdot H_{s,max}$	36.5
Water depth at toe ($h_{toe,min}$)	$\frac{H_{s,max}}{0.45}$	27.1

Table 10.1: Hydrodynamic requirements detailed research phase

In the preliminary research phase, the height of the structure was approximately 35cm. Therefore, the minimum depth requirements cannot be satisfied by that structure. A minimum height of the structure height of 45.2cm is set to allow test series with freeboards $R_c/H_{s,d} = 0.5$ and $R_c/H_{s,d} = 1.0$. The additional height also allows a test run with $H_{s,max} = 1.5 \cdot H_s$ for $R_c/H_{s,d} = 0.0$ and $R_c/H_{s,d} = 0.5$.

10.1.2. Structure modifications

The constructed crest width in the preliminary research phase was on average equal to $b/H_{s,d} = 1.1$ instead of the theoretical width of $b/H_{s,d} = 1.0$. The slightly wider crest made it easier to place rock filling between 2 back to back placed crest blocks. Therefore, a theoretical crest width of $B/H_{s,d} = 1.1$ is applied to the structure in the test series of the detailed research phase.

Initially, the toe structure was equal to the applied toe structure in the preliminary research phase. However, the armour layer slightly settled in a first test session. Therefore, both toe structures are reinforced with an additional gabion. A cross-section of the model set-up is presented in figure 10.1. All dimensions are in centimetres. The dashed lines indicate the water levels for $R_c/H_{s,d} = 0.0$, $R_c/H_{s,d} = 0.5$ and $R_c/H_{s,d} = 1.0$.

Performance optimised block

This chapter contains the test results of the optimised permeable block. Its performance is compared to the initial permeable block and the berm block that is placed at the Afsluitdijk. For the analysis of the modified test set-up is referred to appendix H.2.

11.1. Optimised permeable block

Six test series were executed to assess the performance of the optimised permeable block. All combinations of $R_c/H_{s,d} = 0.0$, $R_c/H_{s,d} = 0.5$, $s_{0,p} = 2\%$ and $s_{0,p} = 4\%$ were tested to get a better picture of the performance of the optimised permeable block. The test series with conditions $s_{0,p} = 2\%$ and $s_{0,p} = 4\%$ with zero freeboard were executed twice. Per condition, a trend line is drawn to get a better representation of a single condition. The failure progression of crest blocks is presented in figure 11.1. The percentage on the Y-axis shows the percentage of failed crest blocks related to the total number of crest blocks on the front and rear slope. The total number of crest blocks in the test set-up is 20. The X-axis represents the performed test runs expressed by the stability number.

Surprisingly, the normative wave steepness is not in line with the expected normative wave steepness for interlocking armour units. Instead of $s_{0,p} = 2\%$ being normative, the crest blocks were least stable for $R_c/H_{s,d} = 0.0$ and $s_{0,p} = 4\%$. The critical stability numbers for this condition are $N_{s,c} = 3.0$ and $N_{s,c} = 3.10$. The average of these critical stability numbers is just larger than the target stability number of 3.0.

No failure is observed in test series with wave steepness $s_{0,p} = 2\%$. Even an additional run with $H_s = 150\%$ $H_{s,d}$ did not result in failure of crest blocks. Moreover, failure is not observed in test series with relative freeboard $R_c/H_{s,d} = 0.5$. As a matter of fact, displacements were hardly observed in test series with $R_c/H_{s,d} = 0.5$. Despite the reduced water depth for $R_c/H_{s,d} = 0.5$, no differences could be observed in the extreme wave height distribution. Therefore, it can be concluded that the optimised crest block is very stable for $R_c/H_{s,d} = 0.5$.

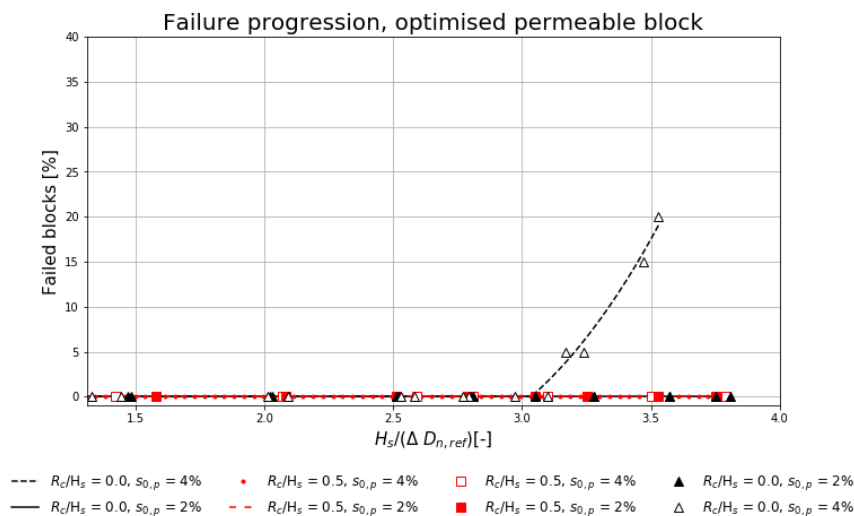


Figure 11.1: Failure progression for crest armoured with optimised permeable blocks

11.1.1. Displacements front slope

Displacements and their relation to failure of crest blocks, are further investigated for the test series with $R_c/H_{s,d} = 0.0$. Figures 11.2 and 11.3 show the failure and displacement progression of crest blocks on the front slope, caused by waves with steepness $s_{0,p} = 2\%$ and $s_{0,p} = 4\%$. Again, trend lines were used to merge the results of two test series into one. The percentage on the Y-axis shows the percentage of failed crest blocks related to the total number of crest blocks on the front slope. The displacement categories are specified in paragraph 5.2.2. Displacements of all categories appeared before failure. The scatter in the start of displacement was rather large for category 1 & 3 (resp. $\Delta N_s = 0.8$ and $\Delta N_s = 0.6$). However, the general displacement patterns of the individual test show similarity.

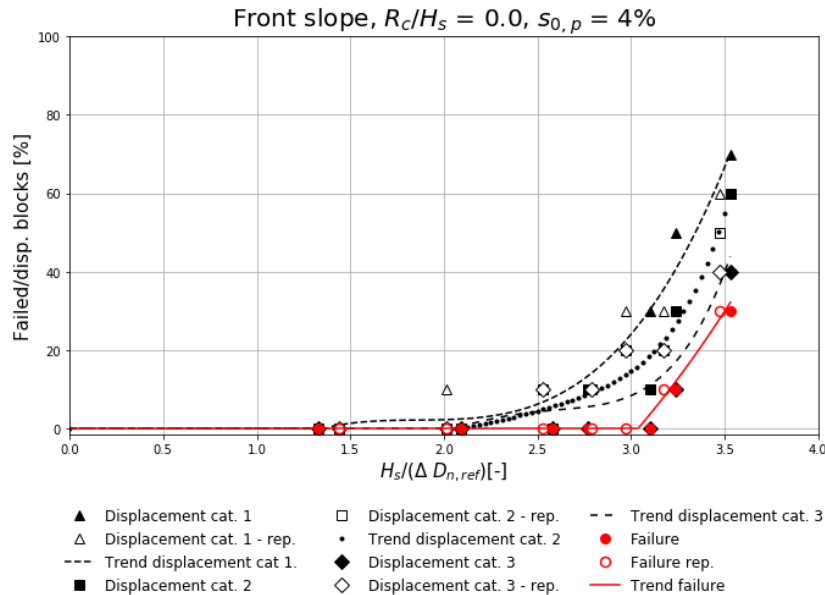


Figure 11.2: Front slope, failure and displacements ($R_c/H_{s,d} = 0.0$ & $s_{0,p} = 4\%$)

In contrast to the test series with $s_{0,p} = 4\%$, no crest blocks failed in the test series with $R_c/H_{s,d} = 0.0$ and $s_{0,p} = 2\%$. Neither displacements of category 2 & 3 were observed. The scatter in category 1 displacements was very large. This large difference might be caused by differences in placement before the start of the test series.

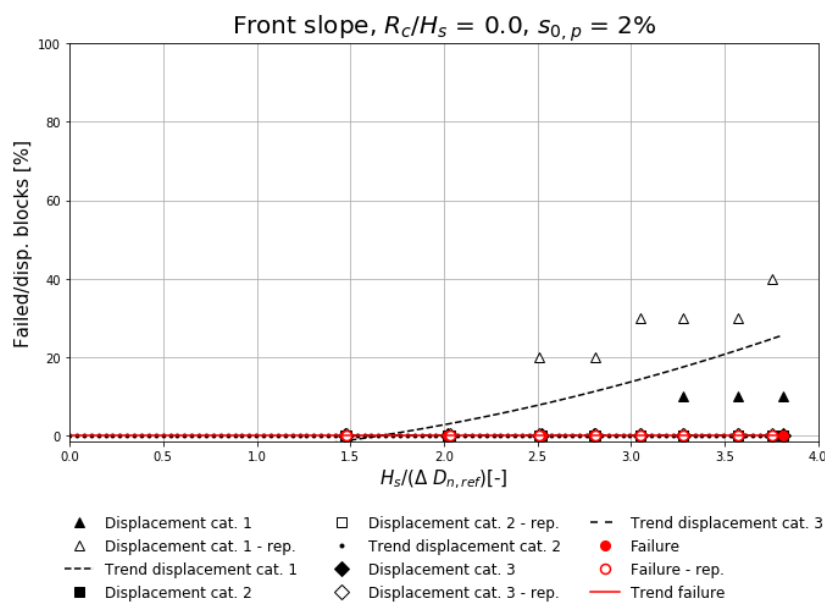


Figure 11.3: Front slope, failure and displacements ($R_c/H_{s,d} = 0.0$ & $s_{0,p} = 2\%$)

11.1.2. Displacements rear slope

Figure 11.4 shows the failure and displacement progression of the rear slope crest blocks exposed to waves with steepness $s_{0,p} = 4\%$. It becomes directly clear that the damage to blocks at the rear slope is much smaller compared to the blocks on the front slope. Failure of one crest block was observed in just one of the two test series. The crest block failed after failure of its neighbouring block on the front row.

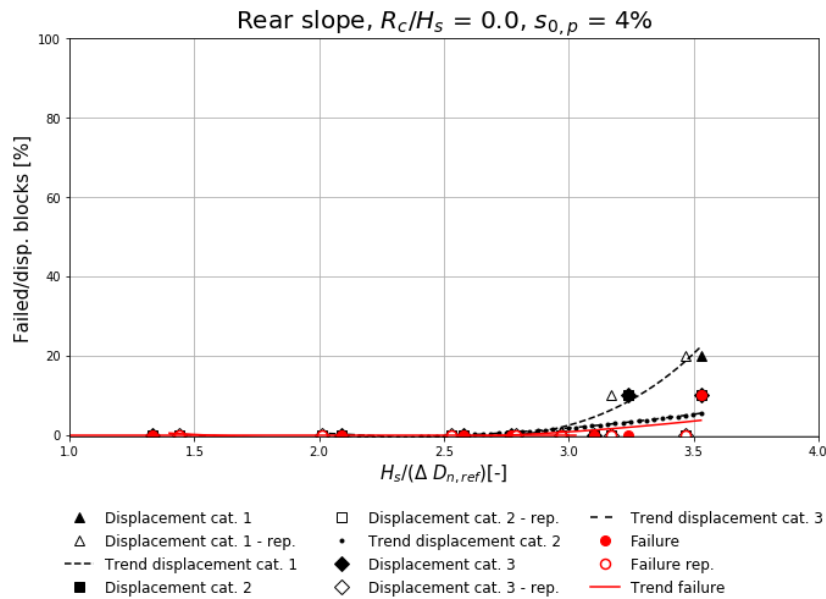


Figure 11.4: Rear slope, failure and displacements ($R_c/H_{s,d} = 0.0$ & $s_{0,p} = 4\%$)

For $s_{0,p} = 2\%$, damage to the crest blocks on the rear slope is even smaller. No failure occurred and displacements hardly occurred. The results are presented in Figure 11.5.

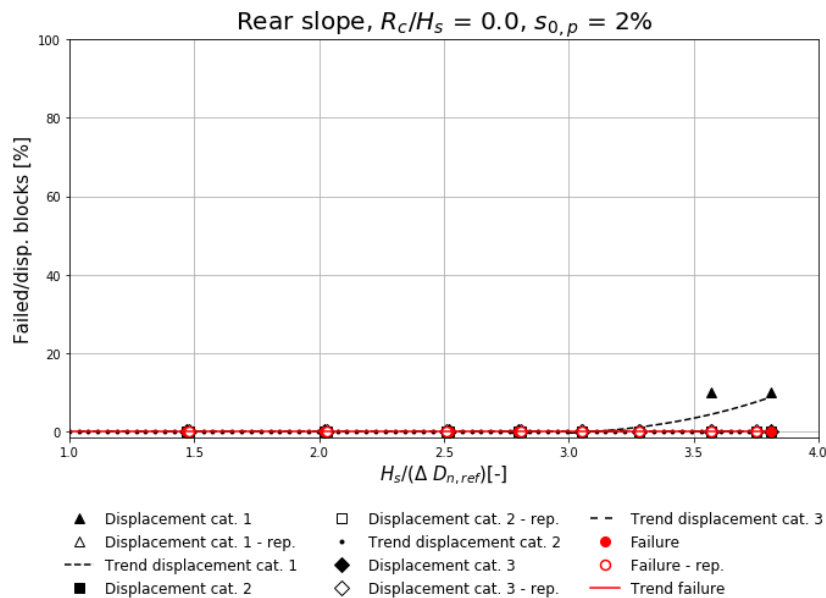


Figure 11.5: Rear slope, failure and displacements ($R_c/H_{s,d} = 0.0$ & $s_{0,p} = 2\%$)

11.1.3. Conclusion

From the test results of the optimised block can be concluded that it is least stable for $R_c/H_{s,d} = 0.0$ and $s_{0,p} = 4\%$. However, the target stability of $N_s = 3.0$ is met. Damage is predominantly caused to the crest blocks on the front slope. Therefore, it can be concluded that the crest blocks on the front slope are normative for the crest stability. $N_{s,c} \geq 3.8$ for the conditions $R_c/H_{s,d} \geq 0.0$ with $s_{0,p} = 2\%$ and $R_c/H_{s,d} = 0.5$ with $s_{0,p} = 4\%$. Only displacements of category 1 could be observed for $R_c/H_{s,d} = 0.0$ and $s_{0,p} = 2\%$. For $R_c/H_{s,d} =$

0.5, displacements were hardly observed. This makes it likely that the crest blocks were not close to their critical stability.

The combination of $R_c/H_{s,d} = 0.0$ and $s_{0,p} = 4\%$ appeared to be normative instead of $R_c/H_{s,d} = 0.0$ and $s_{0,p} = 2\%$. For waves with steepness $s_{0,p} = 4\%$, the wave breaking on the structure is close to the collapsing wave regime. It can be concluded that the crest block stability is most affected by the energetic impact that comes up with the collapsing waves. The large run-up caused by waves with 2% wave steepness has a smaller influence on the crest block stability (appendices A.4.1 and A.4.2).

The start of category 1 displacements seems not very predictable. The number of blocks that showed displacements of category 1 is probably most affected by their placement before the test. Displacements of category 3 were not always observed before failure. Displacements of category 2 were most suitable to relate displacements to failure of crest blocks. Although the results contain some scatter, ΔN_s between the start of category 2 displacement and failure was at most 0.6.

11.2. Comparison blocks

11.2.1. Initial permeable block

In this section, the failure progression of the optimised permeable block is compared to that of the initial permeable block. Thereby, the effectiveness of the block optimisation is assessed. The failure progression of both blocks is shown in figures 11.6 and 11.7. The percentage on the Y-axis represents the ratio between the number of failed crest blocks per slope and the total number of crest blocks on that specific slope. For waves of steepness $s_{0,p} = 4\%$, the optimised permeable blocks achieved a stability value of $N_{s,c} = 3.0$. The initial permeable block achieved $N_{s,c} = 2.8$. Waves with steepness $s_{0,p} = 2\%$ caused no failure of the optimised permeable block whereas one initial permeable block failed on the front slope. The stability values were respectively $N_{s,c} \geq 3.8$ and $N_{s,c} = 3.6$. Therefore, it can be concluded that the optimised permeable block performs better than the initial permeable block. The optimised block achieves higher stability values while it has a smaller volume than the initial permeable block.

The only crest block that failed in the test series with the initial permeable block and wave steepness $s_{0,p} = 2\%$, was the crest block next to the wall. As a result, there might be some influence of the wall. However, the test series with wave steepness $s_{0,p} = 4\%$ clearly indicate that the optimised block performs better than the initial block. Therefore, it can still be concluded that the optimised permeable block performs better than the initial permeable block.

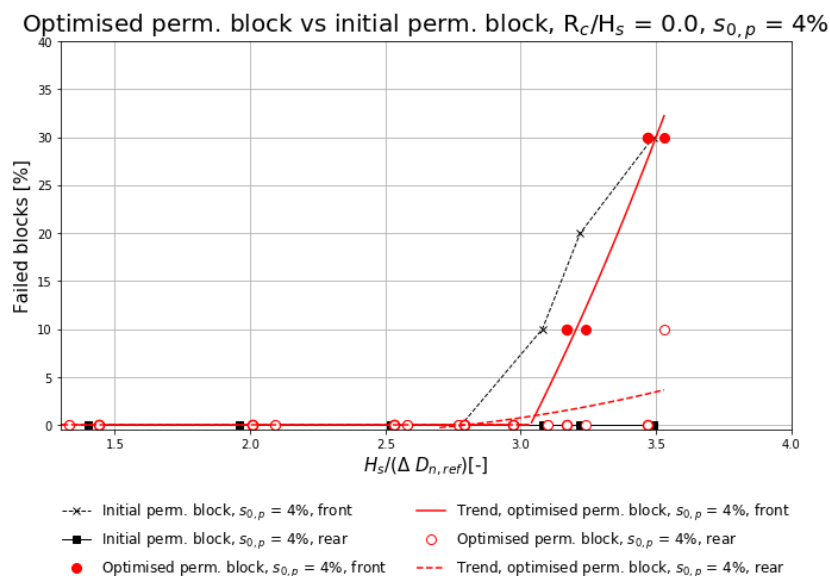


Figure 11.6: Optimised permeable block vs initial permeable block, $s_{0,p} = 4\%$

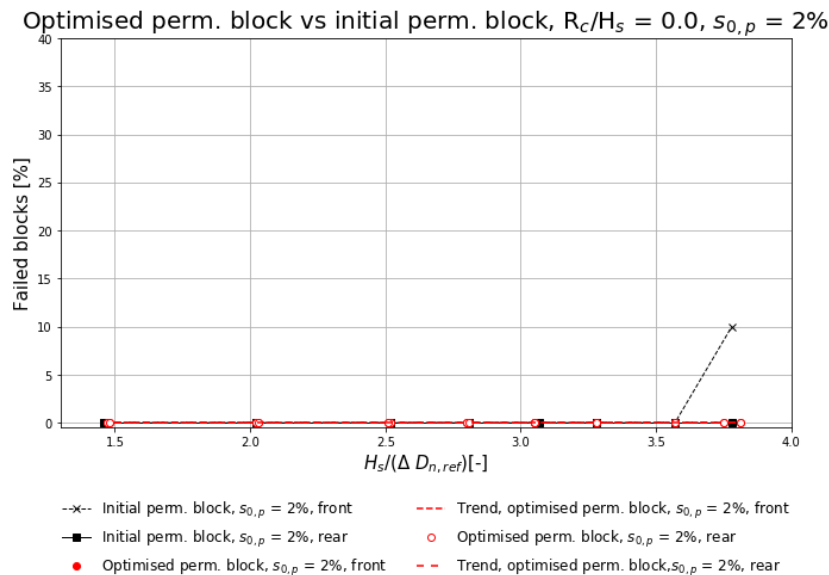


Figure 11.7: Optimised permeable block vs initial permeable block, $s_{0,p} = 2\%$

11.2.2. Berm block Afsluitdijk

The berm block is the only existing modified XblocPlus block so far. It is applied in the Afsluitdijk renovation project. The berm block is almost 5% longer than the optimised permeable block. However, it is much bulkier than the optimised permeable block. The berm block volume is 32% larger than the volume of the optimised permeable block. The dimensions of the berm block are presented in appendix C.2.2.

The performance of the final berm block design is merely tested in the Delta flume of Deltares. Small scale berm blocks were constructed and tested to compare the performance of the optimised permeable block to the performance of the berm block. In addition, a small scale test makes it possible to estimate the performance of the optimised permeable block on a larger scale. The blocks tested in the Delta flume are approximately factor 4000 heavier than the test blocks applied in the small scale tests.

11.2.3. Small scale test

Figure 11.8 shows an overview of the crest set-up with berm blocks. Rock is used to fill the semicircles of two neighbouring blocks. The rock should provide some interlocking.

The test results, presented in figure 11.9, clearly indicate that the berm block performed less than the optimised permeable block. A critical stability ($N_{s,c}$) of 2.8 is achieved for the berm block. $N_{s,c} = 3.0$ and $N_{s,c} = 3.1$ were achieved in the test series with the optimised permeable block. It can be concluded that the berm block performs less than the optimised permeable block while it is 32% heavier.

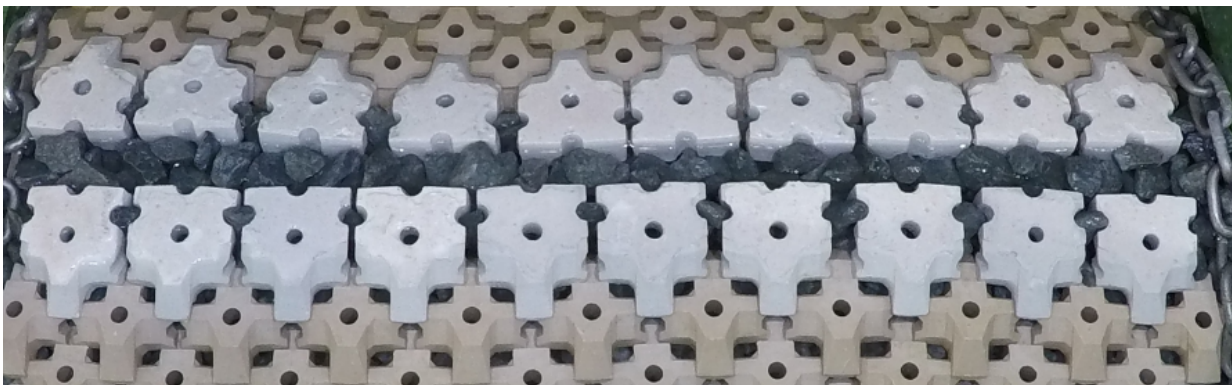


Figure 11.8: Crest armoured with berm blocks

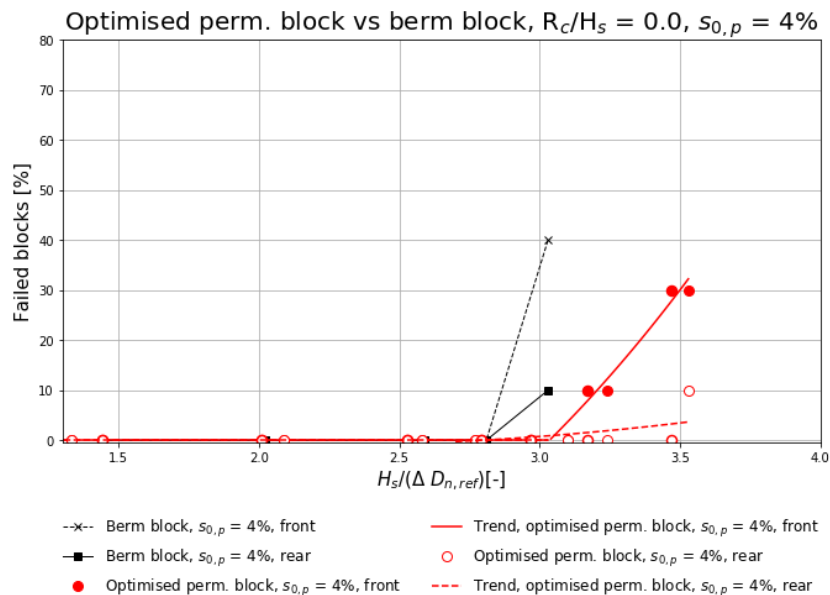


Figure 11.9: Berm block vs optimised permeable block

The failure mode of the berm block has some interesting points to mention. Due to displacements of the crest blocks, the rock between the blocks settled down. However, the rock should provide more stability by interlocking the crest blocks. Based on the small scale test, the increased stability generated by the interlocking is expected to be small. Another point to mention is that one block on the rear slope rolled over before failure of its neighbouring block on the front slope. This is not observed in any of the other test series.

11.2.4. Berm block Delta flume

The performance of the berm block in the small scale test is compared to the performance of the berm block in the Delta flume. However, a comparison of those test results is not completely fair due to differences in test setup. Differences in test setup and test conditions undoubtedly give different test results. Important parametric differences and their effect on the crest block stability are explained before comparing the results of the small scale test and the Delta flume test [22].

- Armour:

- The armour slope was 1V:2H in the Delta flume test whereas it was 3V:4H in the small scale test.
- The Delta flume structure had no rear slope. In contrast to the small scale test, a stiff concrete element behind the berm block had to prevent its backwards displacement. The crest block stability at the front slope is normative for the entire crest. Therefore, this difference is not expected to have a major influence on the comparison of the berm block test results.

- Wave height:

- H_s in the Delta flume test is measured in relatively deep water located approximately 25m located from the breakwater toe. Numerical model tests demonstrated that $H_s \approx 1.06 H_{s,toe}$. However, no measurement of $H_{m0,toe}$ is available. Therefore, H_{m0} is used in the stability number. This slightly overestimates the stability of the berm blocks in the Delta flume test.
- At first sight, the wave height distribution of the Delta flume test and the small scale test seem comparable (Delta flume test: $H_{2\%}/H_s = 1.4$ & $H_{max}/H_s = 1.85$, small scale test: $H_{2\%}/H_s = 1.34$ & $H_{max}/H_s = 1.93$). However, in the Delta flume test, these values were measured at 25m from the toe. The water depth at the toe was approximately 50% of the water depth in the deep section. The reduced H_s value at the toe indicates that wave breaking did occur. This is in line with the observations mentioned in the test report. As a result, H_{max}/H_s & $H_{2\%}/H_s$ at the toe are expected to be smaller than in the small scale test. Considering that the block stability is affected by the largest waves in the wave distribution, the berm block stability is expected to be higher in the Delta flume test.

- Breaking regime:
 - In the Delta flume test and in the small scale test, the $s_{0,p}$ values were resp. 0.047 and 0.043. In combination with the armour slope, surf similarity values of respectively $\xi_{m-1,0} = 2.1$ and $\xi_{m-1,0} = 3.3$ were achieved (appendices A.3.2 and A.4.1). Consequently, the collapsing waves in the Delta flume are expected to cause more damage to the crest blocks than the surging waves in the small scale test.

In the Delta flume test, no failure occurred. Based on the deep water wave height, the berm blocks remained stable till $N_s = 2.95$. The berm blocks in the small-scale test remained stable until a stability number of 2.8. Considering the differences just mentioned, stability differences appear to be small. Substitution of the deep water wave height by the estimated wave height at the toe ($H_{s,toe}$) also gives a stability number of 2.8. The critical stability value of the small-scale test seems comparable to that Delta flume test. However, the different conditions make a straight comparison hard. The optimised permeable block performed much better than the berm block that was tested on a small scale. Therefore, it would be likely that the optimised permeable block would also have achieved a higher stability number in the Delta flume. However, it is ambitious to claim it.

11.2.5. Summary of all blocks

Figure 11.10 gives a stability overview of all tests in the detailed research phase. The wave steepness is on the X-axis and the critical stability number ($N_{s,c}$) is on the y-axis. The obtained stability in the Delta flume test is also shown in the overview. The optimised permeable block performs best. However, it has the smallest block volume of all tested alternatives. The condition $R_c/H_{s,d} = 0$ & $s_{0,p} = 4\%$ is the normative condition for all blocks. In two test sessions of the initial permeable block with conditions $s_{0,p} = 2\%$ and $R_c/H_{s,d} = 0.0$, the critical stability number was significantly lower than the obtained stability number in a third test. Paragraph 11.3 further elaborates on that.

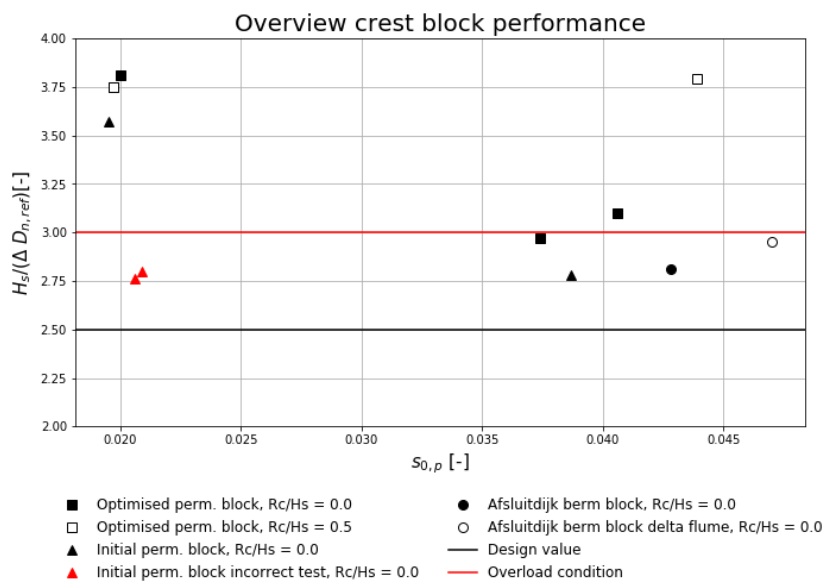


Figure 11.10: Crest stability of all tests

Just like in the preliminary research phase, a gain factor is used to indicate the block efficiency (paragraph 8.1). Again, the reference parameters ($N_{s,ref}$ and V_{ref}) are based on an original XblocPlus block. The critical stability number, found in the test session with the normative condition ($R_c/H_{s,d} = 0.0$, $s_{0,p} = 4\%$), is used as input for the computation. The results are shown in table 11.1. The high gain factor of the optimised permeable block clearly indicates that it performs better than the initial permeable block and the berm block.

11.3. Placement accuracy

As mentioned in the previous paragraph, the critical crest stability of the initial permeable block in test series 2.3.1 and 2.3.2 appeared to be much lower than the critical stability number found in test series 2.3.3. The lower performance is caused by loss of interlocking and underlayer variations.

Block	Gain factor (G)
Optimised permeable block	2.10
Initial permeable block	1.75
Afsluitdijk berm block (Delta flume)	1.57
Afsluitdijk berm block (small scale)	1.50

Table 11.1: Block efficiency detailed research phase

11.3.1. Interlocking

During test series 2.3.1, the entire front armour layer settled due to insufficient toe stability. As a result, the interlocking capacity of the crest blocks reduced because the space between the crest blocks was too large for the present filling material to lock them up. Settling of the armour blocks is a mechanism that is not of major importance for this research. However, it strikes the importance of the interlocking of crest blocks exposed to waves with steepness $s_{0,p} = 2\%$.

For steepness $s_{0,p} = 4\%$, the interlocking might be less important than for steepness $s_{0,p} = 2\%$. The test series with the initial and the optimised permeable blocks, exposed to critical condition $R_c/H_{s,d} = 0.0$ & $s_{0,p} = 4\%$, might indicate that. In both tests, one or two crests blocks displaced in a way that the interlocking effect disappeared. These blocks didn't fail quickly after displacement. The difference between $s_{0,p} = 2\%$ and $s_{0,p} = 4\%$ might be caused by the mechanism that causes failure. Interlocking could be more important to withstand the large up-rush for $s_{0,p} = 2\%$. On the contrary, the interlocking might be less important to withstand the energetic wave impact of waves close to the collapsing regime ($s_{0,p} = 4\%$).

11.3.2. Underlayer variations

In test series 2.3.2, the crest blocks remained stable till $N_{s,c} = 2.8$. Just after the start of the test series was observed that a few crest blocks were not resting with their nose on the XblocPlus blocks in the row beneath (figure 11.11). As a result, the nose became more exposed to the wave load than is the case for a correctly placed crest block (figure 11.12). The area of the nose, that is exposed to the wave load, is indicated by a green plane.

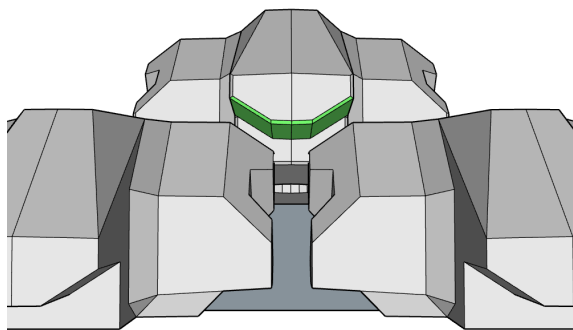


Figure 11.11: More exposed block due to incorrect placement

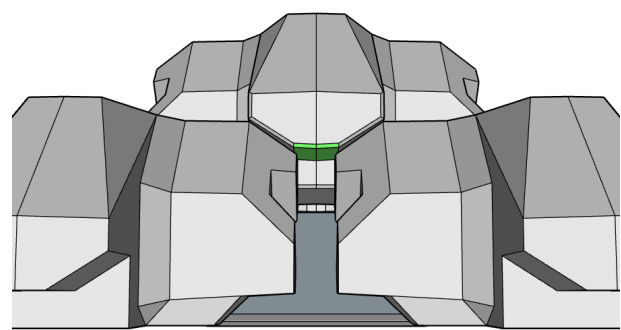


Figure 11.12: Correct placed block

The block's nose becomes more exposed to the wave forcing if it is tilted forwards compared to its ideal position. This is caused by underlayer deviations at the crest. Like mentioned in paragraph 7.1.1, the height of the constructed underlayer should deviate at most $0.5 \cdot d_{n50,underlayer}$ from the design profile. However, the underlayer level at the crest should be sufficiently high to prevent the crest blocks from being tilted forwards. Theoretically, for a crest block exactly at his design position, the underlayer should not be lower than the theoretical level and it should be at most $+0.5 \cdot d_{n50,underlayer}$ higher than the theoretical height. This reduces the tolerance interval by 50%. However, in practice, the crest blocks are not exactly at its theoretical position. This makes it harder to indicate the effect on the tolerance margins.

The importance of the placement accuracy may depend on the block shape and the wave conditions. Theoretically, the consequence of the incorrectly placed blocks is larger for blocks that fail due to rotational instability than for blocks that fail due to uplift. This has to do with the large distance between the nose and the rotation point. The large distance makes the contribution of the block's nose to the overturning moment

relatively large. The optimised permeable blocks fail, for wave steepness $s_{0,p} = 4\%$, mainly due to uplift. However, this could be different for $s_{0,p} = 2\%$ (paragraph 11.4). The wave steepness might also affect the importance of the placement accuracy. The influence of the large run-up velocity, caused by waves with steepness $s_{0,p} = 2\%$, might be larger than the influence of energetic wave breaking caused by waves with steepness $s_{0,p} = 4\%$. Moreover, for wave steepness $s_{0,p} = 4\%$, displacements of crest blocks before failure were relatively large. Consequently, the initial position of the crest blocks is expected to be less important. However, further research into the tolerance bounds is required to assess what deviations are acceptable.

11.4. Failure mode

The failure mode of the crest blocks on the front row is assessed to acquire knowledge about the destabilising mechanisms that cause failure. Crest block failure on the rear slope is neglected because it happened for one block in a single test. This makes it nearly impossible to draw conclusions about the failure of crest blocks on the rear slope.

Per failed block is indicated whether the block failed due to uplift or rotational instability. All test results, including the data of incorrect tests mentioned in the paragraph 11.3, are used to find a pattern. Although those tests were incorrect, the failure mode of these blocks gives useful information. This means that data of 3 tests are used to assess failure of the initial permeable block for condition $R_c/H_{s,d} = 0.0$ & $s_{0,p} = 2\%$. The test results of the optimised permeable block, exposed to $R_c/H_{s,d} = 0.0$ & $s_{0,p} = 4\%$, are also taken together. Per single test is assessed whether the blocks failed due to uplift or rotational instability. The results are given in table 11.2. Important to mention is that 2 failed blocks (1 for optimised permeable block with $R_c/H_{s,d} = 0.0$ & $s_{0,p} = 4\%$ and 1 for the initial permeable block with $R_c/H_{s,d} = 0.0$ & $s_{0,p} = 4\%$) are left out of the assessment since the way they failed couldn't be assessed properly.

Block	$R_c/H_{s,d}$	$s_{0,p}$	Uplift	Rot. instability	Tot. failed blocks
Initial permeable block - preliminary phase	0.0	2%	1	2	3
Initial permeable block	0.0	2%	3	3	6
		4%	1	1	2
Optimised permeable block	0.0	2%	0	0	0
		4%	4	1	5

Table 11.2: Failure cause initial and optimised permeable blocks

In the detailed research phase, the number of initial permeable blocks that failed due to uplift is in balance with the number of blocks that failed due to rotational instability. The results seem to be independent of the wave steepness. Important to mention is that the results slightly differ from the results of the initial permeable block in the preliminary research phase. In the preliminary research phase, 2 out of 3 failed blocks failed due to rotational instability. The third block failed due to a combination of uplift and rotational instability.

In contrast to the initial permeable block, uplift dominates failure for the optimised permeable block for wave steepness $s_{0,p} = 4\%$. The failure mode for $s_{0,p} = 2\%$ cannot be assessed due to absence of failure. The different failure mode might be caused by the applied streamlining measures that make it easier for the water to flow through and along the block. This results in and a lower pressure build-up below the block and so smaller drag and lift forces. Presumably, the optimised block shape reduced the drag force slightly more than the lift force. Therefore, uplift started dominating the failure mode.

Another plausible reason is that the weight distribution over the block changed. Most volume reduction took place at the rear half of the block. As a result, the centre of gravity (COG) slightly shifted towards the centre of the block. That could have resulted in an increased probability of the block being lifted up instead of rotated. An assessment of the relative position of the block's centre of gravity to the block length indicates that this is not the case. The horizontal distance between the rotation point and the centre of gravity is compared to the block length. These numbers, and the ratio between these numbers, are presented in table 11.3. The starting block, the initial permeable block and the optimised permeable block have roughly equal ratios. In contrast to the uplift that mainly caused failure of the optimised permeable blocks, the rotational instability caused failure of the starting blocks. This makes it not very likely that the

COG position relative to the total block length resulted in a different failure mode. However, it might have contributed slightly.

Block	Length	Hor. distance COG - rotation point	Ratio
starting block (preliminary phase)	2.06 $D_{n,ref}$	1.23 $D_{n,ref}$	0.403
Initial permeable block	2.06 $D_{n,ref}$	1.22 $D_{n,ref}$	0.406
Optimised permeable block	2.01 $D_{n,ref}$	1.18 $D_{n,ref}$	0.414

Table 11.3: Location COG

11.5. Wave transmission

The wave transmission was measured to acquire information about the effectiveness of the breakwater. The effectiveness is assessed by comparing the XblocPlus wave transmission with the theoretical wave transmission equation for rock (appendix A.4.4.1). The results are shown in figure 11.13. It clearly indicates that the wave transmission for XblocPlus armoured breakwaters is lower than for rock armoured breakwaters. This is independent of the relative freeboard and the wave steepness. Deviations between the theoretical transmission for rock and the measured transmission for XblocPlus become larger for increasing wave height. The type of crest bock on the structure hardly affects the wave transmission.

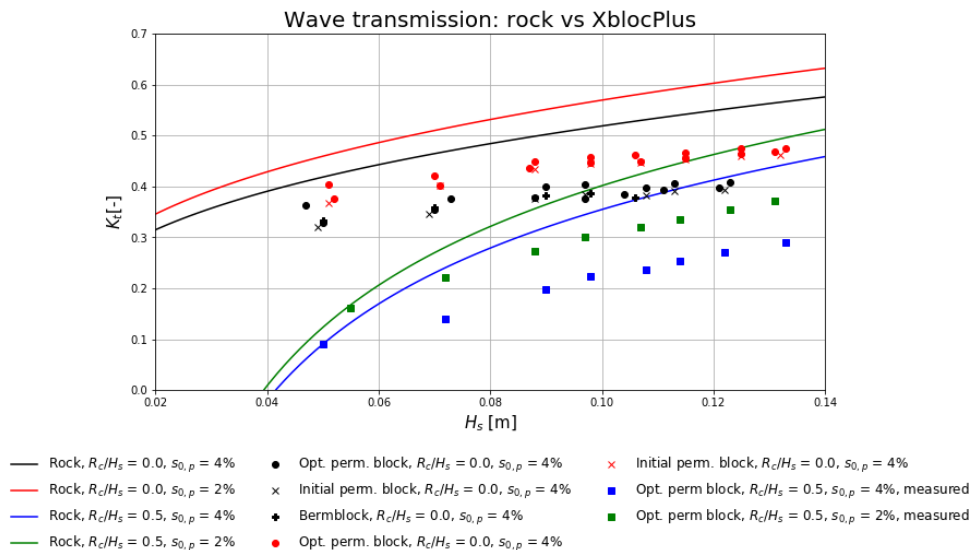


Figure 11.13: Comparison wave transmission for XblocPlus and rock

11.5.1. Stability rear crest armour

The wave load caused more damage on the top row of the front slope compared to the top row on the rear slope. However, it does not automatically mean that the rear slope crest armour is more stable than the front slope crest armour. This is primarily caused by the sheltered position of rear slope crest blocks behind the crest blocks on the front slope, the underlayer and the core. As a result, the load of the incoming waves on the rear slope crest armour is smaller than the wave load on the front slope armour. The critical stability number of the rear slope is determined with the transmitted wave height $H_{s,t}$. Per test, the rear slope stability number is shown in table 11.4. The '≥' sign is used if no crest blocks on the rear slope failed.

Block	$R_c/H_{s,d}$	$s_{0,p}$	$N_{s,rear}$
Initial permeable block	0.0	2%	≥ 1.75
		4%	≥ 1.37
Optimised permeable block	0.0	2%	≥ 1.76
		4%	1.32
	0.5	2%	≥ 1.40
		4%	≥ 1.11
Berm block Afsluitdijk	0.0	4%	1.08

Table 11.4: Stability rear slope crest armour

It is worth mentioning that the rear slope armoured with the optimised permeable block seems less stable than the initial permeable block for $R_c/H_{s,d} = 0.0$ & $s_{0,p} = 4\%$. However, one optimised permeable block on the rear slope failed after it became more exposed to the waves. The increased wave load was caused by failure of a neighbouring block on the front slope. This makes a fair comparison impossible. Second, it becomes clear that the increasing freeboard causes a strong reduction in the transmitted wave height. It confirms that the crest becomes less exposed to the wave load when the freeboard increases.

11.5.2. Comparison with target crest width

In chapter 3 was theoretically assessed how effective heightening and widening of the crest are for wave transmission reduction. The wave transmission equation for rock was used in this assessment to determine the target crest width. It was assumed that comparable values of the reflection coefficient and the friction factor would result in comparable wave transmission results. The test results of the optimised block with $R_c/H_{s,d} = 0.0$ and $R_c/H_{s,d} = 0.5$ make it possible to assess whether this assumption was right.

The results of the wave transmission reduction, caused by the shift in relative freeboard from $R_c/H_{s,d} = 0.0$ to $R_c/H_{s,d} = 0.5$, are indicated by the squares in figure 11.14. The test series with $R_c/H_{s,d} = 0.5$ were performed by lowering the water level instead of heightening the structure. Therefore, the cross-sectional area growth (X-axis) for the XblocPlus armoured structure is artificially created to make the comparison possible. No differences in H_s , $H_{2\%}/H_s$ and $H_{1\%}/H_s$ could be observed. This makes it very likely that the wave height distribution was not affected by the reduced water depth. As a result, the same results were obtained if the structure was heightened.

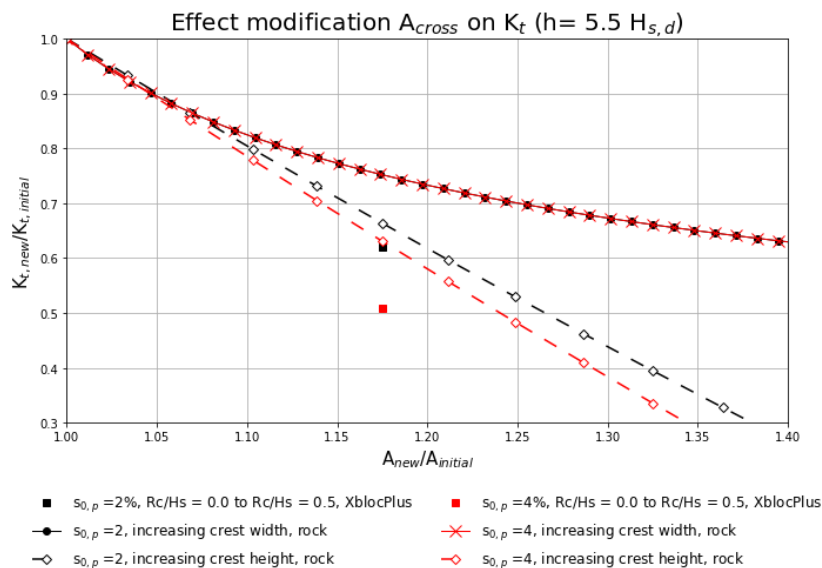


Figure 11.14: Effect cross-section modifications on wave transmission

The effect of the increased crest height on the wave transmission reduction for XblocPlus armoured structures is comparable to the reduction for rock structures. An XblocPlus armoured structure causes a slightly

stronger reduction in wave transmission. There are no data available about the reduction of the wave transmission reduction after an enlargement of the crest width. However, the current results make it possible to conclude that, for height modifications, the wave transmission reduction for XblocPlus armoured structures behaves similar to structures armoured with rock. Presumably, the same holds for width modifications. To concluded, no large mistakes were made by assuming that a relatively high structure with a small crest is preferred above a relatively low structure with a wide crest.

11.6. Important notes

In this section, some important observations are addressed:

- **Crest width:** In theory, the crest armoured with the optimised crest blocks has a width of 10.7cm. This is $1.1 H_{s,d}$, where $H_{s,d}$ is the design wave height for XblocPlus with a correct relative density of 1.36. In the flume tests the crest width varied between 10.5 and 12cm ($1.06 \leq B/H_{s,d} \leq 1.21$). The maximum crest width in the flume is larger than the maximum theoretical crest width. However, no errors are expected. It only required more filling material between the crest blocks.
- **Erosion filling material:** Filling material eroded in every test. During construction, as much as possible rock is placed between the crest blocks. Surplus rock eroded predominantly in early test runs and in test runs that caused failure of crest blocks. On average, slightly more than 10 stones eroded in a test series. The erosion of filling material is not related to the varying crest width. Figure 11.15 gives an indication of the filling material erosion.



Figure 11.15: Erosion filling material

Discussion

12.1. Handmade crest blocks

The modified crest blocks were handmade. As a result, every crest block is unique and variations in weight, volume and density appear. The wave program for modified crest blocks is based on a density of 2200 kg/m³ because all block types have a mean density close to that value. Mean values and 95% confidence intervals are used to indicate the effect of weight, volume and density variations on the block stability. The results, based on the block data in appendix E, are shown in table 12.1. The stability number represents the critical stability number that is based on the last successful test run session without failure of crest blocks. Since the optimised permeable block is tested twice, two stability ranges are presented in the table. From the stability ranges can be concluded that the target stability number of 3.0 is not necessarily met.

Block	\bar{W} (g), CI _{95%}	\bar{V} (mm ³), CI _{95%}	$\bar{\rho}$ (kg/m ³), CI _{95%}	$\bar{N}_{s,c}$ (-), CI _{95%}
Initial permeable block	84.4, (82.2, 86.6)	38675, (37531, 39819)	2182, (2122, 2242)	2.8, (2.7, 3.0)
Optimised permeable block	76.3, (75.3, 77.3)	34440, (33508, 35372)	2215, (2161, 2269)	3.0, (2.8, 3.1)
				3.1 (2.9, 3.2)

Table 12.1: 95% confidence intervals

The scatter in the block density data causes overlap in the stability ranges of the initial permeable block and the optimised permeable block. From the intervals can be obtained that a higher stability number of the optimised permeable block cannot be guaranteed. However, the volume confidence intervals show something remarkable. The theoretical block volumes (resp. 39781 mm³ and 35423 mm³ for the initial permeable block and the optimised permeable block) are relatively close to the upper bound of the confidence intervals. For both blocks, the mean measured block volume is approximately 3% smaller than the theoretical block volume. Small deviations may be caused by inaccuracies. These rather large deviations might have another cause, for example the method that is used to determine the block volume of each block (appendix D). Although the applied method is simple, it is not the most accurate method since it induces errors rather easy. For both blocks, the difference between the measured and the theoretical volume is of equal magnitude. This suggests that the obtained measurement errors are more or less equal for both blocks. The density of both blocks might be overestimated due to the underestimated block volumes. Consequently, both blocks possibly have a higher stability number than presented in the test results. Table 12.2 shows the 95% confidence intervals of the density and the stability numbers based on the theoretical block volume. The theoretical volume is used to indicate the effect of a more accurate volume determination method that probably measures volumes closer to the theoretical block volumes. The stability values obtained with the theoretical block volumes are between 3 and 7% higher than the stability values obtained with the measured block volumes.

Block	$\bar{\rho}$ (kg/m ³), CI _{95%}	$\overline{N_{s,c}}$ (-), CI _{95%}
Initial permeable block	2122, (2066, 2177)	(2.8, 3.1)
Optimised permeable block	2154, (2126,2182)	3.1, (3.0, 3.2)
		3.2 (3.1, 3.3)

Table 12.2: 95% confidence intervals with theoretical block volume

12.2. Foreshore

The presence of the foreshore appears to have a significant influence on the crest block stability. Although no large differences could be observed in the wave height distribution, stability differences were large. The large stability differences caused by the foreshore could not be assigned to a specific mechanism. However, the influence of a certain mechanism could be larger or smaller without a foreshore. That might have affected the test results and thereby the performance of the optimised permeable block.

12.3. Target volume reduction

The target volume reduction that is specified for the initial permeable block to transform it in an optimised version, is based on the rotational stability number (chapter 9). Some uncertainty is involved in this method because the target volume reduction is based on the assumption that the drag force is twice as large as the lift force. It did result in an optimised permeable block that reaches the target stability for all wave conditions. However, it is hard to conclude whether the applied drag over lift ratio is sufficiently close to the real drag over lift ratio. The applied streamlining measures, which did not lead to volume reduction, also have a beneficial impact on the block stability. Consequently, it becomes complicated to assess the correctness of the assumed drag over lift ratio. Numerical model tests are required to obtain that answer.

In the test series with a foreshore (preliminary research phase), the normative failure mode of the initial permeable blocks differed from normative failure mode found in the test series without a foreshore. The rotational stability turned out to be normative in the test series with a foreshore (preliminary research phase). The target volume reduction with the rotational stability number is based on that result. In the test series without a foreshore (detailed research phase), the number of blocks that failed due to rotational instability was equal to the number of blocks that failed due to uplift. Consequently, the decision to base the target volume reduction on the rotational stability number becomes somewhat doubtful. It cannot be fully guaranteed that the applied method is the best method to determine the volume reduction.

12.4. Wall effect

The crest block stability near the walls of the 60cm wide wave flume might be influenced these the walls. A consideration would be to neglect the blocks next to the wall in the stability analysis. This reduces the number of crest blocks in the assessment from 10 to 8. However, in one test series of the preliminary research phase, the 2 leftmost blocks were influenced by the wall. Always taking out the first 2 crest blocks next to the wall reduces the number of crest blocks in the assessment to 6 blocks. By taking just 6 blocks in the assessment makes the impact of one block rather large. As a result, a small number of blocks in the assessment causes a relatively large scatter in the results. No wall influence is observed in most of the tests. Consequently, the impact of the reduced number of crest blocks in the assessment is expected to be larger than the possible wall influence. However, influence of the wall could be unnoticed.

Conclusions and recommendations

In this chapter, the research questions are answered to form the conclusions of this study. Recommendations for further research are formed based on the conclusions.

13.1. Conclusions

The main research was defined as follows:

What crest configuration(s) for low crested XblocPlus armoured breakwaters result(s) in the best hydraulic performance with respect to the economically most feasible breakwater dimensions?

Specification of the phrase 'best hydraulic performance with respect to the economically most feasible breakwater dimensions' have resulted in requirements regarding the stability and the crest width. The designs of the crest configurations with XblocPlus crest armour and modified XblocPlus crest armour were based on these requirements.

- The hydraulic performance of the crest is indicated by the stability number. The critical stability ($N_{s,c}$; Stability just before failure of the first crest block) value should be equal or larger than the target stability of 3.0.
- The economically most feasible breakwater dimensions depend on wave transmission, overtopping and construction. Regarding the cross-sectional area of a breakwater, increasing the crest level turns out to be more effective than widening the crest if wave transmission and/or overtopping requirements are violated. Consequently, the economically most feasible breakwater dimensions are achieved by a structure with the recommended minimum relative crest width ($B/H_{s,d} = 1$). Therefore, a crest configuration should meet the target stability and its relative crest width should be as close as possible to $B/H_{s,d} = 1$.

13.1.1. XblocPlus crest armour

Table 13.1 contains test results of test series with XblocPlus crest armour.

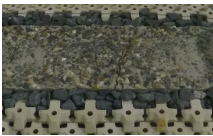



Name	Overview crest	Overview block	V/V_{ref}	$B/H_{s,d}$	$N_{s,c}$
XblocPlus top row large crest element (Reference situation)			1	2.7	2.4
XblocPlus top row small crest element			1	1.9	2.6

Table 13.1: Performance of XblocPlus crest armour

Three conclusions can be drawn about crest configurations with original XblocPlus armour that are exposed to conditions $R_c/H_{s,d} = 0.0$ and $s_{0,p} = 2\%$:

- Despite the support of the rock fill and the concrete element, the XblocPlus armour on the top row of the front slope does not meet the target stability of 3.0. It can be concluded that the weight of the XblocPlus blocks on the front top row is too small to withstand the destabilising forces.
- Damage to the crest starts at the top row of the front slope. The crest blocks on the rear slope are less affected by the wave load.
- The crest width becomes very wide due to the supporting crest element. Even a relatively small crest element results in a crest width that is almost double the target crest width.

13.1.2. Modified XblocPlus crest armour

13.1.2.1. General block shape

The performance of several modified XblocPlus blocks is summarised in table 13.2. The stability numbers are obtained after test series with conditions $R_c/H_{s,d} = 0.0$ and $s_{0,p} = 2\%$.


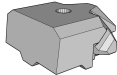

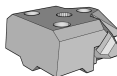

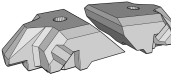

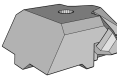
Name	Overview crest	Overview block	V/V_{ref}	$B/H_{s,d}$	$N_{s,c}$
Starting block			1.77	1.1	3.2
Permeable block			1.62	1.1	3.1
Interlocking blocks			1.72 & 1.71	1.0	2.8
Extended bottom block			1.76	1.1	2.8

Table 13.2: Modified XblocPlus crest armour, concept study

Conclusions about modified XblocPlus crest armour are presented by 5 bullet points:

- Crest configurations with modified XblocPlus blocks are more stable than crest configurations with original XblocPlus blocks and a supporting crest element. The crest blocks on front slope are normative for the crest stability. Failure starts at the front slope where crest blocks fail due to rotational instability. Damage to the crest blocks at the rear slope does barely happen.
- Rock between back to back placed crest blocks is an effective measure to lock them up. The interlocking enhances the crest stability. The almost vertical back of the starting block and the permeable block makes the interlocking very effective. The extended bottom block, which is designed to enlarge the resistance against rotation, is less stable than the starting block. The lower stability is caused by the less effective interlocking between the crest blocks and the rock fill. The enlarged resistance against rotation caused by its sloped back does not compensate the reduced interlocking capacity. The same applies to the set of interlocking blocks. The crest block on the rear slope (block with long top) should enlarge the resistance against rotation of the crest block on the front slope (block with short top). However, the crest blocks on the front slope push the crest blocks on the rear slope to a less favourable position. This less favourable position causes failure of the crest blocks on the rear slope. Compared to back to back placed starting blocks, the interlocking between the interlocking

blocks is less effective. As a result, a crest armoured with interlocking blocks is not as stable as a crest that is armoured with starting blocks.

- Underlayer rock as filling material is effective to lock up the crest blocks. Surplus rock between the back to back placed crest blocks is likely to erode. The crest stability is not affected by the erosion of surplus rock.
- Compared to the reference situation, the relative crest width is much smaller for crest configurations with modified XblocPlus.
- Increasing the block's permeability is an effective measure to reduce the block weight without reduction of the crest stability. Without wall influence in the test series of the permeable block, its stability would probably be even higher than the stability of the starting block.

13.1.2.2. Detailed block shape

By further optimisation of the permeable block, an increased crest stability can be achieved with significantly smaller crest blocks. The optimised permeable block performs better than the initial block for wave steepnesses 2% and 4% ($s_{0,p}$). The stability results of the initial and the optimised permeable blocks are summarised in table 13.3. The absence of a foreshore makes the test results of the permeable block different from the results in table 13.2. A combination of measures contributes to the improvement of the block efficiency:

- Streamlining measures: The modified bottom profile and the modified region just behind the block wings facilitate the flow from the wings to the 2 holes at the rear part of the block.
- Improving the permeability: The 8% enlargement of the diameter of the 3 additional holes increased the block's permeability.
- Effective weight reduction: Enlargement of the tolerance margins at the bottom of the rear part of the block reduced the block volume without significant stability loss.

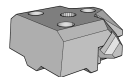
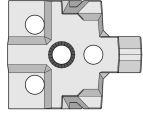
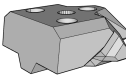
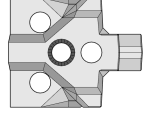
Name	Overview	Bottom view	V/V_{ref}	$B/H_{s,d}$	$s_{0,p}$	$R_c/H_{s,d}$	$N_{s,c}$
Permeable block			1.62	1.1	2%	0.0	3.6
					4%	0.0	2.8
Optimised permeable block			1.44	1.1	2%	0.0	≥ 3.8
						0.5	≥ 3.8
					4%	0.0	3.0
						0.5	≥ 3.8

Table 13.3: Performance optimised permeable block

13.1.3. Performance at varying wave conditions

The optimised permeable block meets the target stability for all combinations of $R_c/H_{s,d} = 0.0$, $R_c/H_{s,d} = 0.5$, $s_{0,p} = 2\%$ and $s_{0,p} = 4\%$. However, the wave steepness and the relative freeboard do affect the crest stability:

- Wave steepness: The lowest crest stability is obtained if the structure is loaded by waves with 4% wave steepness in combination with zero freeboard ($R_c/H_s = 0.0$). The surf similarity parameter indicates that the wave breaking on the structure is close to the collapsing wave regime. It can be concluded that the crest block stability is most affected by the energetic impact caused by the collapsing waves. The large run-up caused by waves with 2% wave steepness has a smaller influence on the crest block stability.
- Relative freeboard: From test series with 4% wave steepness can be concluded that the crest stability number is lowest for structures with zero freeboard. None of the crest blocks failed for waves with 2% steepness. However, the smallest displacements in test series with $R_c/H_{s,d} = 0.5$ were less frequently observed than in test series with $R_c/H_{s,d} = 0.0$. Consequently, crest blocks loaded by waves with 2% steepness are also less stable for $R_c/H_{s,d} = 0.0$.

13.1.4. Performance optimised permeable block

The main objective of this research was to find a crest configuration with the best hydraulic performance with respect to the economically most feasible dimensions. Of all tested variants, a crest armoured with the optimised permeable block has the best hydraulic performance with respect to the economically most feasible breakwater dimensions. The target stability is met and the crest width is just 10% larger than the target crest width. The crest blocks have a volume that is 44% larger than the original XblocPlus volume. In comparison to the berm block applied at the Afsluitdijk, the optimised permeable block is a very efficient block. The berm block is the only applied modified XblocPlus block in a real-life project so far. The volume of the berm block is 32% larger than the volume of the optimised permeable block. However, at critical conditions $R_c/H_{s,d} = 0.0$ and $s_{0,p} = 4\%$, the berm blocks are less stable than the optimised permeable blocks (table 13.4). It can be concluded that the optimised permeable block is a very efficient and effective block to armour the crest of a low crested breakwater.


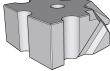
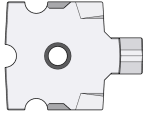
Name	Overview crest	Overview block	Bottom view	V/V_{ref}	$B/H_{s,d}$	$N_{s,c}$
Berm block Afsluitdijk				1.91	1.1	2.8

Table 13.4: Performance berm block Afsluitdijk

13.2. Recommendations

In this study is investigated how an effective and efficient modified XblocPlus crest block looks like. However, the block shape can be further optimised by gaining more knowledge about several aspects. The effect and the importance of these aspects are explained in this paragraph. The most important recommendations are explained first.

13.2.1. Numerical model tests

Physical model tests made accurate stability assessment of crest blocks possible. However, it does not give a clear indication of the bottlenecks regarding the block stability. In this study, it is found that the permeability, back to back interlocking and the additional mass are important for the crest block stability. The location with the largest pressure build-up remains unknown due to the lack of detailed understanding. Consequently, it is hard to come up with effective measures for further reduction of the block's permeability. Another disadvantage is that the values of the drag force and the lift force remain unknown. The ratio between the drag and lift force on the initial permeable block makes it possible to assess whether the assumption of $F_d/F_l = 2$ was good enough to define the target volume reduction. All those answers can be found by tests with a numerical model like a CFD-model. This makes a numerical model highly recommended for further optimisation of the block volume.

13.2.2. Structural stability

The optimising measures applied to the crest blocks were based on the wave load. The internal stability is solely based on engineering experience. Requirements for maximum concrete stresses may be exceeded, in particular near the holes in the block. Further investigation into concrete stresses is recommended before application of the optimised permeable block.

13.2.3. Effect of placement accuracy

The importance of the underlayer placement accuracy for the initial permeable block is described in paragraph 11.3. No height measurements of the underlayer below the crest blocks were performed. This makes it impossible to indicate the required underlayer level to let the nose of the crest blocks rest on the regular XblocPlus armour in the row beneath. This is important to investigate. Moreover, the underlayer level is considered to be important for the initial permeable block loaded by waves with wave steepness $s_{0,p} = 2\%$. It cannot be guaranteed that the placement accuracy is equally important for the optimised permeable block. Also, the fact that the collapsing waves determine the block stability for $s_{0,p} = 4\%$, whereas the run-up velocity determines the block stability for $s_{0,p} = 2\%$, might influence the importance of the placement accuracy. These topics are important to investigate.

13.2.4. Repetition tests

The test series with the optimised permeable block were executed twice. Both tests gave more or less equal results. However, more tests are preferred to investigate the scatter in the results. Insight in the scatter of the test results makes the results more reliable.

13.2.5. Foreshore

Like mentioned in the discussion, significant stability differences appeared for the initial permeable block with and without foreshore. These differences appeared for $R_c/H_{s,d} = 0.0$ and $s_{0,p} = 2\%$. The optimised permeable block is solely tested without foreshore. Tests with a foreshore are recommended to prevent the appearance of unexpected stability differences.

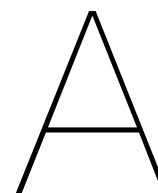
13.2.6. Structure slope

A standard 3V:4H slope is used for this research into crest stability. The crest blocks are slightly tilted backwards on a 3V:4H slope. The crest blocks are exactly horizontal on a 2V:3H slope. No problems are expected by application of the optimised permeable block on this slope. However, applying the crest blocks on a 1V:2H armour slope might cause problems. The armour blocks are tilted forwards by approximately 7 degrees at a 1V:2H slope. As a result, this might cause difficulties during placement of the rock fill between the crest blocks. The crest blocks cannot be locked up if the rock fill does not fit between the crest blocks.

Bibliography

- [1] Hans F Burcharth and T Lykke Andersen. Scale effects related to small scale physical modelling of overtopping of rubble mound breakwaters. In *Coastal Structures 2007: (In 2 Volumes)*, pages 1532–1541. World Scientific, 2009. URL <https://core.ac.uk/download/pdf/60398304.pdf>.
- [2] Hans F Burcharth, Morten Kramer, Alberto Lamberti, and Barbara Zanuttigh. Structural stability of detached low crested breakwaters. *Coastal Engineering*, 53(4):381–394, 2006. URL <https://core.ac.uk/download/pdf/60351545.pdf>.
- [3] HF Burcharth and OK Andersen. On the one-dimensional steady and unsteady porous flow equations. *Coastal engineering*, 24(3-4):233–257, 1995. URL https://vbn.aau.dk/ws/files/65299460/On_the_one_dimensional_steady_and_unsteady_porous_flow_equations.pdf.
- [4] CIRIA; CUR; CETMEF. *Rock Manual*, 2007. URL <http://www.kennisbank-waterbouw.nl/DesignCodes/rockmanual/BWchapter%205.pdf>.
- [5] Cobouw. Afsluitdijk 2 meter hoger: 4 jaar ‘blokken’ voor bam en van oord. website, April 2019.
- [6] Delta Marine Consultants. General specifications for application of xbloc and xblocplus. Report number: 968000-rap-u-100.
- [7] Delta Marine Consultants. *Instruction Xbloc Model Testing*. Delta Marine Consultants, January 2017.
- [8] Kees d’Angremond, Jentsje W Van Der Meer, and Rutger J De Jong. Wave transmission at low-crested structures. In *Coastal Engineering 1996*, pages 2418–2427. 1997.
- [9] J.P. Van de Bos H.J. Verhagen. *Breakwater Design*. TU Delft, 2018.
- [10] *Environmental Design of Low Crested Coastal Defence Structures*. Delos, 2002.
- [11] *Guidelines for Xbloc concept design*. DMC, 2018. URL https://www.dmc.nl/sites/default/files/domain-701/xbloc-guidelines_2018-671-1532949730287638300-701-153537962374766937.pdf.
- [12] Eurotop. *EurOtop Manual*, December 2018.
- [13] X. Grigoris. Stability optimisation of the top armour row of a breakwater with xblocplus units. Master’s thesis, Delft university of Technology, 2019. URL <http://resolver.tudelft.nl/uuid:b5a26cd8-b7b9-43d1-8398-54c91a9f13be>.
- [14] Hald. *Wave induced loading and stability of rubble mound breakwaters*. PhD thesis, Aalborg Universitet, 1998. URL https://vbn.aau.dk/ws/files/55248437/Wave_Induced>Loading_and_Stability_of_Rubble_Mound_Breakwaters.pdf.
- [15] L.H. Holthuijsen. *Waves in oceanic and coastal waters*. Cambridge university press, 2007.
- [16] Robert Jacobs, Pieter Bakker, Ineke Vos-Rovers, and Bas Reedijk. Xbloc-plus—development of a regular placed interlocking armour unit. *Coastal Engineering Proceedings*, 1(36):45, 2018. URL <https://www.xbloc.com/sites/default/files/domain-671/documents/xblocplus-development-of-a-regular-placed-interlocking-armour-unit-abstract-2018-671-1.pdf>.
- [17] D. Janssen. Stability analysis of xblocplus crest element. Master’s thesis, Delft University of Technology, 2018. URL <http://resolver.tudelft.nl/uuid:cfc871cd-261e-4f8f-88a2-ebb17d2c3b8f>.
- [18] Alba Jimenez. Experimental study on the wave overtopping performance of xbloc+ armour unit. Master’s thesis, Delft university of Technology, 2017.

- [19] Morten Kramer. *Structural Stability of Low-Crested Breakwaters*. PhD thesis, Aalborg university, Denmark, 2006. URL <https://vbn.aau.dk/en/publications/structural-stability-of-low-crested-breakwaters>. For further informations see <http://www.civil.aau.dk/i5mkr/phd/> PDF for print: 196 pp.
- [20] Etienne PD Mansard and ER Funke. The measurement of incident and reflected spectra using a least squares method. In *Coastal Engineering 1980*, pages 154–172. 1980.
- [21] Markus Muttray, Erik ten Oever, and Bas Reedijk. Stability of low crested and submerged breakwaters with single layer armouring. *Journal of Shipping and Ocean Engineering*, 2(3), 2012. URL https://www.researchgate.net/profile/Markus_Muttray/publication/248398382_Stability_of_Low_Crested_and_Submerged_Breakwaters_with_Single_Layer_Armouring/links/0deec51dfa3dca1f5e000000.pdf.
- [22] W. Ockeloen. Rapportage deltagoot test dijkvak 8b. Technical report, Rijkswaterstaat Grote Projecten en Onderhoud, 2020.
- [23] Bas Reedijk, Tamara Eggeling, Pieter Bakker, Robert Jacobs, and Markus Muttray. Hydraulic stability and overtopping performance of a new type of regular placed armor unit. *Coastal Engineering Proceedings*, 1(36):54, 2018. URL https://www.xbloc.com/sites/default/files/domain-671/documents/icce_2018_paper-_hydraulic_stability_and_overtopping_performance_of_new_type_of_regular_placed_armour_unit-671-15556780551522628530.pdf.
- [24] Ilse van den Bosch, Erik Ten Oever, Pieter Bakker, and Markus Muttray. Stability of interlocking armour units on a breakwater crest. *Coastal Engineering Proceedings*, 1(33):11, 2012. URL <https://www.xbloc.com/sites/default/files/domain-671/documents/xbloc-2012-stability-of-interlocking-armour-units-on-a-breakwater-crest-van-de-bos.pdf>.
- [25] Peter van der Linde. Stability of single layer armour units on low-crested structures. Master's thesis, TU Delft, 2009. URL <http://resolver.tudelft.nl/uuid:1f995447-3078-4d99-801f-60b19d1116f2>.
- [26] Dieter Vanneste and Peter Troch. A revision of the scaling method for core material in rubble-mound breakwaters. In *10th Coasts, Marine Structures and Breakwaters Conference 2013: From Sea to Shore-Meeting the Challenges of the Sea*, pages 112–121. ICE Publishing, 2014.
- [27] G.J. Schiereck H.J. Verhagen. *Introduction to Bed, bank and shore protection*. Delft Academic Press, 2nd edition edition, 2016. ISBN ISBN 90-6562-403-1.
- [28] A. Vos. Exploration into the mechanisms that govern the stability of an xbloc+ v1 armour unit. Master's thesis, Delft university of technology, 2017. URL <http://resolver.tudelft.nl/uuid:dd61dbae-67ea-4a67-b5f2-b9691240f729>.
- [29] G Wolters, M van Gent, W Allsop, L Hamm, and D Mühlestein. Guidelines for physical model testing of breakwaters. rubble mound breakwaters. *Report prepared for Hydralab III, May, 2007*. URL https://www.researchgate.net/publication/301298828_Guidelines_for_physical_model_testing_of_breakwaters_Rubble_mound_breakwaters.
- [30] Guido Wolters, Marcel van Gent, William Allsop, Luc Hamm, and Doris Muhlestein. Hydralab iii: Guidelines for physical model testing of rubble mound breakwaters. In *Coasts, marine structures and breakwaters: Adapting to change: Proceedings of the 9th international conference organised by the Institution of Civil Engineers and held in Edinburgh on 16 to 18 September 2009*, pages 2–559. Thomas Telford Ltd, 2010.



Background information

A.1. Rubble mound breakwaters

Rubble mound breakwaters are structures composed by large heaps of loose elements [9]. The core and the underlayer are not able to resist the wave forcing. An armour layer on top of the structure is required to protect it against the wave forcing. Usually, the armour layer consists of natural rock or concrete armour units.

A.1.1. Natural rock armour

The classical breakwater type is armoured with natural rock [9]. Application of natural rock armour has 2 important limitations. First, many underlayers are often necessary to obtain a gradual transition between the core and the armour layer. This makes the construction of breakwaters with natural rock labour intensive. In the second place, natural rock availability near a construction site is important. In areas like the Netherlands, the rock availability is minor. Transporting rock from elsewhere to a construction site in the Netherlands is very expensive. Especially for a rock armoured structure that requires relatively more rock than a structure armoured with concrete armour units.

A.1.2. Concrete armour units

Concrete armour units are artificial blocks made of concrete that were invented as an interesting alternative to deal with the rare availability of very large rock elements [9]. These blocks are made of non-reinforced concrete to prevent corrosion of the reinforcing steel. In general, the stability of concrete armour units is gained by their own weight, interlocking and friction (paragraph 2.2). The earliest developments of concrete armour units were cube-shaped and relied, just as natural rock, on their own weight. These blocks were placed in a double layer to prevent large holes in the armour layer after displacement. Examples of those elements are the Antifer and Tetrapods. Later, single layer elements were developed to reduce constructional effort. These elements are bulkier shaped than the elements used in double layers. Examples of random placed single layer elements are Accropode and Xbloc. XblocPlus is an example of a regular placed single layer element.

A.1.3. Low crested versus conventional breakwaters

In the problem definition is stated that the stability of the crest armour is critical for low crested breakwaters. Some other important differences between conventional and low crested breakwaters are shown in table A.1 [19].

Conventional breakwater	Low crested breakwater
Low wave transmission	High wave transmission
High wave reflection	Low wave reflection
Little or no overtopping	Significant overtopping
Damage mainly to front slope	Damage to crest, front and rear slope

Table A.1: Conventional versus low-crested breakwaters [19]

A.2. XblocPlus

A.2.1. Main dimensions

The main dimensions of XblocPlus are shown in figure A.1[11]. The relations that hold between the main dimensions are shown in table A.2. They are expressed in relation to the width (L2) and the nominal diameter D_n ($D_n = \sqrt[3]{V_{ref}}$). The XblocPlus elements are placed on the slope with some space in between them with the aim to increase the permeability of the armour layer. The centre to centre distance between two neighbouring elements is $1.1 \cdot L2$, so the space in between 2 elements equals 10% of the width L2.

Dimensions	Relative to width (L2)	Relative to D_n
Height (L1)	0.5 L2	0.83 D_n
Width (L2)	L2	1.66 D_n
Length (L3)	1.27 L2	2.11 D_n

Table A.2: Dimensions XblocPlus [11]

A.2.2. Contact surfaces

Each XblocPlus block has 4 contact surfaces on top, 4 contact planes at the bottom and 1 contact surface with the underlayer. The contact planes with neighbouring blocks are hatched in orange and the contact planes with the underlayer is hatched in green.

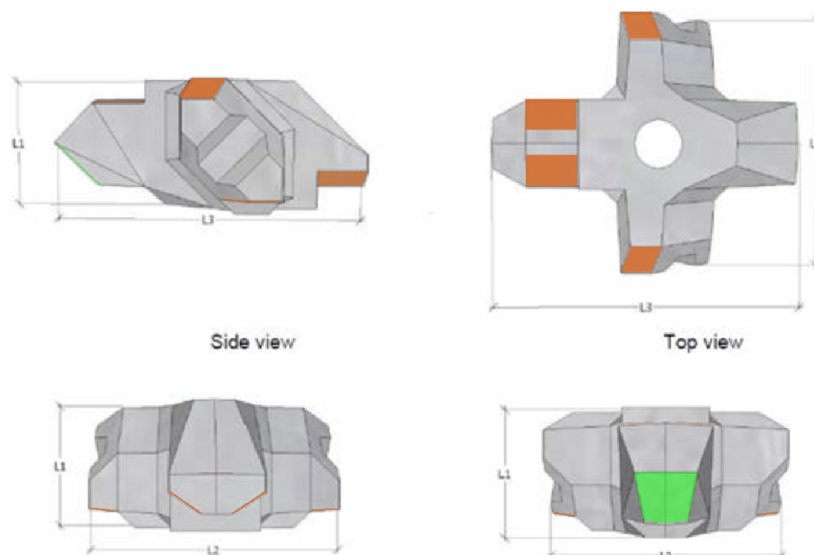


Figure A.1: XblocPlus dimensions [13]

A.2.3. Centre of gravity

Observing the top, front and rear view of an element clearly shows that it is very symmetric (figure A.2). The black cross indicates the location of the centre of gravity (COG). The COG is exactly in the middle of the hole to keep the block position horizontal during construction. The side view in figure A.3 shows the location of the centre of gravity [17].

A.2.4. Friction factor

The friction factor (γ_f) of XblocPlus, which is used for run-up and overtopping computations, is 0.45.

A.3. Wave theory

The water level of the sea is periodically deviating from its mean value due to influence of external factors like the wind. Those deviations follow an irregular pattern and the return period of each deviation is different. A variance density spectrum is used to give a complete description of the surface elevation in a statistical

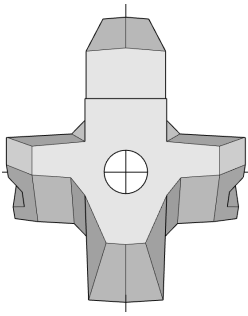


Figure A.2: Centre of gravity

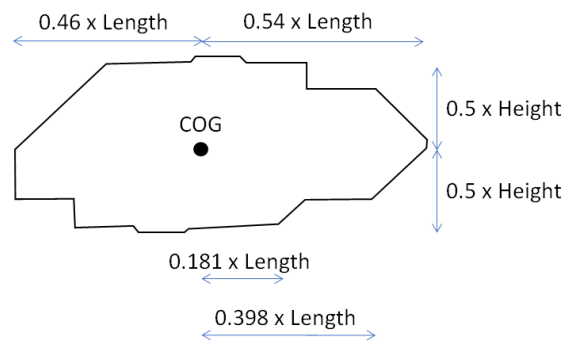


Figure A.3: Centre of gravity side view [17]

sense. Waves are defined as the profile of the surface elevation between 2 successive crossings of the mean sea level [15].

A.3.1. Significant wave height

The wave height is the vertical distance between the maximum and the minimum surface elevation per wave. The significant wave height (H_s) is a measure to express the wave field in one wave height. This wave height, obtained from a wave record, can be described by the average of the highest one-third of the waves in a wave field ($H_{1/3}$). The significant wave height estimated from the spectrum can be expressed by the variance (m_0) of the variance density spectrum (equation A.1). A rule of thumb is that $H_{max} = 2 H_s$.

$$H_{m0} = 4\sqrt{m_0} \quad (\text{A.1})$$

A.3.2. Wave period

Just like the wave height, there are several methods to describe the wave period. Often, those periods are different than the visually observed wave periods between 2 successive crossings of the mean sea level. $T_{1/3}$ is the significant wave period defined as the mean period of the highest one-third of the waves. The peak period T_p is the wave period based on the point of maximum energy from the wave spectrum. T_m is the mean period of all waves in a wave record and $T_{m-1,0}$ is the energy period obtained from the energy wave spectrum. The relations between the mentioned wave periods are given in equations A.2 and A.3 [12].

$$T_p = 1.1 \cdot T_{m-1,0} \quad (\text{A.2})$$

$$T_p = (1.1 - 1.25) \cdot T_m \quad (\text{A.3})$$

A.3.3. Dispersion relation

The dispersion relation describes how the wave period and the wavelength are related to each other. The relation, which is shown in equation A.4, depends on the water depth. From the relation follows that waves with a large period have a large wavelength whereas short waves have a short period. The propagation speed c (L/T) follows the same pattern.

$$L = \frac{gT^2}{2\pi} \cdot \tanh\left(\frac{2\pi d}{L}\right) \quad (\text{A.4})$$

Due to the positive correlation between the wavelength and the propagation speed, waves with a long wave period propagate from their source than short waves do. The phenomenon that describes this, is called frequency dispersion. Waves with approximately equal period and wavelength have almost equal propagation speed. As a result, groups of similar waves with equal steepness are formed far away from their source. Reduction of the depth from deep water conditions ($d/L > 0.5$) to shallow water conditions ($d/L < 0.05$) results in a smaller wavelength and propagation speed. For shallow water, the propagation speed becomes independent of the wave period which makes it non-dispersive.

A.3.4. Fictitious wave steepness

The fictitious wave steepness is defined as the ratio of the spectral wave height (H_{m0}) and deep water wavelength (L_0). Like stated in the paragraph A.3.3, long waves (with a large period) propagate faster

Quantity	Deep water ($d/L > 0.5$)	Shallow water ($d/L < 0.05$)
Wavelength (L)	$\frac{gT^2}{2\pi}$	$T\sqrt{gd}$
Propagation speed (c)	$\frac{gT}{2\pi}$	\sqrt{gd}

Table A.3: Deep and shallow water differences

than waves with a short period. Waves with a clearly visible long wave period are generated far away from their observation location. These waves have a lower wave steepness ($s_0 \approx 0.02$) than shorter wind waves generated relatively close to their existing location ($s_0 = 0.04-0.06$).

A.3.5. Foreshore

A foreshore is a part of the seabed, seaward of the breakwater toe. Its slope varies between horizontal and 1:10 [12]. When waves start feeling the bottom their height increase due to shoaling, their length decreases, and its steepness becomes larger. Closer to the coastline the water depth reduces and eventually, waves will break. The quantity of breaking wave energy depends on the slope of the foreshore and the wave steepness. Hofland [12] concluded that waves with low steepness shoal more than wave with large steepness. Moreover, he concluded that waves at steeper foreshores dissipate less energy than waves at a very mild foreshore. An overview of the wave height transformation according to Hofland is given in figure A.4. The water depth next to the structure, the wave steepness and the foreshore steepness determine whether the $H_{s,toe}$ is smaller or larger than H_{m0} .

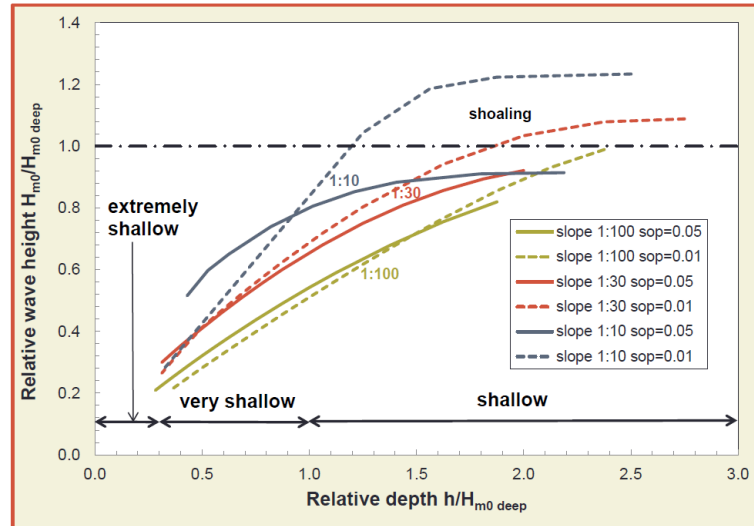


Figure A.4: Influence foreshore [12]

A.3.6. Spectra

A spectrum is used to describe how the variance of the surface elevation is distributed over the frequencies. The Pierson-Moskowitz spectrum is a fully developed spectrum in deep water conditions (equation A.5 [15]). The Jonswap spectrum A.6 is a spectrum which has been established after detailed analysis of observed wave conditions on the North Sea [15]. This a spectrum which is not fully developed and is more relevant for many engineering purposes in the coastal zones.

$$E_{PM}(f) = \alpha_{PM} g^2 (2\pi)^{-4} f^{-5} \exp\left[-\frac{5}{4} \left(\frac{f}{f_{PM}}\right)^{-4}\right] \quad (\text{A.5})$$

$$E_{JONSWAP}(f) = \alpha_J g^2 (2\pi)^{-4} f^{-5} \exp\left[-\frac{5}{4} \left(\frac{f}{f_{peak}}\right)^{-4}\right] \gamma \exp\left[-\frac{1}{2} \left(\frac{f - f_{peak}}{\sigma}\right)^2\right] \quad (\text{A.6})$$

Yamaguchi [15] made good approximations for the zero-, first- and second-order spectral moments for $\sigma = 0.07$ (if $f < f_{peak}$), $\sigma = 0.09$ (if $f > f_{peak}$) and $\gamma = 3.3$.

A.4. Wave-structure interaction

A.4.1. Wave breaking

The impact of a breaking wave on a structure depends on the steepness of the armour slope and the wave steepness. An expression for the surf similarity parameter is given in equation A.7[12]. Since the impact is associated with energy, the deep water wavelength is based on the energy wave period.

$$\xi_{m-1,0} = \frac{\tan(\alpha)}{\sqrt{\frac{H_{m0}}{L_{m-1,0}}}} \quad (\text{A.7})$$

The value of the surf similarity says something about the type of wave breaking. An overview of the different breaking regimes is given in figure A.5. Collapsing is the regime that causes the most impact on the armour of a structure. In combination with a slope of 3V:4H, long waves ($s_{0,p} = 2\%$) give a $\xi_{m-1,0}$ value of 4.8 and wind waves ($s_{0,p} = 4\%$) have a $\xi_{m-1,0}$ value of 3.4. From those numbers can be concluded that the wave impact on the armour is larger for wind waves since the value of the surf similarity parameter for winds waves is closer to the values of the collapsing wave regime.

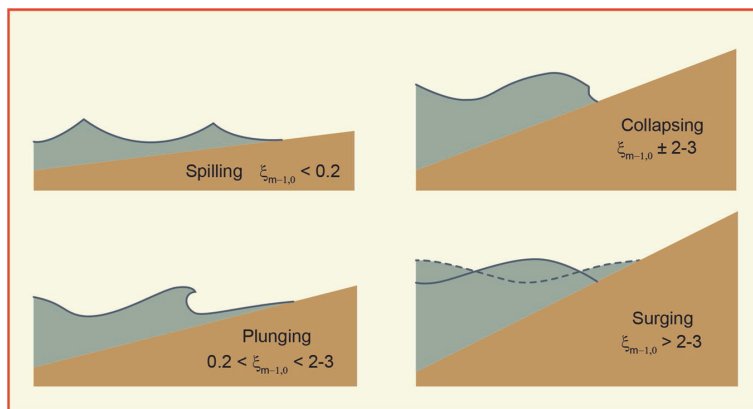


Figure A.5: Breaking regimes [12]

A.4.2. Swash

The run-up and run-up velocity are important phenomena related to the armour stability. In the EurOtop 2018 [12], equations A.8, A.9 and A.10 are used to describe the run-up for a breakwater with rough slopes, without a berm and oblique incoming waves. Equation A.11 describes the run-up velocity. The parameters described in this equation are visualised in figure A.6.

$$\frac{R_{u2\%}}{H_{m0}} = 1.65 \cdot \gamma_f \cdot \xi_{m-1,0} \quad (\text{A.8})$$

With a maximum of:

$$\frac{R_{u2\%}}{H_{m0}} = 1.00 \cdot \gamma_{f \text{ surging}} \cdot \left(4.0 - \frac{1.5}{\sqrt{\xi_{m-1,0}}}\right) \quad (\text{A.9})$$

$$\gamma_{f \text{ surging}} = \gamma_f + (\xi_{m-1,0} - 1.8) \cdot \frac{1 - \gamma_f}{8.2} \quad (\text{A.10})$$

In equation A.10, no larger input values than $R_{u2\%}/H_{m0} = 3.0$ for structures with an impermeable core and 2.0 for a permeable core are allowed.

$$v_{A,2\%} = c_{v2\%} \cdot \sqrt{(g(R_{u2\%} - z_a))} \quad (\text{A.11})$$

From the equations can be concluded that the run-up height is related to the surf similarity number. Long waves ($s_{0,p} = 2\%$) with a larger surf similarity number than wind waves ($s_{0,p} = 4\%$), have a larger run-up and therefore a larger run-up velocity. Consequently, the magnitude of the drag and lift force on the armour blocks is larger.

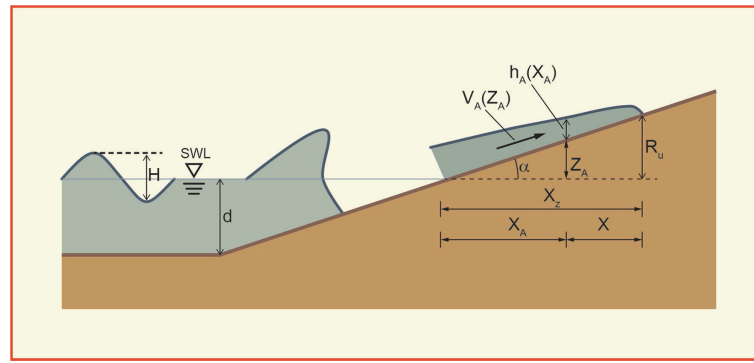


Figure A.6: Run-up velocity parameters [12]

A.4.2.1. Permeability

Run-up measurements during stability tests on rock slopes, performed by Van der Meer, were used to assess the influence of the core permeability on the run-up [12]. An impermeable core (clay) and a permeable (rubble mound) core were compared. The permeability appeared to play a major role in the magnitude of the run-up and the run-up velocity. Permeable structures were able to dissipate more wave energy than impermeable structures. As a result, both run-up and run-up velocity were smaller for permeable structures. This has a favourable impact on the armour stability.

A.4.3. Overtopping discharge

The mean overtopping discharge or overtopping rate is often used to judge allowable overtopping [12]. The overtopping discharge for rubble mound breakwaters with a slope between 1:2 and 1:4/3 is given in equation A.12. The formula is applicable for $R_c/H_{s,d} > 0$ [12]. A higher crest level results in less overtopping. Just as the crest height, the crest width is important because it can dissipate more energy over the wider crest [12]. Equation A.13 is a reduction factor for the overtopping discharge which depends on the crest width. To obtain the overtopping discharge, the C_r value should be multiplied with q .

$$\frac{q}{\sqrt{g \cdot H_{m0}^3}} = 0.09 \cdot \exp\left[-\left(1.5 \left(\frac{R_c}{H_{m0} \cdot \gamma_f \cdot \gamma_\beta}\right)^{1.3}\right)\right] \quad (\text{A.12})$$

$$C_r = 3.06 \exp\left(\frac{-1.5B}{H_{m0}}\right) \quad (\text{A.13})$$

A.4.4. Energy propagation

Wave energy going towards a structure is reflected, absorbed and transmitted. The armour blocks, underlayer and core absorb wave energy. The reflected waves go seaward after hitting the structure and transmitted waves go further in landward direction after being reduced in height by the structure. In sections A.4.4.1 and A.4.4.2 is explained how they are affected by the structure.

A.4.4.1. Wave transmission

The wave transmission is an important indication for the effectiveness of a breakwater. The wave transmission coefficient is the ratio between the incoming wave height (H_{si}) and the wave height after passing the structure (H_{st}). The wave transmission depends mainly on the wave forcing, the crest height and the crest width. In addition, factors like the core permeability and the armour roughness play a role. d'Angremond specified equation A.14 for the transmission coefficient of a narrow crested breakwater armoured with rock ($B/H_s < 10$) [4]. Although the structure's permeability and the armour roughness are not directly included in this formula, they do affect the wave transmission. The effect of the permeability is governed in the formula by a constant (0.64 for permeable rock structures) [8]. The equation is only valid for $0.075 < K_t < 0.8$.

$$K_t = -0.4 \frac{R_c}{H_{si}} + 0.64 \left(\frac{B}{H_{si}}\right)^{-0.31} (1 - \exp(-0.5\xi)) \quad (\text{A.14})$$

A.4.4.2. Wave reflection

Incoming waves do partly reflect after hitting the breakwater. The reflection coefficient is given by the ratio between the incoming wave height (H_{si}) and the height of the wave propagating in the opposite direction

after hitting structure (H_{st}). The reflection for long waves is relatively larger than for short waves. Equation A.15 is an equation for the reflection coefficient for rough and permeable slopes [4].

$$K_r = 0.14 \cdot \xi_p^{0.73} \quad (\text{A.15})$$

B

Scaling core material

Burcharth's method is a practical pore pressure calculation method. The method can be used to compute both in space and time varying wave-induced pore pressures that are required to determine porous flow velocities. The method contains 6 steps that are described by bullet points. A more detailed explanation and equations per step can be found in Vanneste (2014) [26].

- Compute the damping coefficient $\delta(z)$ for every point in figure B.1.
- Compute the horizontal component of the pressure gradient for every point ($l_{x'}(z)$), varying over time within the first half of the wave period.
- Set the computed pressure gradient per point equal to the hydraulic gradient in the Forchheimer equation. Next, compute the filter velocity per point over the first half of the wave period.
- Take the average filter velocity of the prototype and scale it down to the average model filter velocity. The scale formula, with scale factor λ , is given in equation B.1.
- Use the downscaled filter velocity to compute the D_{50} of the core with the Forchheimer equation.
- Compute the Reynolds number to estimate the flow regime. The Reynolds number in the core should be higher than 300 to guarantee turbulent flow.

$$U_m = \frac{U_p}{\sqrt{\lambda}} \quad (\text{B.1})$$

In the scale equation, the value of the scale factor λ between the prototype and the model is 49.5 (paragraph 4.4.1).

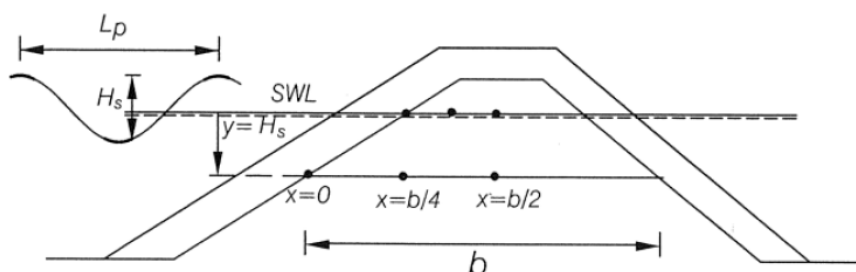


Figure B.1: Schematic model Burcharth

Several assumptions have been made during the process of finding a core grading:

- The porosity of the core material is often between 0.3 and 0.4. Small porosity values result in a low permeability of the core, a large run-up and therefore a reduced armour stability. For this reason, a rather small porosity value is chosen ($n = 0.33$).

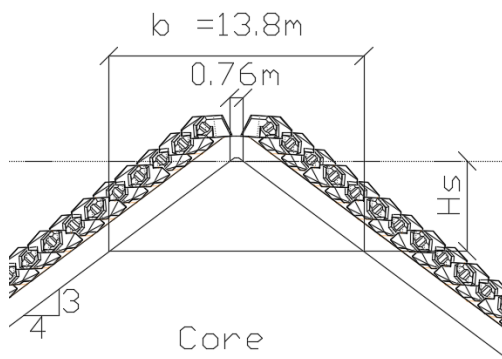


Figure B.2: Geometry small crested breakwater

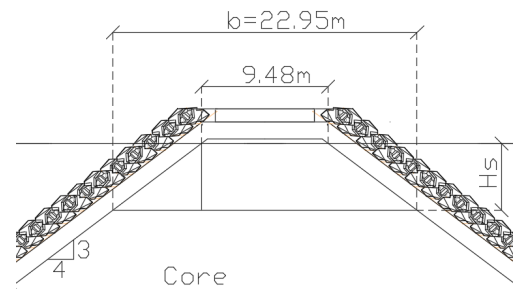


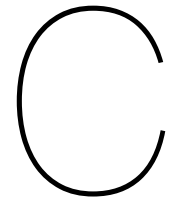
Figure B.3: Geometry small crested breakwater

- The shape factors α and β in the Forchheimer equation differ per flow case and have to be determined experimentally. Without further information, standard values $\alpha = 1000$ and $\beta = 1.1$ are used to estimate the core grading [27].
- The ratio between D_{n50} and D_{50} is 0.84 [4].

In this study, physical model tests with a relative freeboard of 0.0 and 0.5 are performed. For the core material computation, the case with $R_c/H_{s,d} = 0.5$ is used because this makes it easier to implement the core width at the still water line. No large differences in core grading are expected for $R_c/H_{s,d} = 0.0$ and $R_c/H_{s,d} = 0.5$. The input values for the prototype are given in table 4.3. b_{target} and $b_{reference}$ are defined in figures B.2 and B.3 respectively.

Parameter	Value (m)
H_s	5.05
L_p	150.6
b_{target}	13.8
$b_{reference}$	22.95

Table B.1: Prototype parameter values



Drawings

All dimensions are given in millimeters.

C.1. Preliminary research phase

C.1.1. Starting block

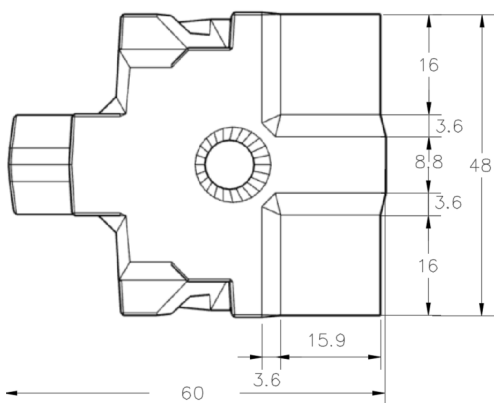


Figure C.1: Bottom view

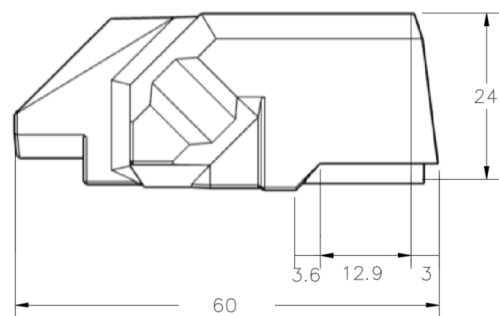


Figure C.2: Side view

C.1.2. Permeable block

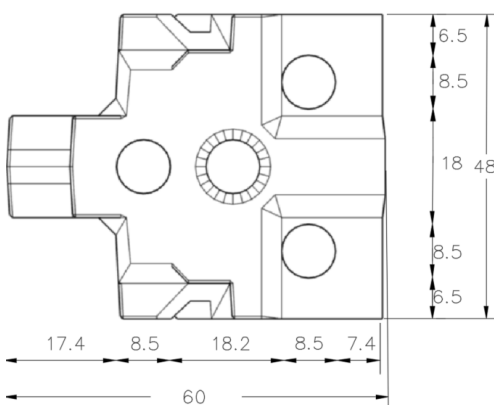


Figure C.3: Bottom view

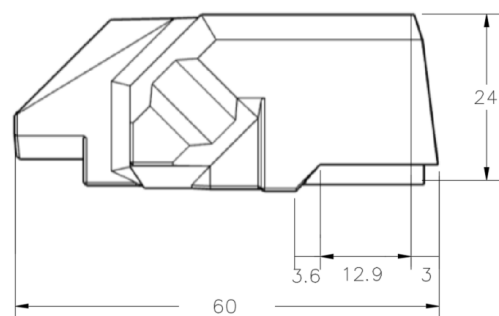


Figure C.4: Side view

C.1.3. Extended bottom block

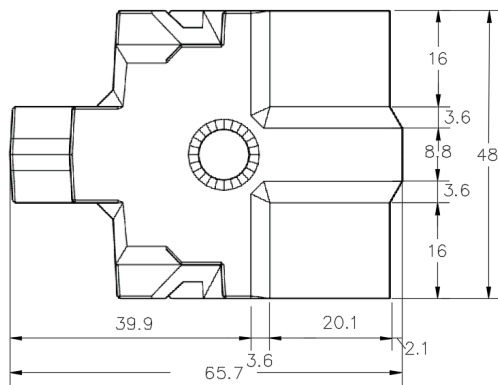


Figure C.5: Bottom view

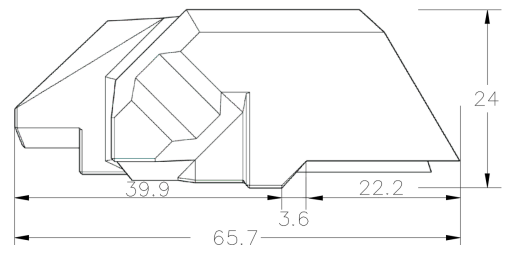


Figure C.6: Side view

C.1.4. Interlocking block

C.1.4.1. Block 1

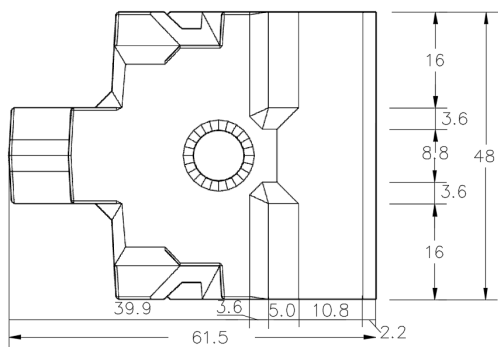


Figure C.7: Bottom view

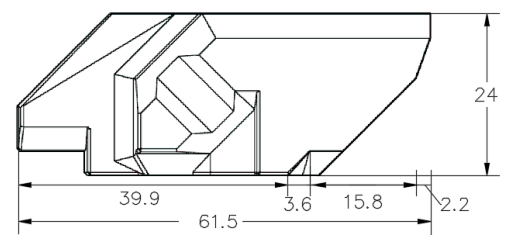


Figure C.8: Side view

C.1.4.2. Block 2

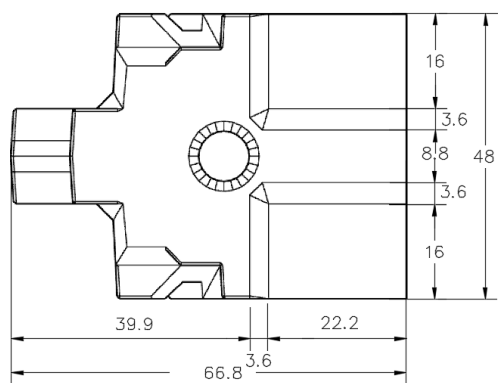


Figure C.9: Bottom view

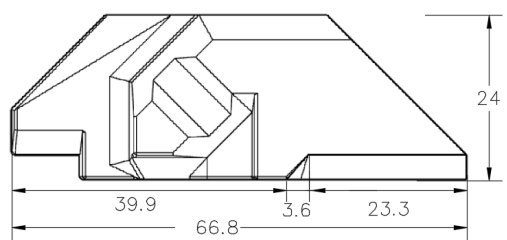


Figure C.10: Side view

C.2. Detailed research phase

C.2.1. Optimised permeable block

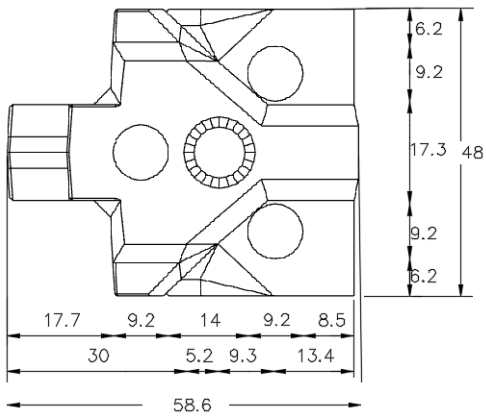


Figure C.11: Bottom view

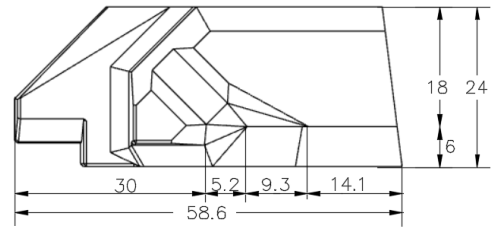


Figure C.12: Side view

C.2.2. Berm block Afsluitdijk

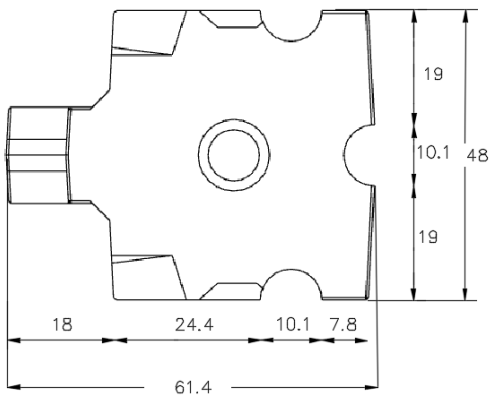


Figure C.13: Bottom view

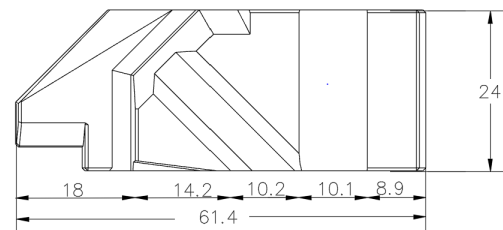
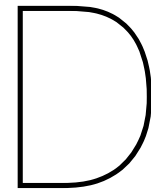


Figure C.14: Side view



Construction modified XblocPlus

To test the modified XblocPlus blocks, handmade model units were constructed. Using solely 3D prints is impossible because the density of 3D printed blocks is limited. The construction procedure is explained in 5 steps.

- The designed blocks were 3D printed (figure D.1).
- Moulds were constructed with the 3D model units by using small PVC tubes and cast rubber. Clay is used to make the bottom of the PVC tube fluid tight (figure D.2). The 3D print is placed upside down in the PVC tube. Subsequently, the PVC tube is filled with moulding rubber. After filling, weight is placed on top of the 3D print to keep it submerged. Six to eight hours later, a mould like the mould presented in figure D.3 is obtained.
- The test blocks are constructed by filling moulds with Acrystal Aqua (figure D.4). The blocks are demoulded 18-24 hours after the filling (figure D.5).
- To finish off the testing blocks, the blocks were polished (figure D.6).

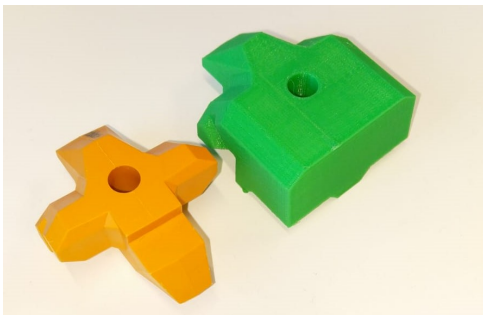


Figure D.1: Original XblocPlus and 3D print



Figure D.2: Mould construction



Figure D.3: Empty mould

D.1. Determination block density

The density of the testing units is determined after finishing off the testing blocks. To determine the block density, every block is weighted first. The volume is determined by making use of a water cup that is filled to the brim. A test block is put into the cup. Consequently, a certain quantity of water, equal to the block volume, flows over. The weight of the cup is measured with and without the test block. In combination with the known block weight, the weight of the overflowed water is determined. This volume is equal to the block volume. The block density can be determined with the obtained weight and volume.



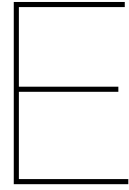
Figure D.4: Mould filled with Acrystal Aqua



Figure D.5: Before polishing



Figure D.6: After polishing



Block density

E.1. Blocks preliminary research phase

E.1.1. starting block

Block nr.	Weight (g)	Volume (mm ³)	Density (kg/m ³)
1	94.1	42100	2235
2	89.1	41100	2168
3	90.9	40900	2222
4	93.1	40600	2293
5	92.3	42100	2192
6	87.4	41200	2121
7	92.0	42900	2145
8	88.0	41400	2126
9	86.0	40100	2145
10	90.0	41500	2169
11	93.0	41400	2246
12	92.1	41900	2198
13	92.4	41800	2211
14	89.3	41000	2178
15	93.4	41200	2267
16	94.2	42500	2216
17	90.1	40800	2208
18	89.2	42900	2079
19	88.2	39600	2227
20	90.4	41200	2194

Table E.1: Block information starting block

μ_{weight} (g)	σ_{weight} (g)	μ_{volume} (mm ³)	σ_{volume} (mm ³)	$\mu_{density}$ (kg/m ³)	$\sigma_{density}$ (kg/m ³)
90.8	2.3	41740	852	2176	51

Table E.2: Statistical values starting block

E.1.2. Permeable block

Block nr.	Weight (g)	Volume (mm ³)	Density (kg/m ³)
1	84.0	39100	2148
2	83.8	38400	2182
3	85.3	39300	2170
4	83.6	38700	2160
5	85.7	39400	2175
6	85.1	38000	2239
7	85.1	39200	2171
8	82.0	37700	2175
9	83.8	38700	2165
10	84.0	37400	2246
11	82.8	38900	2129
12	85.0	38600	2202
13	84.2	39000	2159
14	85.8	38900	2206
15	85.0	39100	2174
16	83.4	38300	2178
17	83.9	37700	2225
18	87.0	39300	2214
19	84.1	39100	2151
20	83.8	38700	2165

Table E.3: Block information permeable block

μ_{weight} (g)	σ_{weight} (g)	μ_{volume} (mm ³)	σ_{volume} (mm ³)	$\mu_{density}$ (kg/m ³)	$\sigma_{density}$ (kg/m ³)
84.4	1.1	38675	572	2182	30

Table E.4: Statistical values permeable block

E.1.3. Extended bottom block

Block nr.	Weight (g)	Volume (mm ³)	Density (kg/m ³)
1	91.7	42700	2148
2	94.5	42500	2224
3	96.0	43200	2222
4	93.2	41200	2262
5	96.1	44100	2179
6	92.8	42400	2189
7	94.1	42100	2235
8	93.2	42200	2209
9	94.4	42400	2226
10	93.3	42300	2206
11	95.2	42200	2256
12	93.2	41700	2235
13	94.5	41800	2261
14	95.5	43800	2180
15	92.3	41300	2235
16	93.7	44200	2120
17	93.6	42400	2208
18	92.8	41800	2220
19	93.9	41900	2241
20	92.3	41300	2235

Table E.5: Block information extended bottom block

μ_{weight} (g)	σ_{weight} (g)	μ_{volume} (mm ³)	σ_{volume} (mm ³)	$\mu_{density}$ (kg/m ³)	$\sigma_{density}$ (kg/m ³)
93.8	1.2	42375	846	2214	36

Table E.6: Statistical values extended bottom block

E.1.4. Interlocking block

E.1.4.1. Interlocking block 1

Block nr.	Weight (g)	Volume (mm ³)	Density (kg/m ³)
1	91.0	42000	2167
2	90.1	39900	2258
3	91.0	42000	2167
4	89.1	40600	2195
5	89.2	41200	2165
6	90.9	39800	2284
7	91.3	41200	2216
8	89.9	39200	2293
9	90.8	39800	2281
10	90.7	40200	2256

Table E.7: Block information interlocking block 1

μ_{weight} (g)	σ_{weight} (g)	μ_{volume} (mm ³)	σ_{volume} (mm ³)	$\mu_{density}$ (kg/m ³)	$\sigma_{density}$ (kg/m ³)
90.4	0.7	40590	924	2228	50

Table E.8: Statistical values interlocking block 1

E.1.4.2. Interlocking block 2

Block nr.	Weight (g)	Volume (mm ³)	Density (kg/m ³)
1	91.3	41300	2210
2	90.5	41500	2180
3	92.5	41500	2228
4	92.7	41400	2239
5	91.8	41800	2196
6	91.0	42000	2166
7	90.5	40300	2245
8	92.2	42700	2159
9	91.4	40900	2234
10	91.5	41500	2204

Table E.9: Block information interlocking block 2

μ_{weight} (g)	σ_{weight} (g)	μ_{volume} (mm ³)	σ_{volume} (mm ³)	$\mu_{density}$ (kg/m ³)	$\sigma_{density}$ (kg/m ³)
91.5	0.7	41490	602	2207	29

Table E.10: Statistical values interlocking block 2

E.2. Blocks detailed research phase

E.2.1. Optimised permeable block

Block nr.	Weight (g)	Volume (mm ³)	Density (kg/m ³)
1	76.0	34600	2197
2	76.4	35600	2146
3	75.3	34000	2215
4	76.9	34200	2249
5	77.0	34200	2251
6	76.5	33700	2270
7	76.8	34800	2207
8	76.6	35000	2189
9	76.6	34700	2207
10	75.9	33700	2252
11	76.2	34700	2196
12	75.2	33800	2225
13	75.6	34100	2217
14	76.1	34100	2232
15	76.8	34800	2207
16	76.3	34700	2199
17	75.9	34300	2213
18	76.6	34500	2220
19	76.4	34500	2214
20	76.6	34800	2201

Table E.11: Block information optimised permeable block

μ_{weight} (g)	σ_{weight} (g)	μ_{volume} (mm ³)	σ_{volume} (mm ³)	$\mu_{density}$ (kg/m ³)	$\sigma_{density}$ (kg/m ³)
76.3	0.5	34440	466	2215	27

Table E.12: Statistical values optimised permeable block

E.2.2. Berm block Afsluitdijk

Block nr.	Weight (g)	Volume (mm ³)	Density (kg/m ³)
1	104.0	47000	2213
2	99.4	44900	2214
3	99.5	44600	2231
4	105.5	47500	2221
5	102.9	46900	2194
6	105.1	48000	2190
7	100.5	45600	2204
8	100.0	44500	2247
9	102.9	46700	2203
10	103.8	45600	2276
11	105.4	48600	2169
12	104.9	47000	2232
13	101.9	45600	2235
14	102.7	46800	2194
15	101.4	46140	2198
16	100.5	46000	2185
17	99.9	45200	2210
18	103.9	46800	2220
19	103.8	47500	2185
20	103.1	47000	2194

Table E.13: Block information berm bloc Afsluitdijk

μ_{weight} (g)	σ_{weight} (g)	μ_{volume} (mm ³)	σ_{volume} (mm ³)	$\mu_{density}$ (kg/m ³)	$\sigma_{density}$ (kg/m ³)
102.6	2.0	46397	1101	2211	24

Table E.14: Statistical values berm bloc Afsluitdijk



Test data

1.1.1, ref. non-modified XblocPlus, $s_{0,p} = 2\%$, $R_c/H_{s,d} = 0.0$

$\% \cdot H_{s,d}$	H_s (m)	$H_{s,theory}$ (m)	T_p (s)	$s_{0,p}$ (-)	h_0 (m)	h_{toe} (m)	R_c (m)	$R_c/H_{s,d}$ (-)	time(h,m,s)
60%	0.037	0.059	1.422	0.0118	0.648	0.372	0.0	0.0	00:25:39
80%	0.078	0.079	1.641	0.0186	0.648	0.372	0.0	0.0	00:21:31
100%	0.094	0.099	1.829	0.0181	0.648	0.372	0.0	0.0	00:23:56
110%	0.104	0.109	1.882	0.0189	0.648	0.372	0.0	0.0	00:25:05

1.1.2, small crest block, $s_{0,p} = 2\%$, $R_c/H_{s,d} = 0.0$

$\% \cdot H_{s,d}$	H_s (m)	$H_{s,theory}$ (m)	T_p (s)	$s_{0,p}$ (-)	h_0 (m)	h_{toe} (m)	R_c (m)	$R_c/H_{s,d}$ (-)	time(h,m,s)
60%	0.056	0.059	1.422	0.0179	0.638	0.357	0.0	0.0	00:19:02
80%	0.082	0.079	1.561	0.0215	0.638	0.357	0.0	0.0	00:21:33
100%	0.101	0.099	1.778	0.0205	0.638	0.357	0.0	0.0	00:24:19
110%	0.112	0.109	1.882	0.0202	0.638	0.357	0.0	0.0	00:25:04
120%	0.121	0.119	1.939	0.0206	0.638	0.357	0.0	0.0	00:26:03

1.2.1, starting block, $s_{0,p} = 2\%$, $R_c/H_{s,d} = 0.0$

$\% \cdot H_{s,d}$	H_s (m)	$H_{s,theory}$ (m)	T_p (s)	$s_{0,p}$ (-)	h_0 (m)	h_{toe} (m)	R_c (m)	$R_c/H_{s,d}$ (-)	time(h,m,s)
60%	0.052	0.052	1.306	0.0197	0.638	0.355	0.0	0.0	00:18:42
80%	0.072	0.070	1.488	0.0209	0.638	0.355	0.0	0.0	00:20:58
100%	0.091	0.087	1.730	0.0195	0.638	0.355	0.0	0.0	00:22:24
110%	0.093	0.096	1.730	0.0200	0.638	0.355	0.0	0.0	00:23:50
120%	0.111	0.105	1.882	0.0200	0.638	0.355	0.0	0.0	00:24:31
130%	0.114	0.113	1.939	0.0195	0.638	0.355	0.0	0.0	00:25:52

1.2.2, starting block, $s_{0,p} = 2\%$, $R_c/H_{s,d} = 0.5$

$\% \cdot H_{s,d}$	H_s (m)	$H_{s,theory}$ (m)	T_p (s)	$s_{0,p}$ (-)	h_0 (m)	h_{toe} (m)	R_c (m)	$R_c/H_{s,d}$ (-)	time(h,m,s)
60%	0.047	0.052	1.306	0.0176	0.595	0.316	0.039	0.43	00:18:02
80%	0.072	0.070	1.488	0.0208	0.595	0.316	0.039	0.43	00:21:00
100%	0.091	0.087	1.641	0.0216	0.595	0.316	0.039	0.43	00:22:33
110%	0.100	0.096	1.778	0.0202	0.595	0.316	0.039	0.43	00:23:50
120%	0.109	0.105	1.882	0.0197	0.595	0.316	0.039	0.43	00:25:17
130%	0.116	0.113	1.939	0.0198	0.595	0.316	0.039	0.43	00:25:52
140%	0.124	0.122	1.939	0.0212	0.595	0.316	0.039	0.43	00:26:31

1.3.1, permeable block, $s_{0,p} = 2\%$, $R_c/H_{s,d} = 0.0$

$\% \cdot H_{s,d}$	H_s (m)	$H_{s,theory}$ (m)	T_p (s)	$s_{0,p}$ (-)	h_0 (m)	h_{toe} (m)	R_c (m)	$R_c/H_{s,d}$ (-)	time(h,m,s)
60%	0.050	0.052	1.306	0.0188	0.635	0.352	0.0	0.0	00:18:08
80%	0.071	0.070	1.488	0.0205	0.635	0.352	0.0	0.0	00:20:45
100%	0.091	0.087	1.641	0.0216	0.635	0.352	0.0	0.0	00:22:42
110%	0.098	0.096	1.778	0.0199	0.635	0.352	0.0	0.0	00:23:50
120%	0.107	0.105	1.882	0.0194	0.635	0.352	0.0	0.0	00:27:59
130%	0.116	0.113	1.939	0.0197	0.635	0.352	0.0	0.0	00:25:51
140%	0.123	0.122	1.939	0.0210	0.635	0.352	0.0	0.0	00:27:10

1.4.1, extended bottom block, $s_{0,p} = 2\%$, $R_c/H_{s,d} = 0.0$

$\% \cdot H_{s,d}$	H_s (m)	$H_{s,theory}$ (m)	T_p (s)	$s_{0,p}$ (-)	h_0 (m)	h_{toe} (m)	R_c (m)	$R_c/H_{s,d}$ (-)	time(h,m,s)
60%	0.052	0.052	1.306	0.0196	0.635	0.353	0.0	0.0	00:18:07
80%	0.071	0.070	1.455	0.0214	0.635	0.353	0.0	0.0	00:20:23
100%	0.089	0.087	1.641	0.0212	0.635	0.353	0.0	0.0	00:22:42
110%	0.097	0.096	1.730	0.0208	0.635	0.353	0.0	0.0	00:23:47
120%	0.108	0.105	1.882	0.0195	0.635	0.353	0.0	0.0	00:24:51

1.5.1, interlocking block attempt 1, $s_{0,p} = 2\%$, $R_c/H_{s,d} = 0.0$

$\% \cdot H_{s,d}$	H_s (m)	$H_{s,theory}$ (m)	T_p (s)	$s_{0,p}$ (-)	h_0 (m)	h_{toe} (m)	R_c (m)	$R_c/H_{s,d}$ (-)	time(h,m,s)
60%	0.051	0.052	1.306	0.0193	0.642	0.359	0.0	0.0	00:18:02
80%	0.072	0.070	1.455	0.0219	0.642	0.359	0.0	0.0	00:20:29
100%	0.088	0.087	1.641	0.0209	0.642	0.359	0.0	0.0	00:23:15
110%	0.098	0.096	1.730	0.0210	0.642	0.359	0.0	0.0	00:23:42

1.5.2, interlocking block attempt 2, $s_{0,p} = 2\%$, $R_c/H_{s,d} = 0.0$

$\% \cdot H_{s,d}$	H_s (m)	$H_{s,theory}$ (m)	T_p (s)	$s_{0,p}$ (-)	h_0 (m)	h_{toe} (m)	R_c (m)	$R_c/H_{s,d}$ (-)	time(h,m,s)
60%	0.049	0.052	1.306	0.0185	0.642	0.36	0.0	0.0	00:18:05
80%	0.070	0.070	1.455	0.0212	0.642	0.36	0.0	0.0	00:20:22
100%	0.091	0.087	1.641	0.0216	0.642	0.36	0.0	0.0	00:23:01
110%	0.096	0.096	1.730	0.0206	0.642	0.36	0.0	0.0	00:23:42
120%	0.109	0.105	1.882	0.0197	0.642	0.36	0.0	0.0	00:24:07
130%	0.114	0.113	1.939	0.0195	0.642	0.36	0.0	0.0	00:25:53

1.6.1, reversed interlocking block, $s_{0,p} = 2\%$, $R_c/H_{s,d} = 0.0$

$\% \cdot H_{s,d}$	H_s (m)	$H_{s,theory}$ (m)	T_p (s)	$s_{0,p}$ (-)	h_0 (m)	h_{toe} (m)	R_c (m)	$R_c/H_{s,d}$ (-)	time(h,m,s)
60%	0.059	0.052	1.306	0.0220	0.642	0.359	0.0	0.0	00:18:10
80%	0.069	0.070	1.455	0.0210	0.642	0.359	0.0	0.0	00:20:22
100%	0.088	0.087	1.641	0.0209	0.642	0.359	0.0	0.0	00:22:23
110%	0.096	0.096	1.730	0.0205	0.642	0.359	0.0	0.0	00:24:15
120%	0.107	0.105	1.882	0.0193	0.642	0.359	0.0	0.0	00:24:33

2.1.1, optimised permeable block, $s_{0,p} = 2\%$, $R_c/H_{s,d} = 0.0$

$\% \cdot H_{s,d}$	H_s (m)	$H_{s,theory}$ (m)	T_p (s)	$s_{0,p}$ (-)	$H_{s,t}$ (m)	h_{toe} (m)	R_c (m)	$R_c/H_{s,d}$ (-)	time(h,m,s)
60%	0.051	0.052	1.333	0.0185	0.02073	0.482	0.0	0.000	00:18:31
80%	0.070	0.070	1.455	0.0213	0.02969	0.482	0.0	0.000	00:20:38
100%	0.088	0.087	1.684	0.0198	0.03946	0.482	0.0	0.000	00:22:38
110%	0.098	0.096	1.73	0.0209	0.04481	0.482	0.0	0.000	00:24:03
120%	0.106	0.105	1.778	0.0216	0.04914	0.482	0.0	0.000	00:25:03
130%	0.115	0.113	1.939	0.0195	0.0535	0.482	0.0	0.000	00:26:08
140%	0.125	0.122	1.939	0.0213	0.05922	0.482	0.0	0.000	00:26:44
150%	0.133	0.131	2.065	0.0200	0.06327	0.482	0.0	0.000	00:27:49

2.1.2, optimised permeable block, $s_{0,p} = 4\%$, $R_c/H_{s,d} = 0.0$

$\% \cdot H_{s,d}$	H_s (m)	$H_{s,theory}$ (m)	T_p (s)	$s_{0,p}$ (-)	$H_{s,t}$ (m)	h_{toe} (m)	R_c (m)	$R_c/H_{s,d}$ (-)	time(h,m,s)
60%	0.047	0.052	0.9275	0.0347	0.017	0.48	0.0	0.000	00:13:55
80%	0.073	0.070	1.067	0.0410	0.027	0.48	0.0	0.000	00:15:31
100%	0.090	0.087	1.185	0.0411	0.036	0.48	0.0	0.000	00:17:13
110%	0.097	0.096	1.208	0.0424	0.039	0.48	0.0	0.000	00:18:45
120%	0.108	0.105	1.306	0.0406	0.043	0.48	0.0	0.000	00:18:06
130%	0.113	0.113	1.333	0.0408	0.046	0.48	0.0	0.000	00:18:55
140%	0.123	0.122	1.391	0.0408	0.050	0.48	0.0	0.000	00:19:43

2.1.3, optimised permeable block, $s_{0,p} = 2\%$, $R_c/H_{s,d} = 0.5$

$\% \cdot H_{s,d}$	H_s (m)	$H_{s,theory}$ (m)	T_p (s)	$s_{0,p}$ (-)	$H_{s,t}$ (m)	h_{toe} (m)	R_c (m)	$R_c/H_{s,d}$ (-)	time(h,m,s)
60%	0.055	0.052	1.231	0.0233	0.009	0.439	0.042	0.478	00:18:31
80%	0.072	0.070	1.561	0.0190	0.016	0.439	0.042	0.478	00:21:08
100%	0.088	0.087	1.561	0.0230	0.024	0.439	0.042	0.478	00:22:39
110%	0.097	0.096	1.778	0.0197	0.029	0.439	0.042	0.478	00:24:10
120%	0.107	0.105	1.778	0.0216	0.034	0.439	0.042	0.478	00:24:44
130%	0.114	0.113	1.829	0.0217	0.038	0.439	0.042	0.478	00:26:13
140%	0.123	0.122	1.939	0.0210	0.044	0.439	0.042	0.478	00:27:09
150%	0.131	0.131	2.065	0.0197	0.049	0.439	0.042	0.478	00:28:24

2.1.4, optimised permeable block, $s_{0,p} = 4\%$, $R_c/H_{s,d} = 0.5$

$\% \cdot H_{s,d}$	H_s (m)	$H_{s,theory}$ (m)	T_p (s)	$s_{0,p}$ (-)	$H_{s,t}$ (m)	h_{toe} (m)	R_c (m)	$R_c/H_{s,d}$ (-)	time(h,m,s)
60%	0.050	0.052	0.9275	0.0370	0.005	0.438	0.041	0.467	00:09:12
80%	0.072	0.070	1.067	0.0407	0.010	0.438	0.041	0.467	00:09:28
100%	0.090	0.087	1.123	0.0459	0.018	0.438	0.041	0.467	00:11:57
110%	0.098	0.096	1.231	0.0415	0.022	0.438	0.041	0.467	00:12:47
120%	0.108	0.105	1.255	0.0441	0.026	0.438	0.041	0.467	00:18:40
130%	0.114	0.113	1.362	0.0392	0.029	0.438	0.041	0.467	00:19:08
140%	0.122	0.122	1.391	0.0405	0.033	0.438	0.041	0.467	00:18:48
150%	0.133	0.131	1.391	0.0439	0.039	0.438	0.041	0.467	00:20:13

2.1.5, optimised permeable block - rep, $s_{0,p} = 2\%$, $R_c/H_{s,d} = 0.0$

$\% \cdot H_{s,d}$	H_s (m)	$H_{s,theory}$ (m)	T_p (s)	$s_{0,p}$ (-)	$H_{s,t}$ (m)	h_{toe} (m)	R_c (m)	$R_c/H_{s,d}$ (-)	time(h,m,s)
60%	0.052	0.052	1.333	0.0186	0.019	0.478	0.000	0.000	00:18:19
80%	0.071	0.070	1.488	0.0205	0.028	0.478	0.000	0.000	00:20:41
100%	0.087	0.087	1.730	0.0187	0.038	0.478	0.000	0.000	00:23:45
110%	0.098	0.096	1.730	0.0210	0.044	0.478	0.000	0.000	00:24:03
120%	0.107	0.105	1.778	0.0216	0.048	0.478	0.000	0.000	00:25:00
130%	0.115	0.113	1.939	0.0195	0.052	0.478	0.000	0.000	00:26:10
140%	0.125	0.122	1.939	0.0213	0.058	0.478	0.000	0.000	00:26:52
150%	0.131	0.131	2.065	0.0197	0.062	0.478	0.000	0.000	00:27:40

2.1.6, optimised permeable block - rep, $s_{0,p} = 4\%$, $R_c/H_{s,d} = 0.0$

$\% \cdot H_{s,d}$	H_s (m)	$H_{s,theory}$ (m)	T_p (s)	$s_{0,p}$ (-)	$H_{s,t}$ (m)	h_{toe} (m)	R_c (m)	$R_c/H_{s,d}$ (-)	time(h,m,s)
60%	0.050	0.052	0.9275	0.0375	0.017	0.478	0.000	0.000	00:14:18
80%	0.070	0.070	1.067	0.0395	0.025	0.478	0.000	0.000	00:16:04
100%	0.088	0.087	1.185	0.0402	0.033	0.478	0.000	0.000	00:16:53
110%	0.097	0.096	1.208	0.0428	0.037	0.478	0.000	0.000	00:17:42
120%	0.104	0.105	1.333	0.0374	0.040	0.478	0.000	0.000	00:18:14
130%	0.111	0.113	1.362	0.0383	0.044	0.478	0.000	0.000	00:19:16
140%	0.121	0.122	1.391	0.0402	0.048	0.478	0.000	0.000	00:19:52

2.2.1, bermblock Afsluitdijk, $s_{0,p} = 4\%$, $R_c/H_{s,d} = 0.0$

$\% \cdot H_{s,d}$	H_s (m)	$H_{s,theory}$ (m)	T_p (s)	$s_{0,p}$ (-)	$H_{s,t}$ (m)	h_{toe} (m)	R_c (m)	$R_c/H_{s,d}$ (-)	time(h,m,s)
60%	0.050	0.052	0.9275	0.0374	0.017	0.478	0.000	0.000	00:13:53
80%	0.070	0.070	1.067	0.0397	0.025	0.478	0.000	0.000	00:15:36
100%	0.090	0.087	1.164	0.0428	0.035	0.478	0.000	0.000	00:17:37
110%	0.098	0.096	1.208	0.0431	0.038	0.478	0.000	0.000	00:17:36
120%	0.106	0.105	1.333	0.0381	0.040	0.478	0.000	0.000	00:18:14

2.3.1, initial permeable block-1, $s_{0,p} = 2\%$, $R_c/H_{s,d} = 0.0$

$\% \cdot H_{s,d}$	H_s (m)	$H_{s,theory}$ (m)	T_p (s)	$s_{0,p}$ (-)	$H_{s,t}$ (m)	h_{toe} (m)	R_c (m)	$R_c/H_{s,d}$ (-)	time(h,m,s)
60%	0.052	0.052	1.333	0.0188	0.021	0.49	0.0	0.000	00:18:26
80%	0.071	0.070	1.488	0.0206	0.031	0.49	0.0	0.000	00:20:46
100%	0.088	0.087	1.684	0.0199	0.040	0.49	0.0	0.000	00:22:55
110%	0.096	0.096	1.730	0.0206	0.042	0.49	0.0	0.000	00:24:57
120%	0.107	0.105	1.778	0.0216	0.048	0.49	0.0	0.000	00:24:45
130%	0.115	0.113	1.939	0.0195	0.052	0.49	0.0	0.000	00:25:55
140%	0.124	0.122	1.939	0.0211	0.058	0.49	0.0	0.000	00:27:36

2.3.2, initial permeable block-2, $s_{0,p} = 2\%$, $R_c/H_{s,d} = 0.0$

$\% \cdot H_{s,d}$	H_s (m)	$H_{s,theory}$ (m)	T_p (s)	$s_{0,p}$ (-)	$H_{s,t}$ (m)	h_{toe} (m)	R_c (m)	$R_c/H_{s,d}$ (-)	time(h,m,s)
60%	0.051	0.052	1.333	0.0185	0.020	0.485	0.0	0.000	00:18:33
80%	0.070	0.070	1.455	0.0212	0.029	0.485	0.0	0.000	00:20:38
100%	0.088	0.087	1.684	0.0198	0.039	0.485	0.0	0.000	00:22:42
110%	0.098	0.096	1.730	0.0209	0.045	0.485	0.0	0.000	00:24:29
120%	0.107	0.105	1.778	0.0216	0.049	0.485	0.0	0.000	00:24:58

2.3.3, initial permeable block-3, $s_{0,p} = 2\%$, $R_c/H_{s,d} = 0.0$

$\% \cdot H_{s,d}$	H_s (m)	$H_{s,theory}$ (m)	T_p (s)	$s_{0,p}$ (-)	$H_{s,t}$ (m)	h_{toe} (m)	R_c (m)	$R_c/H_{s,d}$ (-)	time(h,m,s)
60%	0.051	0.052	1.333	0.0184	0.019	0.478	0.000	0.000	00:19:05
80%	0.071	0.070	1.488	0.0204	0.028	0.478	0.000	0.000	00:20:52
100%	0.088	0.087	1.730	0.0188	0.038	0.478	0.000	0.000	00:22:45
110%	0.098	0.096	1.730	0.0210	0.043	0.478	0.000	0.000	00:24:46
120%	0.107	0.105	1.778	0.0217	0.048	0.478	0.000	0.000	00:24:44
130%	0.115	0.113	1.939	0.0195	0.052	0.478	0.000	0.000	00:26:01
140%	0.125	0.122	1.939	0.0212	0.057	0.478	0.000	0.000	00:26:34
150%	0.132	0.131	2.065	0.0198	0.061	0.478	0.000	0.000	00:28:35

2.3.4, initial permeable block, $s_{0,p} = 4\%$, $R_c/H_{s,d} = 0.0$

$\% \cdot H_{s,d}$	H_s (m)	$H_{s,theory}$ (m)	T_p (s)	$s_{0,p}$ (-)	$H_{s,t}$ (m)	h_{toe} (m)	R_c (m)	$R_c/H_{s,d}$ (-)	time(h,m,s)
60%	0.049	0.052	0.9275	0.0365	0.016	0.477	0.000	0.000	00:14:02
80%	0.069	0.070	1.067	0.0386	0.024	0.477	0.000	0.000	00:15:32
100%	0.088	0.087	1.164	0.0416	0.033	0.477	0.000	0.000	00:17:18
110%	0.097	0.096	1.208	0.0426	0.037	0.477	0.000	0.000	00:17:57
120%	0.108	0.105	1.333	0.0387	0.041	0.477	0.000	0.000	00:18:23
130%	0.113	0.113	1.362	0.0389	0.044	0.477	0.000	0.000	00:19:36
140%	0.122	0.122	1.391	0.0403	0.048	0.477	0.000	0.000	00:19:57

G

Experiment photos

G.1. Preliminary research phase

G.1.1. Test 1.1.1. - Reference situation



Figure G.1: Initial situation



Figure G.2: After 60% test session ($N_s = 0.94$)



Figure G.3: After 80% test session ($N_s = 1.97$)



Figure G.4: After 100% test session ($N_s = 2.39$)



Figure G.5: After 110% test session ($N_s = 2.64$)

G.1.2. Test 1.1.2. - Small crest block



Figure G.6: Initial situation



Figure G.7: After 60% test session ($N_s = 1.42$)



Figure G.8: After 80% test session ($N_s = 2.07$)

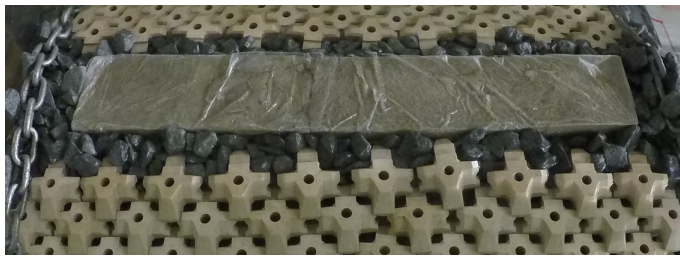


Figure G.9: After 100% test session ($N_s = 2.56$)



Figure G.10: After 110% test session ($N_s = 2.82$)



Figure G.11: After 120% test session ($N_s = 3.06$)

G.1.3. Test 1.2.1. - Start block $R_c/H_{s,d} = 0$



Figure G.12: Initial situation



Figure G.13: After 60% test session ($N_s = 1.50$)



Figure G.14: After 80% test session ($N_s = 2.07$)



Figure G.15: After 100% test session ($N_s = 2.60$)



Figure G.16: After 110% test session ($N_s = 2.68$)



Figure G.17: After 120% test session ($N_s = 3.16$)



Figure G.18: After 130% test session ($N_s = 3.27$)

G.1.4. Test 1.2.2. - Start block $R_c/H_{s,d} = 0.5$



Figure G.19: Initial situation



Figure G.20: After 60% test session ($N_s = 1.34$)



Figure G.21: After 80% test session ($N_s = 2.06$)



Figure G.22: After 100% test session ($N_s = 2.60$)



Figure G.23: After 110% test session ($N_s = 2.86$)



Figure G.24: After 120% test session ($N_s = 3.12$)



Figure G.25: After 130% test session ($N_s = 3.32$)



Figure G.26: After 140% test session ($N_s = 3.56$)

G.1.5. Test 1.3.1. - Permeable block



Figure G.27: Initial situation



Figure G.28: After 60% test session ($N_s = 1.43$)



Figure G.29: After 80% test session ($N_s = 2.03$)



Figure G.30: After 100% test session ($N_s = 2.60$)



Figure G.31: After 110% test session ($N_s = 2.81$)



Figure G.32: After 120% test session ($N_s = 3.07$)



Figure G.33: After 130% test session ($N_s = 3.31$)



Figure G.34: After 140% test session ($N_s = 3.53$)

G.1.6. Test 1.4.1. - Extended bottom block



Figure G.35: Initial situation



Figure G.36: After 60% test session ($N_s = 1.50$)



Figure G.37: After 80% test session ($N_s = 2.02$)

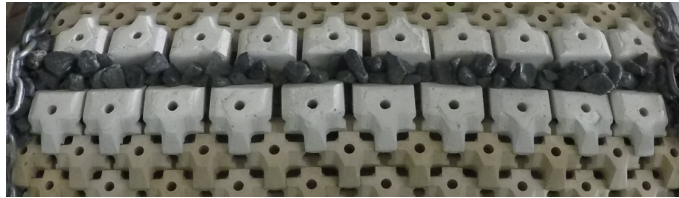


Figure G.38: After 100% test session ($N_s = 2.55$)

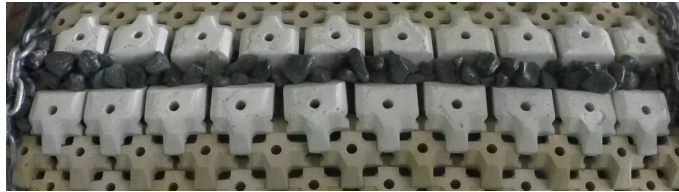


Figure G.39: After 110% test session ($N_s = 2.78$)

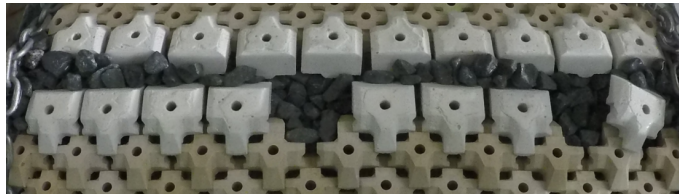


Figure G.40: After 120% test session ($N_s = 3.08$)

G.1.7. Test 1.5.1. - Interlocking block attempt 1



Figure G.41: Initial situation



Figure G.42: After 60% test session ($N_s = 1.47$)



Figure G.43: After 80% test session ($N_s = 2.07$)

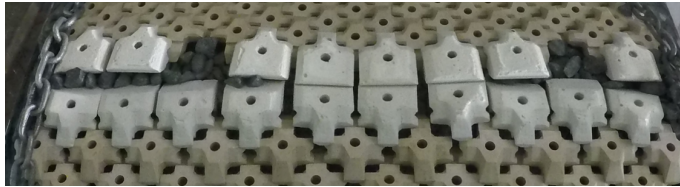


Figure G.44: After 100% test session ($N_s = 2.51$)



Figure G.45: After 110% test session ($N_s = 2.81$)

G.1.8. Test 1.5.2. - Interlocking block attempt 2

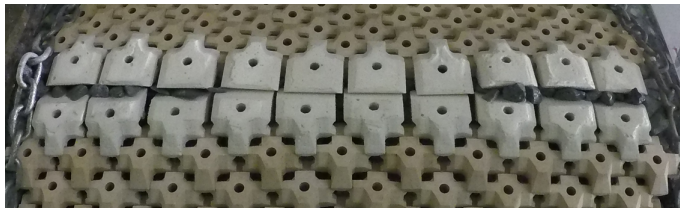


Figure G.46: Initial situation

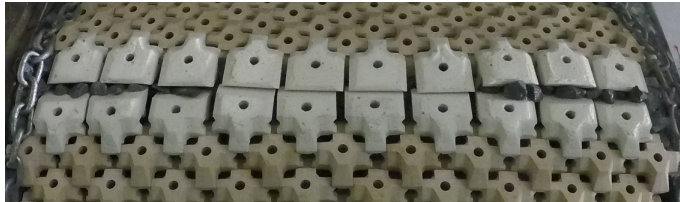


Figure G.47: After 60% test session ($N_s = 1.41$)

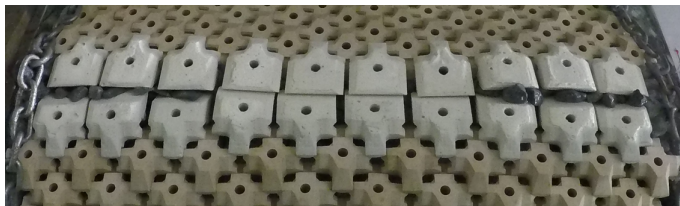


Figure G.48: After 80% test session ($N_s = 2.01$)



Figure G.49: After 100% test session ($N_s = 2.60$)

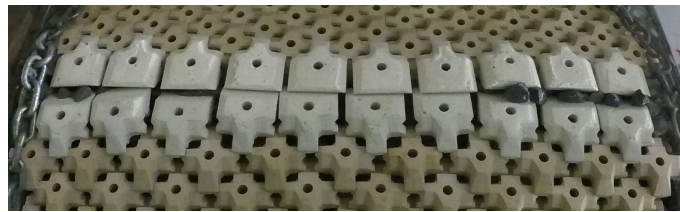


Figure G.50: After 110% test session ($N_s = 2.76$)



Figure G.51: After 120% test session ($N_s = 3.12$)

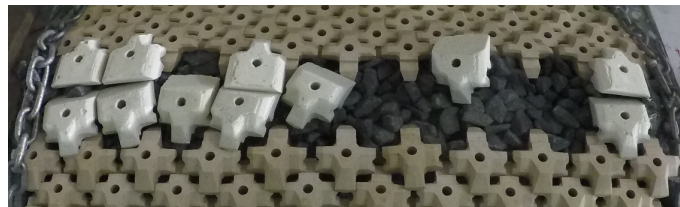


Figure G.52: After 130% test session ($N_s = 3.27$)

G.1.9. Test 1.6.1. - Reversed interlocking blocks

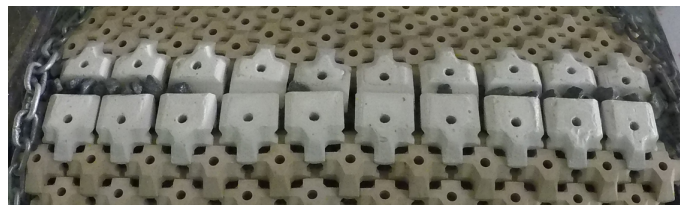


Figure G.53: Initial situation

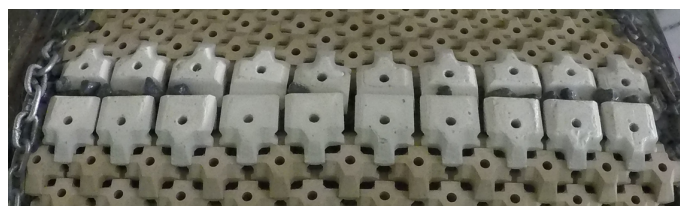


Figure G.54: After 60% test session ($N_s = 1.68$)

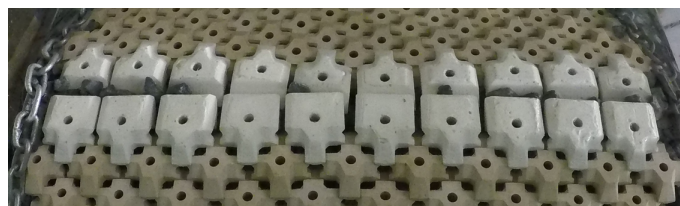


Figure G.55: After 80% test session ($N_s = 1.99$)

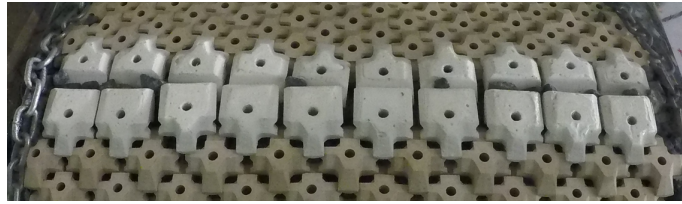


Figure G.56: After 100% test session ($N_s = 2.51$)



Figure G.57: After 110% test session ($N_s = 2.74$)

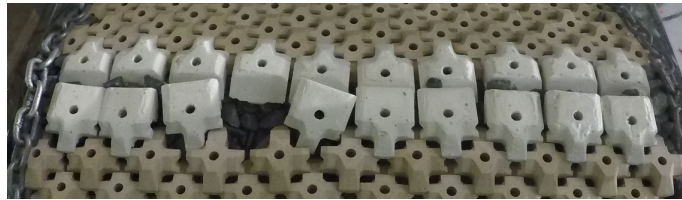


Figure G.58: After 120% test session ($N_s = 3.06$)

G.2. Detailed research phase

G.2.1. Test 2.1.1. - Optimised permeable block ($R_c/H_{s,d} = 0.0$, $s_{0,p} = 2\%$)

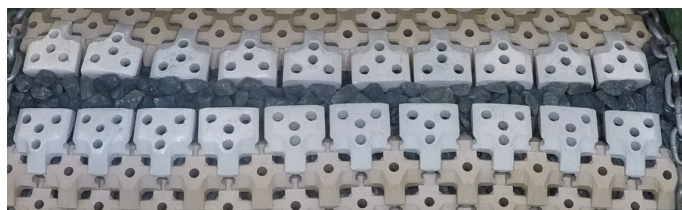


Figure G.59: Initial situation

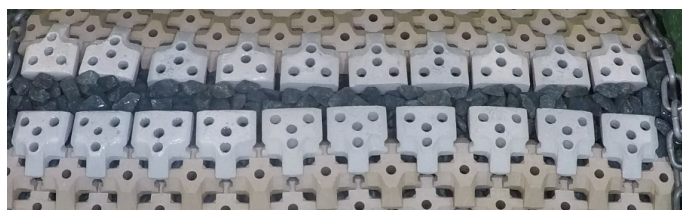


Figure G.60: After 60% test session ($N_s = 1.47$)

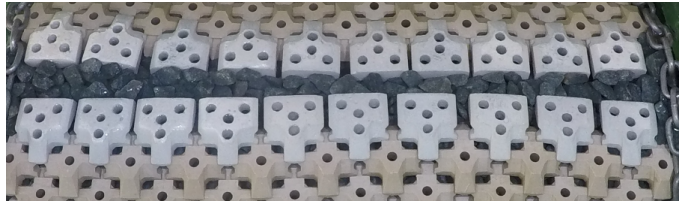


Figure G.61: After 80% test session ($N_s = 2.02$)

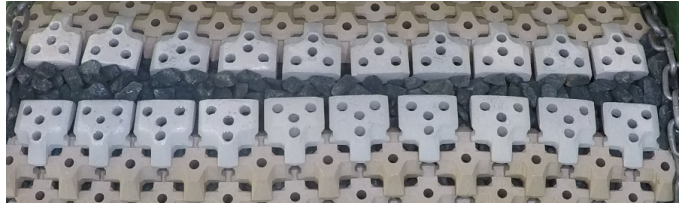


Figure G.62: After 100% test session ($N_s = 2.52$)

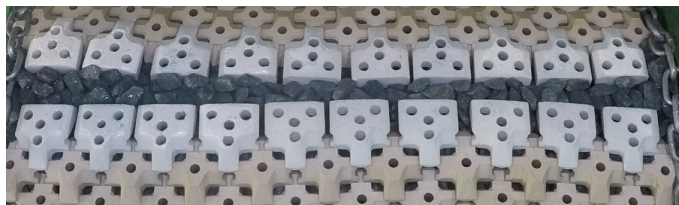


Figure G.63: After 110% test session ($N_s = 2.80$)



Figure G.64: After 120% test session ($N_s = 3.05$)



Figure G.65: After 130% test session ($N_s = 3.28$)

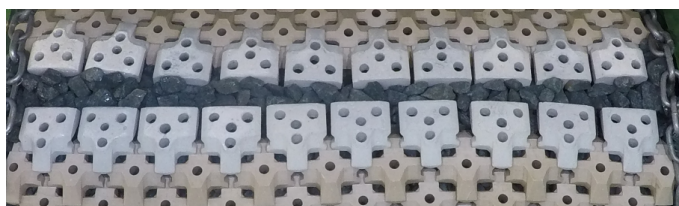


Figure G.66: After 140% test session ($N_s = 3.57$)

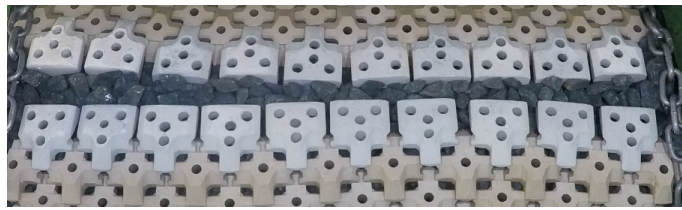


Figure G.67: After 150% test session ($N_s = 3.81$)

G.2.2. Test 2.1.2. - Optimised permeable block ($R_c/H_{s,d} = 0.0$, $s_{0,p} = 4\%$)

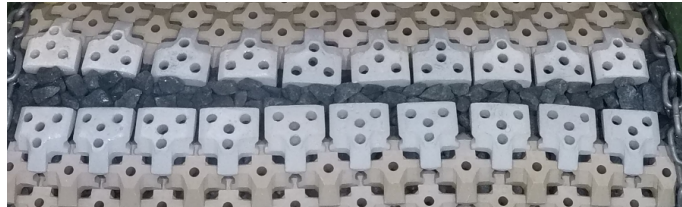


Figure G.68: Initial situation

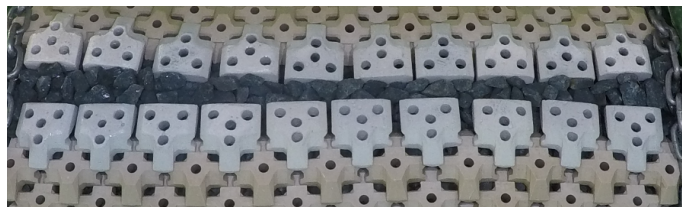


Figure G.69: After 60% test session ($N_s = 1.33$)

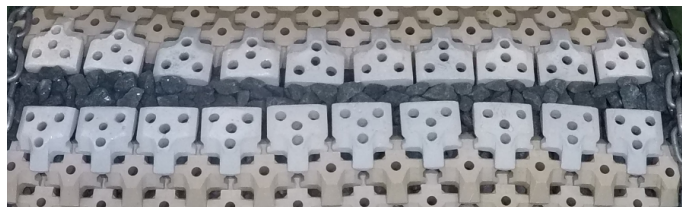


Figure G.70: After 80% test session ($N_s = 2.09$)

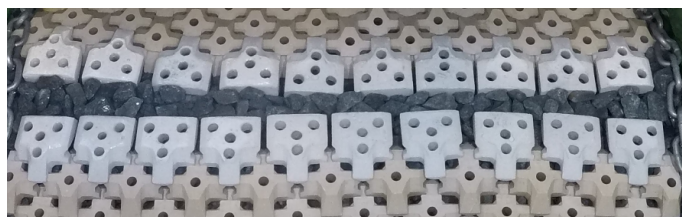


Figure G.71: After 100% test session ($N_s = 2.58$)

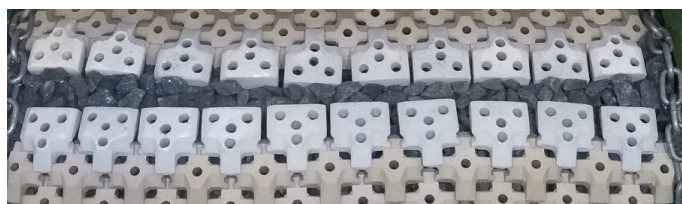


Figure G.72: After 110% test session ($N_s = 2.77$)

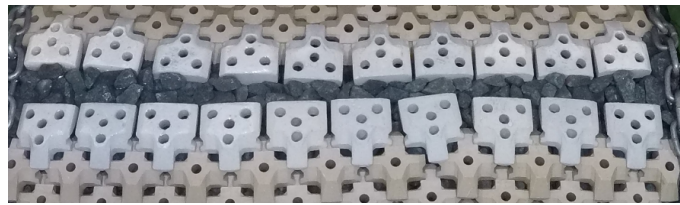


Figure G.73: After 120% test session ($N_s = 3.10$)



Figure G.74: After 130% test session ($N_s = 3.24$)



Figure G.75: After 140% test session ($N_s = 3.53$)

G.2.3. Test 2.1.3. - Optimised permeable block ($R_c/H_{s,d} = 0.5$, $s_{0,p} = 2\%$)

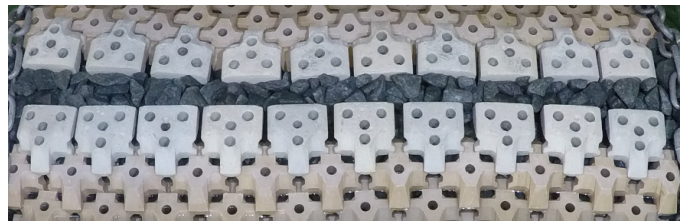


Figure G.76: Initial situation



Figure G.77: After 60% test session ($N_s = 1.58$)

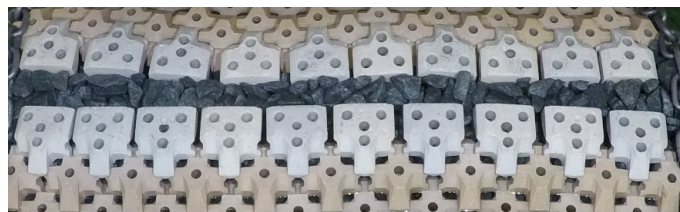


Figure G.78: After 80% test session ($N_s = 2.08$)

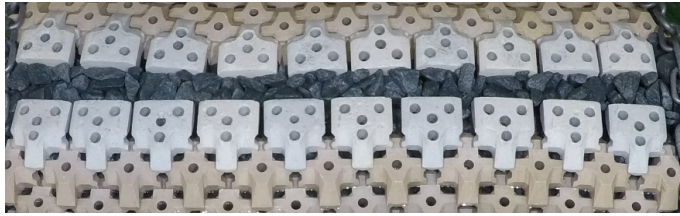


Figure G.79: After 100% test session ($N_s = 2.51$)

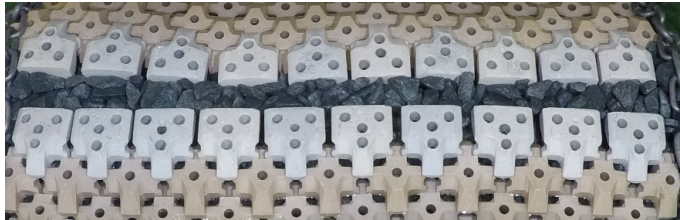


Figure G.80: After 110% test session ($N_s = 2.79$)

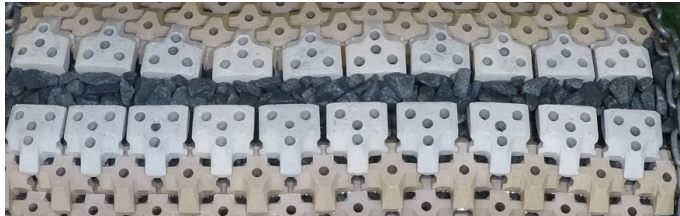


Figure G.81: After 120% test session ($N_s = 3.05$)

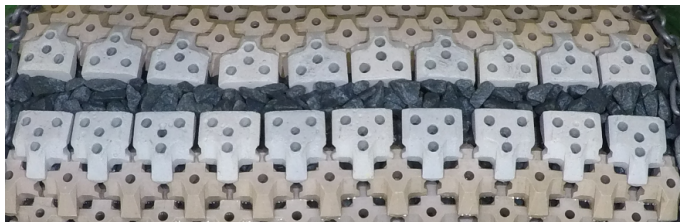


Figure G.82: After 130% test session ($N_s = 3.25$)

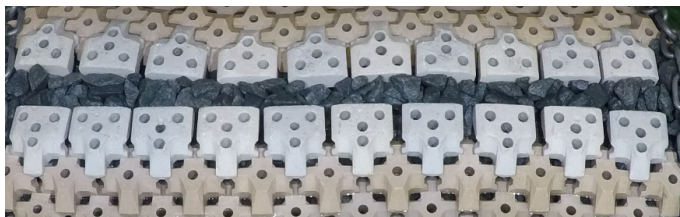


Figure G.83: After 140% test session ($N_s = 3.53$)



Figure G.84: After 150% test session ($N_s = 3.75$)

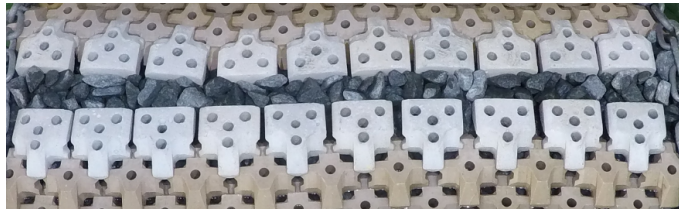
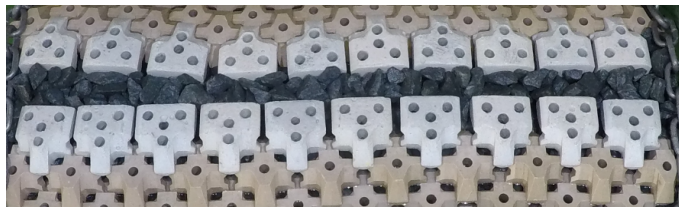
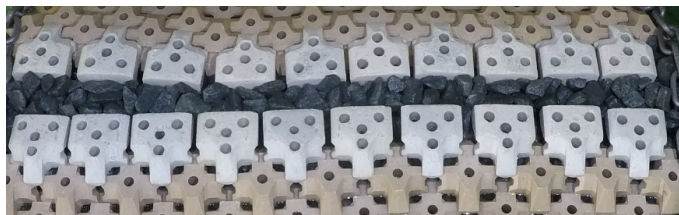
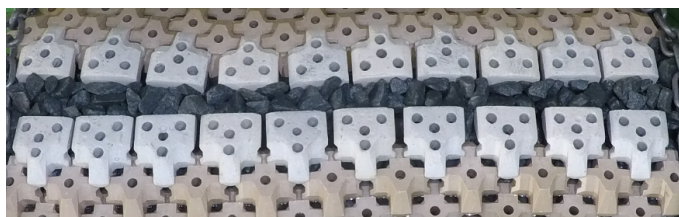
G.2.4. Test 2.1.4. - Optimised permeable block ($R_c/H_{s,d} = 0.5$, $s_{0,p} = 4\%$)

Figure G.85: Initial situation

Figure G.86: After 60% test session ($N_s = 1.42$)Figure G.87: After 80% test session ($N_s = 2.07$)Figure G.88: After 100% test session ($N_s = 2.59$)Figure G.89: After 110% test session ($N_s = 2.81$)

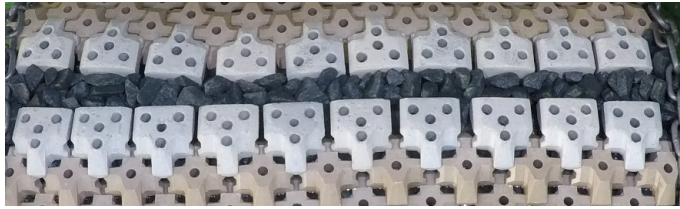


Figure G.90: After 120% test session ($N_s = 3.10$)

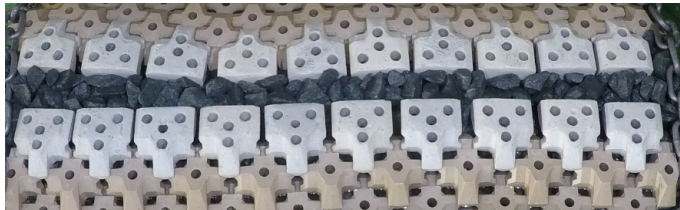


Figure G.91: After 130% test session ($N_s = 3.25$)

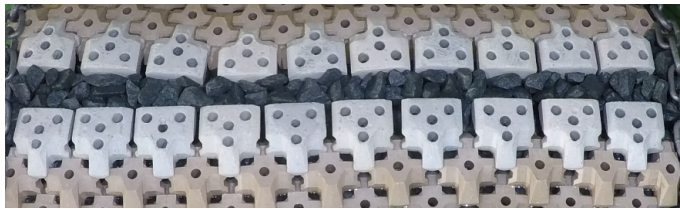


Figure G.92: After 140% test session ($N_s = 3.50$)



Figure G.93: After 150% test session ($N_s = 3.79$)

G.2.5. Test 2.1.5. - Optimised permeable block - repetition ($R_c/H_{s,d} = 0.0$, $s_{0,p} = 2\%$)



Figure G.94: Initial situation



Figure G.95: After 60% test session ($N_s = 1.48$)



Figure G.96: After 80% test session ($N_s = 2.03$)



Figure G.97: After 100% test session ($N_s = 2.51$)



Figure G.98: After 110% test session ($N_s = 2.81$)



Figure G.99: After 120% test session ($N_s = 3.05$)



Figure G.100: After 130% test session ($N_s = 3.28$)



Figure G.101: After 140% test session ($N_s = 3.57$)



Figure G.102: After 150% test session ($N_s = 3.75$)

G.2.6. Test 2.1.6. - Optimised permeable block - repetition ($R_c/H_{s,d} = 0.0$, $s_{0,p} = 4\%$)



Figure G.103: Initial situation



Figure G.104: After 60% test session ($N_s = 1.44$)



Figure G.105: After 80% test session ($N_s = 2.01$)



Figure G.106: After 100% test session ($N_s = 2.53$)



Figure G.107: After 110% test session ($N_s = 2.79$)



Figure G.108: After 120% test session ($N_s = 2.97$)



Figure G.109: After 130% test session ($N_s = 3.17$)



Figure G.110: After 140% test session ($N_s = 3.47$)

G.2.7. Test 2.2.1. - Berm block ($R_c/H_{s,d} = 0.0$, $s_{0,p} = 4\%$)

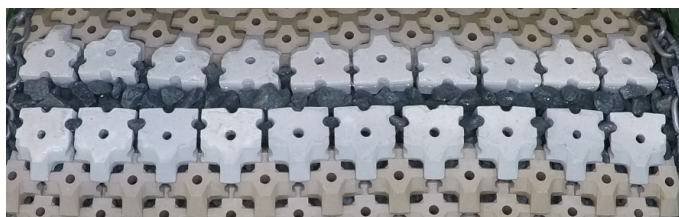


Figure G.111: Initial situation

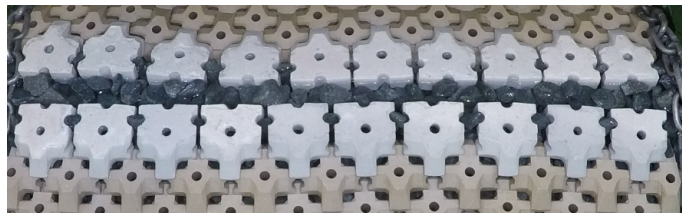


Figure G.112: After 60% test session ($N_s = 1.44$)

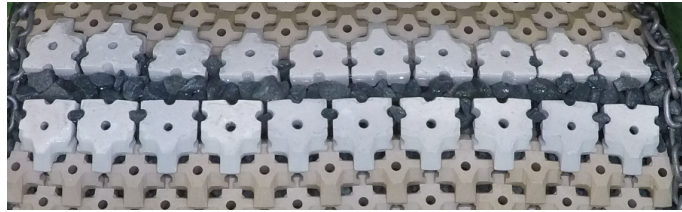


Figure G.113: After 80% test session ($N_s = 2.02$)

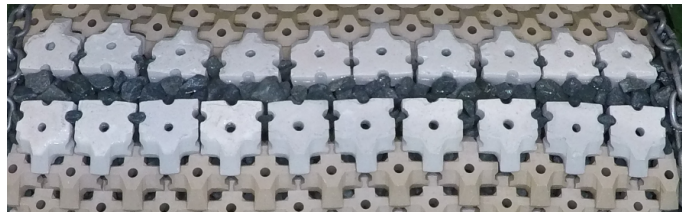


Figure G.114: After 100% test session ($N_s = 2.59$)

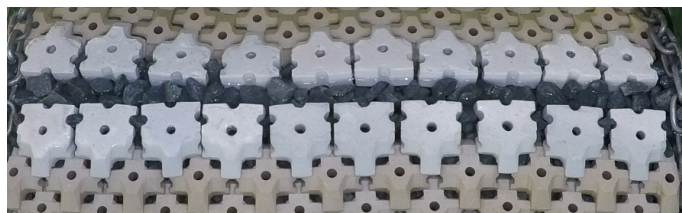


Figure G.115: After 110% test session ($N_s = 2.81$)



Figure G.116: After 120% test session ($N_s = 3.03$)

G.2.8. Test 2.3.1. - Initial permeable block - 1 ($R_c/H_{s,d} = 0.0$, $s_{0,p} = 2\%$)



Figure G.117: Initial situation

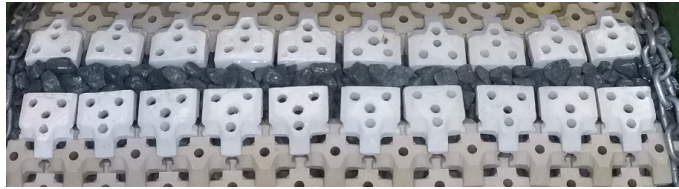


Figure G.118: After 60% test session ($N_s = 1.49$)

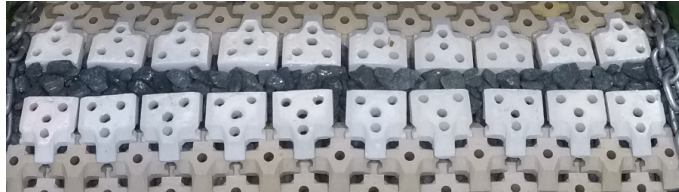


Figure G.119: After 80% test session ($N_s = 2.03$)

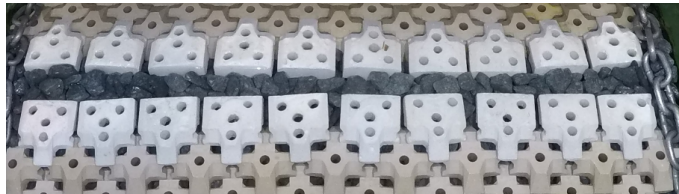


Figure G.120: After 100% test session ($N_s = 2.52$)

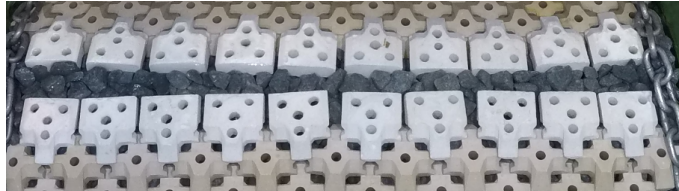


Figure G.121: After 110% test session ($N_s = 2.75$)



Figure G.122: After 120% test session ($N_s = 3.06$)



Figure G.123: After 130% test session ($N_s = 3.29$)



Figure G.124: After 140% test session ($N_s = 3.55$)

G.2.9. Test 2.3.2. - Initial permeable block - 2 ($R_c/H_{s,d} = 0.0$, $s_{0,p} = 2\%$)



Figure G.125: Initial situation



Figure G.126: After 60% test session ($N_s = 1.47$)

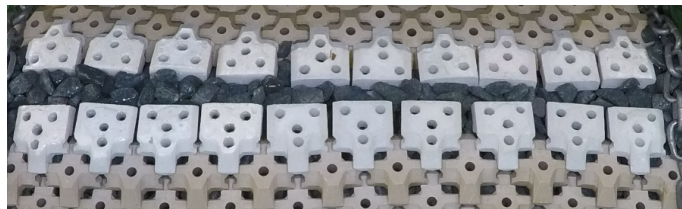


Figure G.127: After 80% test session ($N_s = 2.01$)

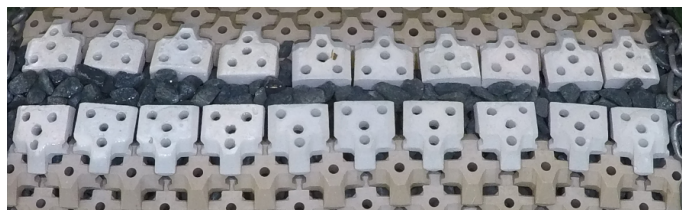


Figure G.128: After 100% test session ($N_s = 2.51$)



Figure G.129: After 110% test session ($N_s = 2.80$)

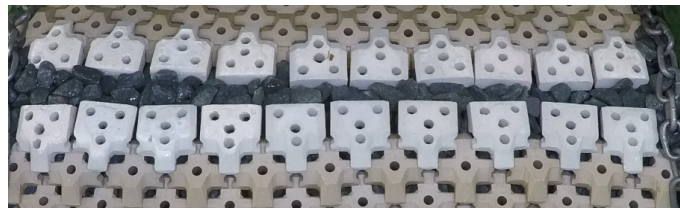


Figure G.130: After 120% test session ($N_s = 3.06$)

G.2.10. Test 2.3.3. - Initial permeable block - 3 ($R_c/H_{s,d} = 0.0$, $s_{0,p} = 2\%$)

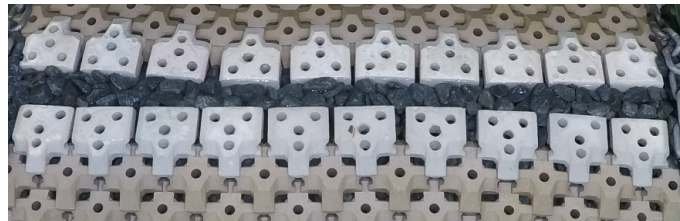


Figure G.131: Initial situation

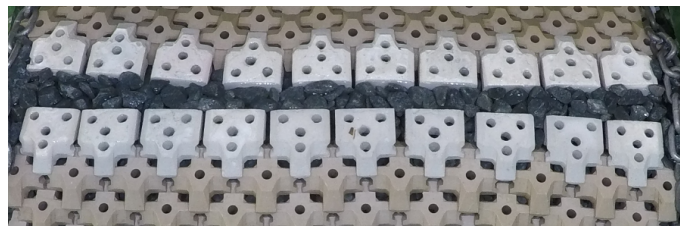


Figure G.132: After 60% test session ($N_s = 1.46$)

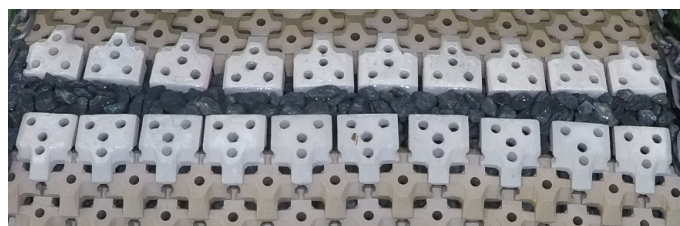


Figure G.133: After 80% test session ($N_s = 2.02$)

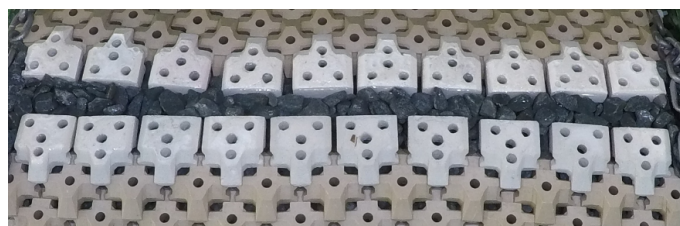


Figure G.134: After 100% test session ($N_s = 2.52$)

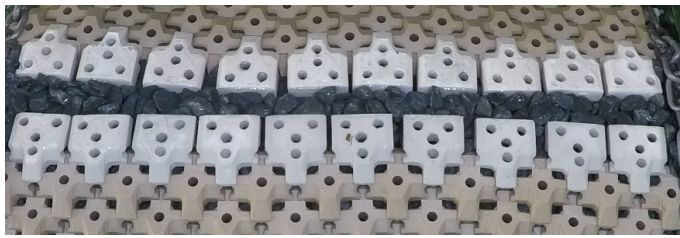


Figure G.135: After 110% test session ($N_s = 2.81$)

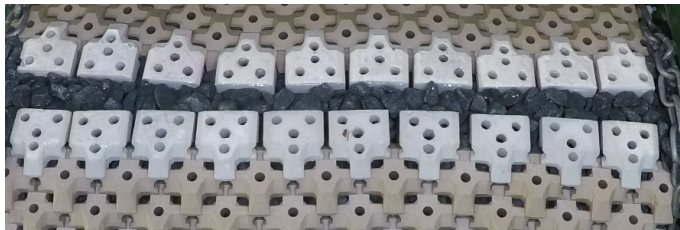


Figure G.136: After 120% test session ($N_s = 3.07$)

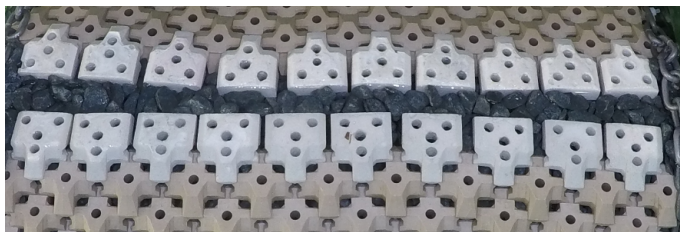


Figure G.137: After 130% test session ($N_s = 3.28$)

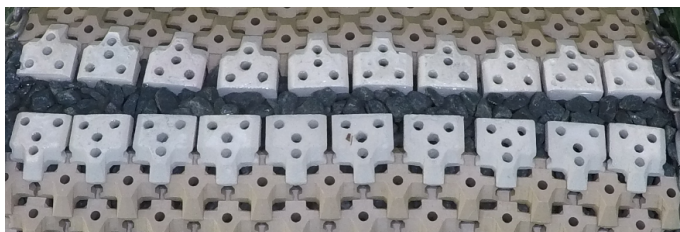


Figure G.138: After 140% test session ($N_s = 3.57$)

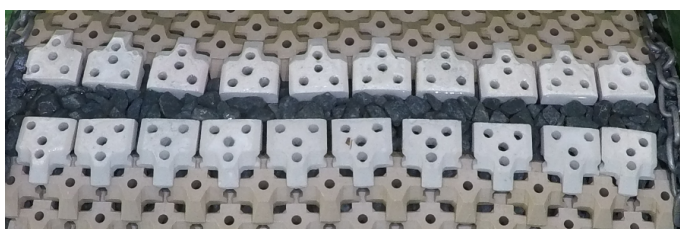


Figure G.139: After 150% test session ($N_s = 3.78$)

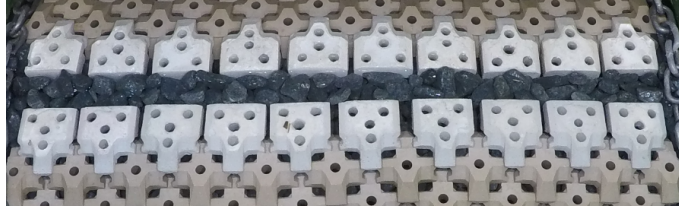
G.2.11. Test 2.3.4. - Initial permeable block ($R_c/H_{s,d} = 0.0$, $s_{0,p} = 4\%$)

Figure G.140: Initial situation

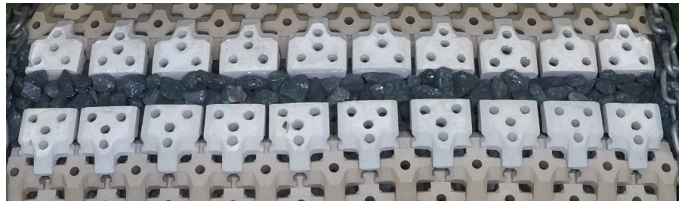
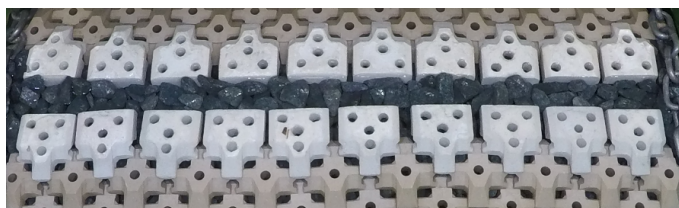
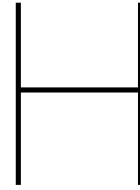
Figure G.141: After 60% test session ($N_s = 1.40$)Figure G.142: After 80% test session ($N_s = 1.96$)Figure G.143: After 100% test session ($N_s = 2.52$)Figure G.144: After 110% test session ($N_s = 2.78$)Figure G.145: After 120% test session ($N_s = 3.08$)



Figure G.146: After 130% test session ($N_s = 3.22$)



Figure G.147: After 140% test session ($N_s = 3.49$)



Additional test material

H.1. Interlocking blocks

H.1.1. Placement accuracy

In paragraph 7.5.3 is already mentioned that precise placement of the interlocking blocks is required to prevent loss of its interlocking capacity. Keeping the crest width very close to the theoretical crest width is crucial. In addition, height variations in the underlayer appear to be very important. During attempt 1, the blocks at the top row of the rear slope were positioned slightly higher than the blocks at the top row of the front slope. As a result, the crest blocks at the rear slope were more exposed to the wave load than they should be. Failure observations indicate that the initial position might have influenced the final stability. In a second attempt, the interlocking blocks were placed more accurately and retested. The test results of both tests are shown in figure H.1. It clearly indicates that the placement accuracy highly determines the outcome of the tests. During attempt one the structure remained stable till $N_{s,c} = 2.1$ whereas at the second attempt the structure remained stable till $N_{s,c} = 2.8$.

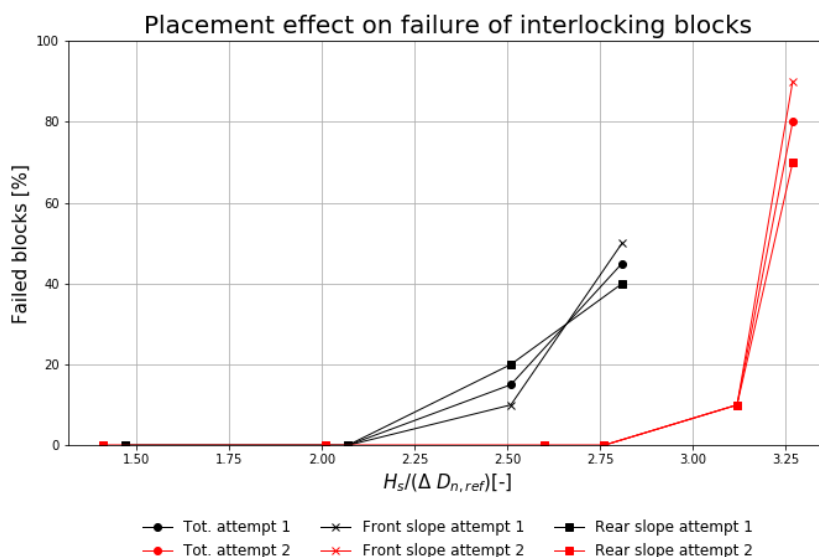


Figure H.1: Effect of initial placement on failure

H.1.2. Reversed placed interlocking blocks

In paragraph 7.5.3 is stated that the also the reversed placed interlocking blocks are tested. The test results are presented in figures H.2 and H.3. $N_{s,c}$ for the reserved interlocking blocks is 2.51 whereas it is 3.16 for the starting block. It can be concluded that the reversed interlocking blocks are less stable than the starting block. In addition, the reversed placed interlocking blocks are less stable than attempt 2 of the interlocking blocks ($N_s = 2.8$). Interesting to note is that rocking is hardly observed for the reversed interlocking blocks.

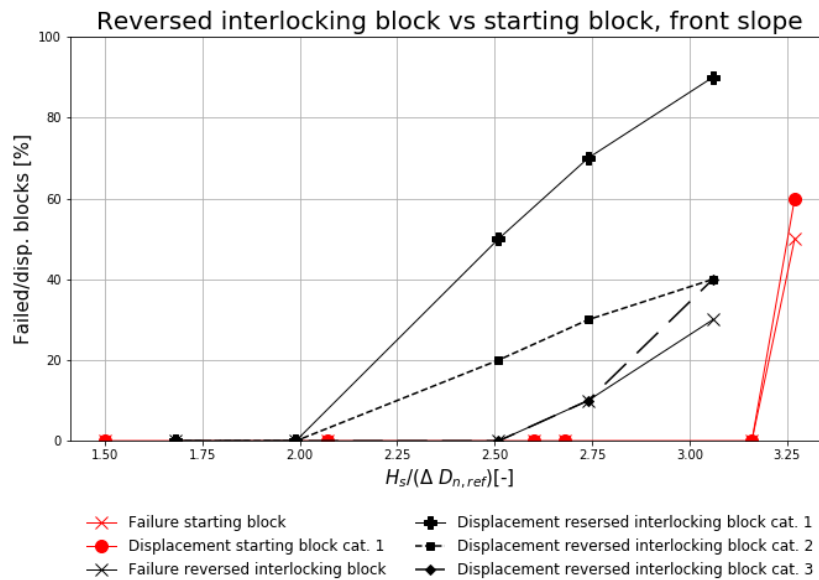


Figure H.2: Results front slope armoured with reversed interlocking blocks

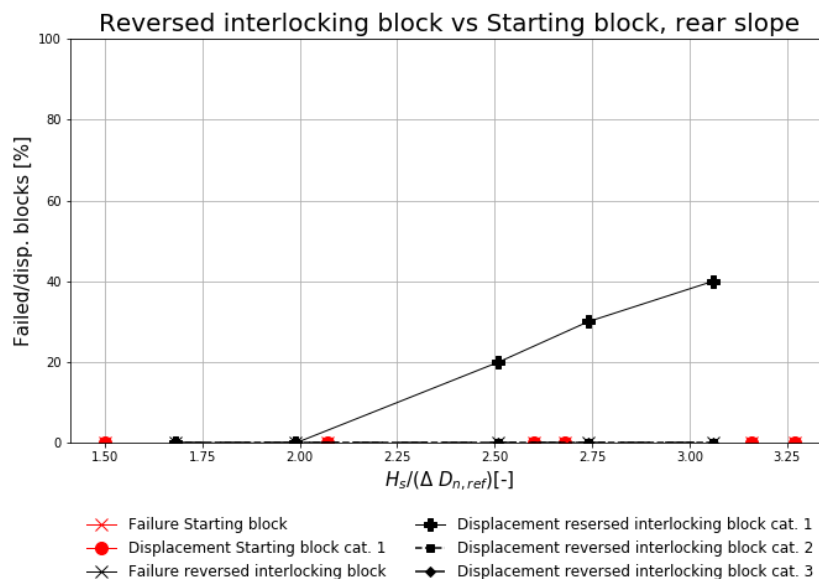


Figure H.3: Results rear slope armoured with reversed interlocking blocks

H.2. Foreshore influence

An assessment of the modified test set-up has been made before assessing the stability of the optimised permeable block. The initial permeable block is tested without a foreshore to make comparison possible. Figure H.4 shows the difference in stability of the initial permeable block with and without a foreshore. It shows the failure progression over a test session of crest blocks on the front and rear slope. The Y-axis expresses the ratio between the number of failed blocks on a crest row and the total number of crest blocks on that row in percentages. The X-axis expresses the test runs in a test series based on the stability number. The graph clearly indicates that failure of crest blocks on the front and rear slope started in an earlier test run for the test series with a foreshore. Differences between the test series with and without a foreshore are much larger than expected. In the set-up without foreshore, a test run with $H_s = 150\% \cdot H_{s,d}$ was necessary to let one crest block fail. The wave height distribution, wave steepness and the wave breaking are assessed to investigate their contribution to those large differences.

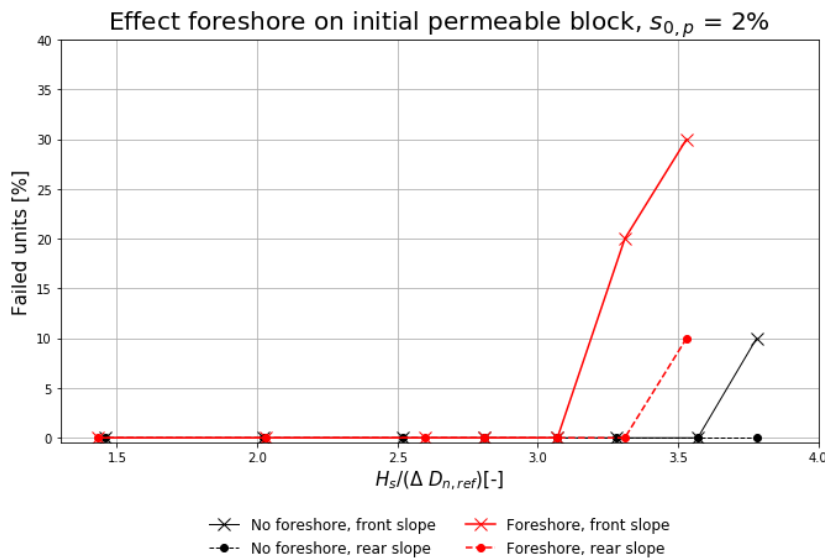


Figure H.4: Effect foreshore on stability initial permeable block, $s_{0,p} = 2\%$

H.2.1. Wave height distribution

The presence of a foreshore causes differences in the water depth near the toe ($h_{foreshore} = 35.5\text{cm}$, $h_{no,foreshore} = 48\text{cm}$). This may cause differences in the wave height distribution at the toe because the limited water depth induced by the foreshore might reduce the height of the largest waves in the distribution. As a result, differences in crest stability may arise because the crest block stability is determined by the largest waves in the wave distribution whereas H_s is in the stability expression. Observing figure H.5 shows that the smaller water depth in the test set-up with a foreshore didn't influence the height of the largest waves. H_s , $H_{2\%}$ and $H_{1\%}$ were nearly equal in the tests with and without foreshore. This makes it possible to conclude that the wave height distribution didn't influence the crest block stability.

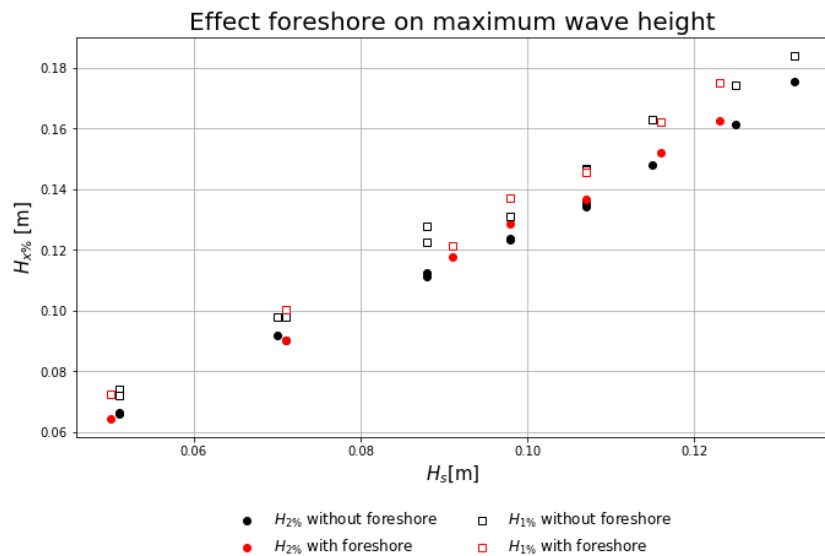


Figure H.5: Effect foreshore on wave distribution

H.2.2. Wave steepness

The local peak wavelength (L_p) decreases due to the reduced water depth caused by the foreshore. As a result, the local wave steepness (H_s/L_p) increases from approximately 3% to 3.5%. For both permeable blocks, the crest stability appeared to be normative for $s_{0,p} = 4\%$ instead of $s_{0,p} = 2\%$ (paragraph 11.1). The larger local wave steepness in the test series with a foreshore might have contributed to the earlier failure for the structure with foreshore.

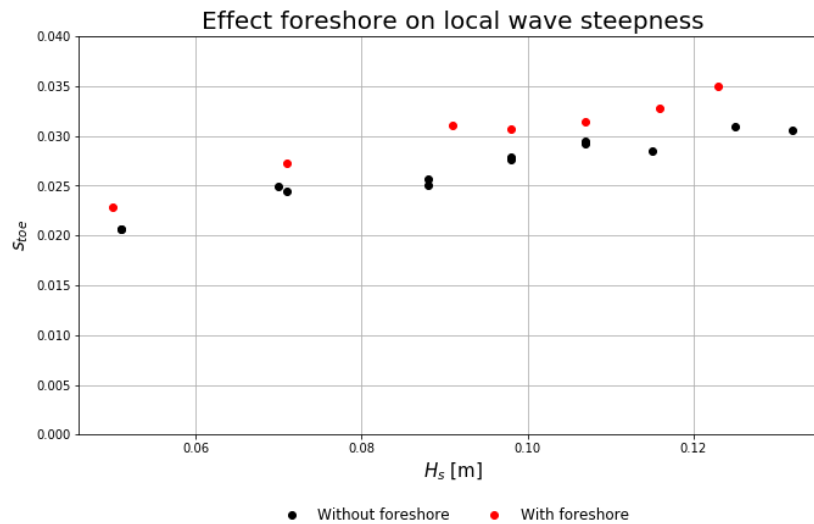


Figure H.6: Effect foreshore on local waves steepness

H.2.3. Wave breaking

Wave breaking occurred frequently in the test series with a foreshore whereas wave breaking hardly occurred in test series without a foreshore. In the initial research phase, failure of crest blocks occurred frequently due to breaking waves. This might be caused by the highly turbulent flow in a breaking wave.

H.2.4. Placement accuracy

The placement accuracy of the crest blocks in the preliminary research phase (and thus the test series with a foreshore) might have been lower than in the test series without a foreshore. This might be caused by differences in lab experience and knowledge about the crest blocks in the two test phases. The nose of some crest blocks in the preliminary research phase might have been more exposed to the wave forcing because they were not exactly resting on the XblocPlus blocks in the row beneath (paragraph 11.3). However, this is not observed.

H.2.5. Conclusion

The stability differences between the test series with and without a foreshore cannot be assigned to a single mechanism. Wave steepness, wave breaking and the placement accuracy might have been contributed. Only the effect of the wave height distribution can be excluded.